UNIVERSITY OF SOUTHAMPTON

FACULTY OF ENGINEERING SCIENCE AND MATHEMATICS

School of Engineering Sciences

Projection schemes for stochastic partial differential equations

by

Surya Mohan Prerapa

Thesis for the degree of Doctor of Philosophy

May 2009

ABSTRACT

FACULTY OF ENGINEERING SCIENCE AND MATHEMATICS

SCHOOL OF ENGINEERING SCIENCES

Doctor of Philosophy

PROJECTION SCHEMES FOR STOCHASTIC PARTIAL DIFFERENTIAL EQUATIONS

by Surya Mohan Prerapa

The focus of the present work is to develop stochastic reduced basis methods (SRBMs) for solving partial differential equations (PDEs) defined on random domains and nonlinear stochastic PDEs (SPDEs). SRBMs have been extended in the following directions:

Firstly, an h-refinement strategy referred to as Multi-Element-SRBMs (ME-SRBMs) is developed for local refinement of the solution process. The random space is decomposed into subdomains where SRBMs are employed in each subdomain resulting in local response statistics. These local statistics are subsequently assimilated to compute the global statistics. Two types of preconditioning strategies namely global and local preconditioning strategies are discussed due to their merits such as degree of parallelizability and better convergence trends. The improved accuracy and convergence trends of ME-SRBMs are demonstrated by numerical investigation of stochastic steady state elasticity and stochastic heat transfer applications.

The second extension involves the development of a computational approach employing SRBMs for solving linear elliptic PDEs defined on random domains. The key idea is to carry out spatial discretization of the governing equations using finite element (FE) methods and mesh deformation strategies. This results in a linear random algebraic system of equations whose coefficients of expansion can be computed nonintrusively either at the element or the global level. SRBMs are subsequently applied to the linear random algebraic system of equations to obtain the response statistics. We establish conditions that the input uncertainty model must satisfy to ensure the well-posedness of the problem. The proposed formulation is demonstrated on two and three dimensional model problems with uncertain boundaries undergoing steady state heat transfer. A large scale study involving a three-dimensional gas turbine model with uncertain boundary, has been presented in this context.

Finally, a numerical scheme that combines SRBMs with the Picard iteration scheme is proposed for solving nonlinear SPDEs. The governing equations are linearized using the response process from the previous iteration and spatially discretized. The resulting linear random algebraic system of equations are solved to obtain the new response process which acts as a guess for the next iteration. These steps of linearization, spatial discretization, solving the system of equations and updating the current guess are repeated until the desired accuracy is achieved. The effectiveness and the limitations of the formulation are demonstrated employing numerical studies in nonlinear heat transfer and the one-dimensional Burger's equation.

to my parents ...

Contents

List of Figures

List of Tables

Declaration of authorship

I, **Surya Mohan Prerapa**, declare that the thesis entitled **Projection schemes for stochastic partial differential equations** and the work presented in it are my own. I confirm that:

- ⋆ this work was done wholly or mainly while in candidature for a research degree at this University;
- ⋆ where any part of this thesis has previously been submitted for a degree or any other qualification at this University or any other institution, this has been clearly stated;
- ⋆ where I have consulted the published work of others, this is always clearly attributed;
- ⋆ where I have quoted from the work of of others, the source is always given. With the exception of such quotations, this thesis is entirely my own work;
- ⋆ I have acknowledged all main sources of help;
- ⋆ where the thesis is based on work done by myself jointly with others, I have made clear exactly what was done by others and what I have contributed myself;
- ⋆ parts of this work have been published and some articles are under review as:

  1. P. Surya Mohan, P. B. Nair and A. J. Keane, "Multi-element stochastic reduced basis methods", *Computer Methods in Applied Mechanics and Engineering*, **197(17-18)**, 2008, pp.1495-1506.
  2. P. Surya Mohan, P. B. Nair and A. J. Keane, "Inexact Picard iterative scheme for steady-state nonlinear diffusion in random heterogeneous media", *Physical Review E*, **79**, 2009, pp. 046706-1–046706-9.
  3. P. Surya Mohan, P. B. Nair and A. J. Keane, "Finite element methods for solving linear elliptic partial differential equations on random domains", submitted for review.

4. P. Surya Mohan, P.B. Nair and A. J. Keane, "Projection schemes for solving linear elliptic stochastic partial differential equations on random domains", accepted at *SIAM Conference on Computational Science and Engineering*, Miami, Florida, 2009.

5. P. Surya Mohan, P.B. Nair and A. J. Keane, "Uncertainty in thermal analysis of gas turbine blades", accepted at 11^{th} *AIAA Non-deterministic Approaches Conference*, Palm Springs, California, 2009.

Signature: _____

Date: _____

Acknowledgements

I would like to thank Dr. P. B. Nair for his guidance, advice, constant encouragement and support. I consider myself very fortunate to undertake this thesis under his able guidance. I am grateful to Rolls-Royce and the University of Southampton for the financial support without which this thesis would not have materialized. I would also like to thank Prof. A. J. Keane for proof reading the thesis and offering his advise that enriched the content of this work.

Special mention to my family and Prof. Vasu who have been my pillars of strength during this undertaking. I would like to acknowledge Prof. Vasu for proof reading the papers. His invaluable insights led to some interesting results presented in this thesis. I have spent many moments to cherish during these three years with Aarti, Abhi, Rupa, Alex, Ananth, Kamal, Apu, Nikita, Arun, Asa, Kevin, Antony, Alistair, Arturo, Dimitra, Ballu, Rakhi, Amrit, Becky, Boss, Rishi, Chincha, Chris, Derek, Felix, Bindu, Ronan, Ghasi, Hatice, Laurence, Dr. Mak, Mundis, Mandar, Sheetal, Shirin, Shubho, Runa, Obul, Phil, Pramod, Sneha, Sree and Pola. I dearly value and appreciate your company. Many thanks to you all and the Southampton Academics Cricket Club for the rejuvenating effect you had on me.

Finally, I would like to take this opportunity to acknowledge the Computational Engineering and Design Group for providing me with excellent research facilities and conducive environment. Many thanks to Ros for providing material support during the course of the PhD.

List of acronyms

PDE	Partial Differential Equation
FE	Finite Elements
SPDE	Stochastic Partial Differential Equation
IID	Identical, Independently Distributed
PDF	Probability Density Function
PCA	Principal Component Analysis
POD	Proper Orthogonal Decomposition
KL	Karhunen-Loève
MCS	Monte-Carlo Simulation
PC	Polynomial Chaos
gPC	generalized Polynomial Chaos
SSFEM	Spectral Stochastic Finite Element Method
SRBM	Stochastic Reduced Basis Method
ME-SRBM	Multi-Element Stochastic Reduced Basis Method

Nomenclature

Bold-faced lower-case alphabets denote vectors

Bold-faced upper-case alphabets denote matrices

$\mathbf{K}$-norm error	$\langle(\mathbf{u}_{true}(\boldsymbol{\theta}) - \mathbf{u}_{approx}(\boldsymbol{\theta}))^T \mathbf{K}(\boldsymbol{\theta})(\mathbf{u}_{true}(\boldsymbol{\theta}) - \mathbf{u}_{approx}(\boldsymbol{\theta}))\rangle$
$\boldsymbol{\theta}$	A set of statistically independent random variables
ϵ_μ	$\frac{\|\boldsymbol{\mu}_{MCS} - \boldsymbol{\mu}_{SRBM}\|}{\|\boldsymbol{\mu}_{MCS}\|}$
ϵ_σ	$\frac{\|\boldsymbol{\sigma}_{MCS} - \boldsymbol{\sigma}_{SRBM}\|}{\|\boldsymbol{\sigma}_{MCS}\|}$
κ	Denotes the conductivity
$\langle \mathbf{uv} \rangle$	Inner product or expectation of $\mathbf{uv}$
$\mathbb{C}$	Complex line
$\mathcal{P}$	Probability measure defined on an appropriate space
$\mathcal{B}$	A boundary operator
$\mathcal{F}$	σ-algebra associated with the sample space
$\mathcal{K}$	Stochastic Krylov subspace
$\mathscr{B}$	Bilinear form
$\mathscr{L}$	Linear form
Ω	Sample space
ω	A simple event on a probability space
$\|\cdot\|$	Norm induced by the inner product on Hilbert space

$\mathbb{R}$ Real line

$\{\phi_i\}$ A set of polynomial chaos basis functions

$\{N\}$ A set of finite element shape functions

C_{uv} Covariance of u and v

D The spatial domain of definition

$H_0^1(D)$ Hilbert space consisting of functions who along with their first order partial derivatives vanish on the boundary

$L_p(\Omega)$ Let $1 \leq p \leq \infty$. Then $L_p(\Omega)$ space is the set of all measurable functions from Ω to $\mathbb{R}$ whose absolute value raised to the p^{th} power has a finite Lebesgue integral

$W_p^k(D)$ For $p \geq 1$, $W_p^k(D)$ refers to the set of all functions $u \in L_p(D)$ such that all derivatives of u of orders lesser than or equal to k belong to $L_p(D)$

$\mathbf{M}$ A deterministic preconditioner

$\mathbf{u}^*$ Complex conjugate transpose of the vector $\mathbf{u}$

Chapter 1

Introduction

1.1 Motivation

In the last two decades, modeling and simulation of highly complex problems have been made possible by tremendous growth in computing power. Sophisticated numerical techniques have also evolved to limit the discretization errors in the numerical simulations. However, some degree of uncertainty is inevitable when dealing with many engineering and natural systems. Disregarding or neglecting these variabilities, idealized (nominal) values of the parameters like boundary, loading, boundary conditions and operating conditions are often selected for modeling and simulation. In such simulations, the correlation between the numerical results and the field response (reality) remain unclear. Lack of information and intrinsic variability may be pointed out as two main reasons for the existence of input uncertainty. For example in a system undergoing diffusion, the micro-mechanical structure of the material may be variable (leading to uncertain diffusivity) or the geometry of the system may be uncertain. Also, some degree of uncertainty may be present in the operating conditions such as forcing and boundary conditions. Reliability and safety of such systems can be questionable, based on the degree of the input uncertainty especially in off-design or failure conditions. Hence a realistic modeling and simulation of complex physical systems should take input uncertainties into account to provide a reliable prognoses of the numerical solutions. This has motivated the development of advanced stochastic solvers which propagate the input uncertainty through the governing equations to obtain the response statistics thereby enabling the quantification of uncertainty in computational predictions.

1.2 Background

Various mathematical theories have been adopted to model uncertainties such as probability theory, possibility theory, evidence (Dempster-Shafer) theory, fuzzy set theory, imprecise probability theory and Bayesian estimation theory; refer to [4] for details. The present work primarily focuses on employing the probabilistic theory approach to deal with all types of uncertainties. It is implicitly assumed here that the uncertainties can be described as random variables or random fields.

Traditionally, physical systems are mathematically modeled by partial differential equations (PDEs) that govern the system response. Treating uncertainties in a probabilistic framework, leads to PDEs with random coefficients called stochastic partial differential equations or SPDEs. The SPDEs with the prescribed deterministic/stochastic initial and boundary conditions govern the system dynamics.

Numerical methods to analyze SPDEs can be broadly classified as parametric and non-parametric approaches. The central idea underpinning non-parametric approaches [5–8] is to employ the mean value of the coefficient matrix in conjunction with the maximum entropy principle to construct a random matrix model. Subsequently, the response statistics are approximated using Monte-Carlo methods. Non-parametric approaches are useful in situations where limited data is available on the uncertain parameters. However the focus of the thesis is on parametric approaches – in other words, we assume that a complete probabilistic characterization of the input uncertain parameters is available.

Figure 1.1(from [1]) lists the steps involved in analysis of uncertain systems employing parametric approaches. Uncertainty models are typically constructed using the field/experimental data or by stochastic micro-mechanical analysis and is characterized by random fields or kernel density estimates. The governing equations namely, the SPDEs in addition to the characterized uncertainty completely define the problem in question. For computational purposes where the variability is required to be expressed in terms of a finite number of random variables, random field discretization is carried out. A number of random field discretization techniques have been discussed in literature; see for example [2, 9–11]. The resulting semi-discretized SPDEs are spatially discretized using finite element, finite difference or finite volume techniques. Statistics of the response can be now computed by *propagating* the uncertainty to the response.

Many existing techniques can be adopted for *uncertainty propagation*. They can be

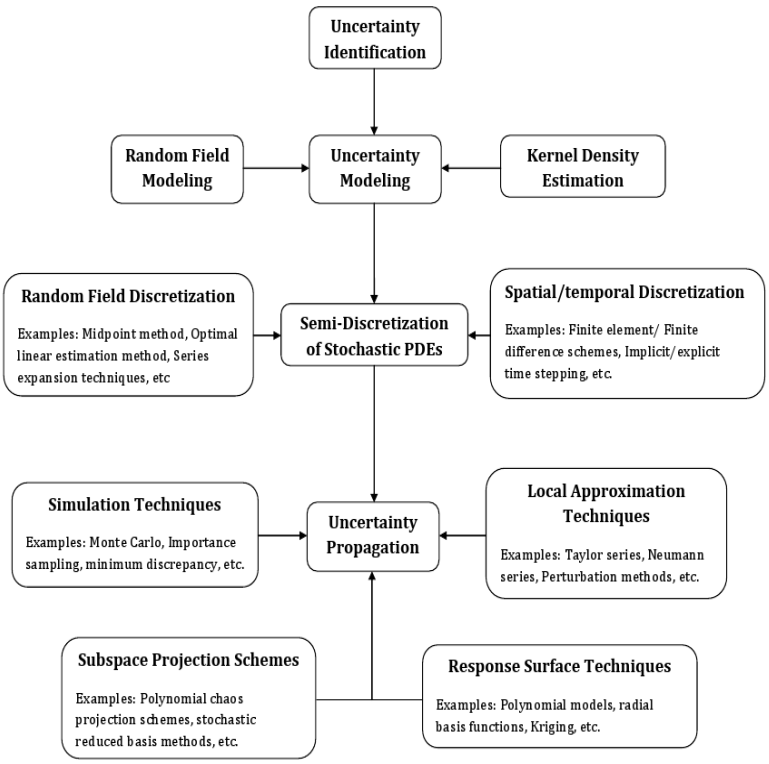

FIGURE 1.1: Physics based parametric uncertainty analysis [1].

broadly classified as simulation techniques, local approximation methods, response surface methods and spectral stochastic projection schemes. Simulation methods are very general purpose in scope and hence can be applied to a variety of problems [12]. Monte-Carlo techniques are widely used simulation methods to approximate the response statistics with an arbitrary degree of accuracy [13, 14]. In practice, however, the associated cost can be computationally prohibitive for large scale applications and high fidelity systems. More efficient alternatives based on sparse quadrature rules have been employed in [15–24]. Sparse quadrature based on Smolyak's construction have been extensively studied in the context of stochastic collocation schemes. These approaches leverage the regularity of stochastic variables in contrast to Monte-Carlo/quasi-Monte-Carlo schemes. Among the local approximation (perturbation) methods, Neumann series offer an efficient alternative to compute the first two statistical moments of the response; see [25–30] for details. The major drawback of this class of methods is that the results become highly inaccurate for large coefficient of variation of the input random variables. The response surface methods are another class of approximation techniques that are usually applied to construct linear or quadratic models of the response quantities as a function of the basic random variables; [31]. By leveraging

the existing literature on function approximations (e.g. [32] [33]), more general nonlinear models can however be constructed. However response surface methods do not scale well to problems with large number of variabilities due to *the curse of dimensionality*[1]; see for example, [34–36] and the references therein..

In recent years, stochastic projection schemes based on polynomial chaos (PC) expansions have emerged as a powerful tool to analyze stochastic systems. The fundamentals underpinning this approach is based on the homogeneous chaos theory proposed by Wiener [37] as a generalization of Fourier series expansion. In the original work of Wiener, multidimensional Hermite polynomials in terms of a set of Gaussian random variables are used as (orthogonal) basis functions for representing stochastic processes. If the undetermined constants are computed as coefficients of Fourier-Hermite expansions, such expansions converge for any second-order stochastic process in the L_2 sense by the theorem of Cameron and Martin [38]. Ghanem et al [39–44] and others [45, 46] have applied PC expansions to a wide class of stochastic PDEs. These results show that unlike perturbation-based methods, good accuracy can be attained with PC methods even when the coefficients of variation of the input random variables is large. Recently, Xiu and Karniadakis [3, 47] proposed generalized Polynomial Chaos (gPC) expansions, where basis functions from the Askey family of hypergeometric polynomials are used. It was shown that by employing appropriate basis functions depending on the input (e.g. Legendre polynomials for uniform distribution, Laguerre polynomial functions for exponential distributions, etc.), faster convergence rates can be attained compared to Hermite polynomials for non-Gaussian distributions. The method is not limited only to continuous distributions but is also applicable to discrete distributions (e.g. Charlier Polynomial functions are used in the case of Poisson's distribution). PC projection schemes present the most general and extensively applied numerical methods for uncertainty quantification and propagation. They have been employed on a wide range of steady state and transient problems ranging from deformation of elasto-plastic bodies [48], fluid flow simulations using Euler and Navier-Stokes equations [49–52], nonlinear vibrations [53] and multiphase flows in heterogeneous random media [34, 35].

Nouy et al [54–56] proposed generalized spectral decomposition (GSD) methods to solve linear and nonlinear SPDEs. GSD methods generalize the classical spectral decomposition, namely the Karhunen-Loève (KL) expansion where the solution is approximated by a series

[1]The curse of dimensionality arises from the fact that the number of hypercubes required to fill out a compact M-dimensional space grows exponentially with M.

of terms, each of which being the product of a scalar stochastic function by a deterministic function. Both these functions are not fixed *a priori* but determined by solving a problem which can be interpreted as an eigenvalue problem. Le Maître et al. [57, 58] introduced *Wiener-Haar expansions* for representing stochastic processes. It has been shown that these basis functions give more accurate representations at discontinuities compared to gPC expansions. Babuška et al. [59] studied the convergence of Galerkin finite element approximations of stochastic elliptic PDEs. A theoretical analysis was presented for the computational costs involved in the Monte-Carlo Simulations (MCS) and the Galerkin projection schemes employing a spectral representation of the solution process. This analysis suggests that for problems with a small number of random variables, the latter method is preferable especially when the accuracy requirement is high. While for problems involving a large number of variables, the Galerkin projection schemes lead to significant increase in the dimensionality of the problem resulting in computational costs comparable to that of MCS.

Stochastic Reduced Basis Methods (SRBMs) were recently introduced in the literature [60, 61] to solve linear random algebraic systems of equations arising from discretization of stochastic PDEs. In this approach, the response process is approximated using basis vectors spanning a preconditioned stochastic Krylov subspace. The Bubnov-Galerkin/Petrov-Galerkin projection scheme is used to compute the undetermined coefficients by solving a reduced order deterministic system of equations. The basis vectors in SRBMs are problem dependent – this is in contrast to gPC expansions where the basis functions are chosen solely depending on the input distribution. Numerical studies on linear stochastic PDEs conducted by Sachdeva et al. [62] suggest that SRBMs can be more accurate for a given order of expansion compared to existing PC based approaches. In addition, it has also been observed that the computational cost incurred by reduced order projection schemes is significantly lower than PC projection schemes. SRBMs are hybridized with PC expansions in [63] to deal with non-Gaussian uncertainties.

However, application of SRBMs have so far been limited to linear systems where the uncertainties arise in the coefficients of PDEs. This motivates the development of advanced stochastic projection schemes applicable to a wider class of SPDEs.

In this thesis, we primarily focus on steady-state heat transfer applications as they are a very important class of partial differential equations (PDEs) which arise from mathematical characterization of a variety of phenomena appearing in nature e.g., heat transfer, diffusion in heterogeneous media, etc. The SPDE underlying stochastic steady state heat transfer

has diverse applications in several areas such as petroleum reservoir characterization, water resources modelling, population genetics, image noise correction, etc. This problem has been studied by many researchers (see, for example [15, 16, 34–36, 64–68]) in the context of steady-state diffusion in random heterogeneous media in the past. Projection schemes based on Polynomial Chaos (PC) expansions have been employed in [64, 66, 67]. Our objective is to propose faster projection schemes to solve both linear and nonlinear variants of this SPDE which are general in scope and applicable to a wider class of problems. Note that all the simulations presented in this thesis are performed over a machine with Intel Core 2 Duo processor having a 2.4GHz clock speed and 1GB RAM.

1.3 Scope of the thesis

The main focus of this work is to develop reduced order projection schemes for complex linear (geometric uncertainty) and nonlinear uncertainty propagation problems. In our model problems, we assume input uncertainty models in order to purely focus on propagating these uncertainties through the governing PDEs. Uncertainty modeling is a very important and involved field of research but it is not the focus of this thesis.

Here we adopt probability theory for uncertainty representation as opposed to possibility theory, evidence theory, fuzzy set theory, etc. However, the applicability of reduced order basis methods is not limited to uncertainty representation employing probability theory, but is very general in scope. They can be applied to any parametrized system of equations irrespective of how the uncertainty is modeled. This is due to the reason that only the post-processing stage is dependent on the measure defined on the space underlying the random parameters.

In addition to the probability theory being employed here for uncertainty representation, it should also be noted that the probabilistic uncertainties considered in this thesis are second order stochastic processes (i.e., a finite variance) in contrast to white noise processes. A wide body of literature can be found on dealing with white noise models (see for e.g. [69, 70] in the context of diffusion in random heterogeneous media) and this topic is beyond the scope of this thesis.

The initial part of the thesis focuses on the formulation of a h-refinement strategy of SRBMs (multi-element-SRBMs (ME-SRBMs)) as compared to the regular p-refinement strategy to improve the accuracy of the single element SRBMs for a given number of basis vectors.

A theoretical result proving the convergence of an error metric employing ME-SRBMs is established. Two preconditioning strategies have been suggested. Local preconditioning results in a better approximation and hence faster convergence while global preconditioning strategy is more realistic for large scale problems with many degrees of freedom. The approach admits a very high degree of coarse-grained and fine-grained parallelizability especially in conjunction with a global preconditioning strategy. The improved accuracy of the method in comparison to the standard single element formulation is demonstrated using three numerical studies dealing with stochastic steady state elasticity on a square domain and stochastic steady state heat transfer on two domains (including a square surface and a 2D gas turbine blade model). Although, the approach focuses on uniform uncertainty, it can be easily extended to other types of distributions.

A novel computational framework employing reduced order projection schemes is presented for solving deterministic/stochastic partial differential equations defined on random domains. The central idea is to employ mesh deformation strategies in conjunction with standard finite element discretization to arrive at a system of linear random algebraic equations. We present a theoretical result on the condition that the input uncertainty model needs to satisfy to ensure the well-posedness of the problem. The method is demonstrated using steady state heat transfer on a square domain with a rough wall represented by a random field model. We also present a numerical study involving steady state heat transfer on a 2D model of a gas turbine blade where the uncertain core locations have a parametric representation. A three dimensional numerical study involving gas turbine blades with a simplified cooling core uncertainty model is also presented. The numerical techniques presented here can be readily applied to complex spatial domains. The stochastic to deterministic mesh deformation can be performed using any of the available tools such as algebraic transformations, trans-finite interpolation and PDE based methods. The proposed approach also renders the existing deterministic solvers reusable for stochastic analysis.

Finally, we present a computational approach to solve nonlinear stochastic PDEs employing SRBM expansions in combination with the Picard iteration scheme. The proposed approach is very simple to implement and can potentially result in orders of magnitude speed-up compared to simulation techniques. A theoretical result has been proved which states the existence of a stochastic fixed point for the model problem (with the uncertainty model) under consideration. It is conjectured that the method is applicable to any nonlinear SPDE where the deterministic version of the governing equations admit an unconditionally

convergent and stable solution employing deterministic fixed-point iteration scheme. Numerical studies are presented using stochastic steady state heat transfer on a square domain and in a L-shaped channel with nonlinear conductivity to showcase the effectiveness of the proposed approach. The limitations of the formulation are demonstrated using a case study involving the Burger equation motivating future work in this direction.

1.4 Layout of the thesis

This thesis is organized as follows:

Chapter 2 introduces the notation used throughout the thesis. Preliminaries such as Karhunen-Loève expansion technique for random field discretization and polynomial chaos expansion to represent a random field are covered. Spatial discretization of SPDEs employing finite element methods is outlined. Finally, stochastic projection schemes including SSFEM and SRBM are reviewed in detail.

In Chapter 3, we present a h-refinement technique to improve the accuracy of SRBMs. Two preconditioning strategies namely global and local preconditioning are discussed due to their merits such as better degree of parallelizability and faster convergence trends. We demonstrate the proposed approach on three numerical studies involving stochastic steady state elasticity on a square domain and stochastic heat transfer over two different domains.

In Chapter 4, a novel method is proposed to solve linear elliptic partial differential equations defined on random domains using SRBMs. We demonstrate two mapping strategies namely mapping in the continuum and discrete sense to map the stochastic domain onto a deterministic domain before carrying out spatial discretization. Mathematical equivalence between both the approaches is established. A condition on the input uncertainty model for the well-posedness of the problem is proposed leading to the details on the spatial discretization of the governing equations on the random domain. The effectiveness of the numerical approach is demonstrated using heat transfer on three spatial domains, namely, a square domain with a rough wall, a two-dimensional profile of a gas turbine blade where the core center locations are considered to be uncertain and finally a three-dimensional gas turbine blade model with a simplified model to represent uncertainty in the geometry. While the first numerical study involves the random field description of the boundary, the other studies have parametric representation of the randomness.

In Chapter 5, we present a numerical approach to solve nonlinear stochastic partial differ-

ential equations using reduced order projection schemes where the Picard iterative scheme has been used to linearize the governing equations. Here, we discuss in detail, the linearization and spatial discretization of the governing equations. Convergence criterion and the issues involved in the current formulation are explained. Numerical studies involving stochastic heat transfer analysis on a square plate and an L-shaped channel are presented to showcase the efficiency of the method. A case study involving the 1D Burger equation is also presented to explore the limitations of the method.

We conclude the thesis in Chapter 6 and outline future research directions.

Chapter 2

Stochastic Galerkin projection schemes

In this chapter we introduce the notation that is followed throughout the thesis. Preliminaries such as generalized polynomial chaos and Karhunen-Loève expansion are briefly discussed. Stochastic Galerkin projection schemes are reviewed and their application is illustrated for a typical SPDE arising in stochastic heat transfer.

2.1 Preliminaries

2.1.1 Notation

Let $(\Omega, \mathcal{F}, \mathcal{P})$ be a probability space, where Ω is the sample space, $\mathcal{F}$ is the σ-algebra associated with Ω and $\mathcal{P}$ is a probability measure. Let $\omega \in \Omega$ be a random event. Then any random vector $\boldsymbol{\theta}(\omega) : \Omega \rightarrow \mathbb{R}^d$ is said to be a second order stochastic process if it has a finite second order moment on $(\Omega, \mathcal{F}, \mathcal{P})$. Here d refers to the dimensionality of the vector $\boldsymbol{\theta}$. By definition, $L_2(\Omega, \mathcal{F}, \mathcal{P})$ is a Hilbert space of random variables. Let $\mathbf{u}(\boldsymbol{\theta}) \in \mathbb{C}^n$ and $\mathbf{v}(\boldsymbol{\theta}) \in \mathbb{C}^n$ be two stochastic vectors, then the expectation operator $\langle \cdot \rangle$ is defined as

$$\langle \mathbf{u}^*(\boldsymbol{\theta})\mathbf{v}(\boldsymbol{\theta}) \rangle = \int \mathbf{u}^*(\boldsymbol{\theta})\mathbf{v}(\boldsymbol{\theta}) \mathrm{d}\mathcal{P}(\boldsymbol{\theta}),$$

where $\boldsymbol{\theta}$ is a continuous random variable and the superscript * denotes the complex conjugate transpose. The norm induced by this inner product on the Hilbert space is defined as

$$\| \mathbf{u}(\boldsymbol{\theta}) \| = \sqrt{\langle \mathbf{u}^*(\boldsymbol{\theta})\mathbf{u}(\boldsymbol{\theta}) \rangle}. \tag{2.1}$$

2.1.2 Karhunen-Loève expansion

The Karhunen-Loève (KL) expansion of a random field $\kappa(x;\omega)$ is a popular method for random field discretization as the expansion is performed over an optimal basis. It is based on the spectral decomposition of the autocovariance function $C_{\kappa\kappa}(x,x')$. The set of deterministic functions over which any realization of the random field $\kappa(x;\omega)$ is expanded are defined by the integral eigenvalue problem:

$$\int_D C_{\kappa\kappa}(x,x')\varphi(x')\mathrm{d}x' = \lambda\varphi(x). \tag{2.2}$$

The above equation is a Fredholm integral equation of the second kind and the kernel of integration $C_{\kappa\kappa}$ is bounded, symmetric and positive definite as it represents an autocovariance function where λ represents the eigenvalues. Thus φ form a complete orthogonal basis on $L_2(\Omega,\mathcal{F},\mathcal{P})$. Also note that the eigen spectrum is real, positive, numerable and has zero as the only possible limit point. Hence a given random field, $\kappa(x;\omega)$, can be expanded around its mean as follows:

$$\kappa(x;\omega) = \mu(x) + \sum_{i=1}^{\infty}\sqrt{\lambda_i}\theta_i(\omega)\varphi_i(x). \tag{2.3}$$

where $\mu(x)$ is the mean of the random field and $\{\theta_i(\omega)\}$ are a set of random variables. For computational applications, the ordered series given in the above equation is truncated to a finite number of terms (d). The following are the properties of the KL expansion scheme

- ⋆ The set of random variables $\{\theta_i\}$ are orthonormal with respect to the inner product. Thus KL expansion separates the space and random variables in $\kappa(x;\omega)$.
- ⋆ The accumulation point of the eigenvalues is zero. Thus the series terms can be re-ordered in a descending order. Hence the expansion can be truncated for computational problems with finite precision machines.
- ⋆ The covariance eigenfunction basis $\{\varphi_i\}$ is optimal such that the mean square error resulting from the d^{th} order truncation is minimized.
- ⋆ KL expansion always under-represents the true variance of the random field.

Equation 2.2 has a closed form solution only for special autocovariance functions defined on simple geometries [39]. Many numerical techniques are available in literature (refer to [71, 72]) to solve the Fredholm integral equation of the second kind given by Equation 2.2. However, we numerically solve this integral eigenvalue problem based on the approximation

proposed by Keese [16]. It is a finite element discretization of KL expansion and the approximation converges uniformly in variance. But it is important to note that the eigenfunction basis so obtained is suboptimal. However, it has been shown that the approximation comes closer to the actual solution by refining the spatial discretization. Typically different spatial resolutions are used for KL expansion and uncertainty propagation. Finer resolutions are used for the random field discretization which is mapped onto a coarser resolution used for uncertainty propagation.

2.1.3 Generalized Polynomial Chaos

In this section, we first review the classical Polynomial Chaos (PC) and then introduce the concept of generalized Polynomial Chaos (gPC). The classical PC approach is based on the homogeneous chaos theory proposed by Wiener [37] as a generalization of Fourier series expansion. PC basis defined on $L_2(\Omega, \mathcal{F}, \mathcal{P})$ is based on Hermite polynomials of standard normal random variables. These polynomials can be written as:

$$h_n(x) = (-1)^n \frac{d^n \left[e^{-\frac{1}{2}x^2}\right]}{dx^n} e^{\frac{1}{2}x^2}.$$

Hermite polynomials of independent standard normal random variables are orthogonal to each other with respect to the inner product defined in Equation 2.1 implying:

$$\langle h_m(\theta_i(\omega)) h_n(\theta_j(\omega)) \rangle = 0, \quad \forall m \neq n.$$

In the original work of Wiener, multi-dimensional Hermite polynomials in terms of a set of independent standard normal random variables are used as (orthogonal) basis functions for representing stochastic processes. Their construction is as follows: Consider the following integer sequences:

$$\begin{aligned} \boldsymbol{\beta} &= \{\beta_1, \beta_2, \cdots, \beta_p\}, \quad \forall\ \beta_j \geq 0, \\ \mathbf{i} &= \{i_1, i_2, \cdots, i_p\}, \quad \forall\ i_j > 0. \end{aligned}$$

The multi-dimensional Hermite polynomial associated with the tuple of sequences $(\mathbf{i}, \boldsymbol{\beta})$ is:

$$\boldsymbol{\Psi}_{\mathbf{i},\boldsymbol{\beta}}(\omega) = \prod_{k=1}^{p} h_{\beta_k}(\theta_{i_k}(\omega)). \tag{2.4}$$

The set of all polynomials $\{\boldsymbol{\Psi}_{\mathbf{i},\boldsymbol{\beta}}(\omega)\}$ associated with all possible sequences $(\mathbf{i}, \boldsymbol{\beta})$ of any length p forms a basis of $L_2(\Omega, \mathcal{F}, \mathcal{P})$. Let

$$\Gamma_p(\theta_{i_1}, \theta_{i_2}, \cdots, \theta_{i_p}) = \Big\{ \boldsymbol{\Psi}_{\mathbf{i},\boldsymbol{\beta}} \ \Big| \ \sum_{k=1}^{p} \beta_k = p \Big\}.$$

The space spanned by $\{\Gamma_p\}$ is a subspace of $L_2(\Omega, \mathcal{F}, \mathcal{P})$ and is called homogeneous chaos of order p. Homogeneous chaoses of order p and q where $p \neq q$ can be proved to be orthogonal on $L_2(\Omega, \mathcal{F}, \mathcal{P})$ giving rise to Wiener decomposition, as

$$\bigoplus_{k=0}^{\infty} \Gamma_k = L_2(\Omega, \mathcal{F}, \mathcal{P}), \tag{2.5}$$

where $\bigoplus$ denotes inner sum of orthogonal subspaces. Due to the completeness property of polynomial chaos, Γ_0 equals unity, as a result of which the following properties hold for PC functions:

$$\begin{aligned} \langle \Gamma_i \rangle &= 0, \quad \forall\, i > 0, \\ \langle \Gamma_i \;\; \Gamma_j \rangle &= 0, \quad \forall\, i \neq j, \end{aligned}$$

in addition to:

$$\Gamma_0 = 1.$$

For computational purposes, a finite dimensional PC is constructed in terms of a finite number (d) of orthonormal Gaussian random variables. Karhunen-Loève expansion of the input random field provides us with such a finite number of random variables. The finite dimensional PC so constructed is called a *homogeneous chaos of dimension d and order p*. The construction of a finite dimensional PC is as follows: Let $\boldsymbol{\beta} = \{\beta_1, \beta_2, \beta_3, \cdots, \beta_d\}$ be a set of integers such that $0 \leq \beta_k \leq p$ and $\sum_{k=1}^{d} \beta_k \leq p$. Then by Equation 2.4, the basis function can be defined as follows:

$$\phi_{\boldsymbol{\beta}} = \prod_{i=1}^{d} h_{\beta_i}(\theta_i). \tag{2.6}$$

The lower dimensional (up to order $p = 4$) PC for up to $d = 4$ have been tabulated by Ghanem and Spanos [39] which is shown in Table 2.1

The total number of basis polynomials P in a d-dimensional p^{th} order basis is given by:

$$P = \sum_{k=0}^{p} \binom{d+k-1}{k}.$$

Table 2.2 shows the number of basis functions P for a desired order p and dimensions d.

The finite dimensional PC basis have the following properties

$$\begin{aligned} \phi_0 &= 1, \\ \langle \phi_i \rangle &= 0, \quad \forall 1 \leq i \leq P, \\ \langle \phi_i \phi_j \rangle &= 0, \quad \forall i \neq j. \end{aligned}$$

TABLE 2.1: Two-dimensional Hermite polynomial chaos basis functions [2]

j	p	j$^{\text{th}}$ basis polynomial ϕ_j
0	$p=0$	1
1	$p=1$	θ_1
2		θ_2
3	$p=2$	θ_1^2-1
4		$\theta_1\theta_2$
5		θ_2^2-1
6	$p=3$	$\theta_1^3-3\theta_1$
7		$\theta_2\big(\theta_1^2-1\big)$
8		$\theta_1\big(\theta_2^2-1\big)$
9		$\theta_2^3-3\theta_2$
10	$p=4$	$\theta_1^4-6\theta_1^2+3$
11		$\theta_2\big(\theta_1^3-3\theta_1\big)$
12		$\big(\theta_1^2-1\big)\big(\theta_2^2-1\big)$
13		$\theta_1\big(\theta_2^3-3\theta_2\big)$
14		$\theta_2^4-6\theta_2^2+3$

TABLE 2.2: Number of basis polynomials P for d-dimensional p^{th} order expansion [2]

d	$p=1$	$p=2$	$p=3$	$p=4$
2	3	6	10	15
4	5	15	35	70
6	7	28	83	210

As a consequence of the above construction of a finite dimensional polynomial chaos basis, any second order stochastic process, $u(\boldsymbol{\theta})$ can be written as:

$$u(\boldsymbol{\theta}) = \sum_{i=0}^{P} \alpha_i \phi_i(\boldsymbol{\theta}).$$

In the equation above, if the undetermined constants $\{\alpha_i\}$ are computed as coefficients of Fourier-Hermite expansions, such expansions converge for any second-order stochastic process in the L_2 sense by the theorem of Cameron and Martin [38]. Although convergence is guaranteed in the random space for any type of uncertainty, the rates of convergence are

TABLE 2.3: Orthogonal polynomials and their support spaces for different types of random variables [3]

	Random variables ($\boldsymbol{\theta}$)	Orthogonal polynomials (ϕ_n)	Support region
Continuous	Gaussian	Hermite	$(-\infty, \infty)$
	Gamma	Laguerre	$[0, \infty)$
	Beta	Jacobi	$[a, b]$
	Uniform	Legendre	$[a, b]$
Discrete	Poisson	Charlier	$\{0, 1, 2, \cdots\}$
	Binomial	Krawtchouk	$\{0, 1, 2, \cdots, N\}$
	Negative Binomial	Meixner	$\{0, 1, 2, \cdots\}$
	Hypergeometric	Hahn	$\{0, 1, 2, \cdots, N\}$

optimal only for the case of Gaussian random variables and near Gaussian random fields. A more general framework called *generalized polynomial chaos* based on Askey chaos was proposed by Karniadakis et al [47] for optimal convergence of other types of uncertainties. In this method, the polynomials are chosen from hypergeometric polynomials of the Askey scheme and are not restricted to Gaussian random variables. The type of the random variables are chosen according to the stochastic input and the weighting function of these random variables determine the type of orthogonal polynomials to be used as the basis in the random space. Table 2.3 shows the class of polynomials corresponding to the type of the random variables exhibiting optimal convergence.

2.2 Discretization of SPDEs

Here, we discuss the steps involved in discretization of SPDEs using the steady state linear stochastic heat equation given below as an example:

$$\left.\begin{aligned} \nabla \cdot [\kappa(x;\omega)\nabla u(x;\omega)] &= f(x;\omega) \qquad (x;\omega) \in D \times \Omega \\ \mathcal{B}u(x;\omega) &= g(x;\omega) \qquad (x;\omega) \in \partial D \times \Omega \end{aligned}\right\}, \tag{2.7}$$

where $\kappa(x;\omega)$[1], $f(x;\omega)$ are random fields defined on $D \times \Omega$ while $g(x;\omega)$ is a random field defined on $\partial D \times \Omega$. D and ∂D denote the physical domain and its boundary, respectively. $\mathcal{B}$ is an operator indicating the type of boundary conditions, e.g., Dirichlet, Neumann, Robin

[1]The random field $\kappa(x;\omega)$ is considered to be independent of the solution process.

or mixed boundary conditions. $u(x;\omega) : D \times \Omega \to \mathbb{R}$ is the solution process whose statistics are of practical interest. Consider the Cartesian product space $H = H_0^1(D) \times L_2(\Omega)$ with the inner product defined as:

$$(v, w)_H = \left\langle \int_D \nabla v \cdot \nabla w \, \mathrm{d}x \right\rangle.$$

Now we seek a solution $u \in H$ such that the bilinear form is equal to the linear form, i.e.

$$\mathscr{B}(u, v) = \mathscr{L}(v), \ \forall v \in H, \tag{2.8}$$

where $\mathscr{B}(u, v)$, the bilinear form is given by

$$\mathscr{B}(u, v) = \left\langle \int_D \kappa \nabla u \cdot \nabla v \, \mathrm{d}x \right\rangle,$$

and the linear form $\mathscr{L}$ is

$$\mathscr{L}(v) = \left\langle \int_D f v \, \mathrm{d}x \right\rangle,$$

$\forall u, v \in H$. We know that the variational formulation represented by Equation 2.8 has a unique solution in H almost everywhere as a consequence of the Lax-Milgram lemma [73] since the bilinear form $\mathscr{B}$ is coercive and continuous provided the conductivity $\kappa(x;\omega)$ is bounded, i.e., $0 < \kappa_{min} \leq \kappa(x;\omega) \leq \kappa_{max} < \infty$.

The conductivity, $\kappa(x;\omega)$ needs to be represented by a finite set of random variables in order to apply spatial discretization techniques namely finite element method, finite difference method, finite volume method, etc. A number of random field discretization techniques are available in the literature including the mid-point method, shape function method, optimal linear estimation, weighted integral methods, orthogonal series expansion and Karhunen-Loève expansion; see, for example, [2, 10, 11] and Section 2.1.2. Random field discretization of $\kappa(x;\omega)$ followed by truncation, using any of the afore-mentioned techniques result in a series expansion in terms of a finite set of uncorrelated random variables $\{\theta_1(\omega), \theta_2(\omega), \cdots, \theta_d(\omega)\}$ and basis functions $\{\varphi_1(x), \varphi_2(x), \cdots, \varphi_d(x)\}$ of the form:

$$\kappa(x;\omega) = \mu(x) + \sum_{i=1}^{d} \theta_i(\omega)\varphi_i(x). \tag{2.9}$$

This sets the stage for the spatial discretization of the SPDE which is performed employing finite element framework. The starting point for the finite element analysis is the weak form of the governing equations. This is obtained by multiplying the governing equation by a test function and integrating by parts; a detailed overview can be be found in [74]. The domain is subsequently divided into a number of elements and the field variables are approximated over

each finite element using a set of shape functions $\mathbf{N}^e(x)$. Substituting the approximations into the weak form, we arrive at the expression for the element stiffness matrix as:

$$\mathbf{K}^e(\omega) = \int_{D^e} \big(\nabla \mathbf{N}^e(x)\big)\kappa(x;\omega)\big(\nabla \mathbf{N}^e(x)\big)^{\mathrm{T}}\mathrm{d}x,$$

where D^e is a typical element.

When the conductivity is a Gaussian random field, then the preceding equation after substitution of the discretized random field $\kappa(x;\omega)$ in Equation 2.9 is given as:

$$\mathbf{K}^e(\boldsymbol{\theta}) = \mathbf{K}_0^e + \sum_{i=1}^{d} \mathbf{K}_i^e \theta_i,$$

where

$$\mathbf{K}_0^e = \int_{D^e} \big(\nabla \mathbf{N}^e(x)\big)\mu(x)\big(\nabla \mathbf{N}^e(x)\big)^{\mathrm{T}}\mathrm{d}x,$$

and

$$\mathbf{K}_i^e = \int_{D^e} \big(\nabla \mathbf{N}^e(x)\big)\varphi_i(x)\big(\nabla \mathbf{N}^e(x)\big)^{\mathrm{T}}\mathrm{d}x.$$

The discretized stochastic conductivity has a more general expression of the form:

$$\kappa(x;\omega) = \mu(x) + \sum_{i=1}^{P} \kappa_i(x)\phi_i(\boldsymbol{\theta}(\omega)), \tag{2.10}$$

for non-Gaussian random field models [2] following which the element stiffness and force matrices can be expressed in general form given as:

$$\begin{aligned} \mathbf{K}^e(\boldsymbol{\theta}) &= \sum_{i=0}^{P} \mathbf{K}_i^e \phi_i(\boldsymbol{\theta}), \\ \mathbf{f}^e(\boldsymbol{\theta}) &= \sum_{i=0}^{P} \mathbf{f}_i^e \phi_i(\boldsymbol{\theta}), \end{aligned} \tag{2.11}$$

for any form of uncertainties for κ, f and g. Here $\{\phi_0, \phi_1, \cdots, \phi_P\}$ is the PC basis for the space of random variables on $L_2(\Omega, \mathcal{F}, \mathcal{P})$.

Notes:

- ⋆ Here $\boldsymbol{\theta}$ denotes the vector of uncorrelated random variables arising from KL expansion of the random fields κ, f and g[‡] .

[2] e.g. lognormal random fields. The reader is referred to Appendix B for a detailed description of the discretization of lognormal random fields.

[‡] Strictly speaking, the random variables appearing in Equation 2.11 for $\mathbf{K}^e(\boldsymbol{\theta})$ are those arising from Karhunen-Loève expansion of $\kappa(x,\omega)$ alone. However, we group together all random variables arising from random field discretizations of κ, f and g in a single vector for notational convenience.

- ⋆ For simplicity of notation and improving the clarity of the presentation, we shall henceforth assume that κ, f and g are statistically independent.

- ⋆ Note that the above representation Equation 2.11 in a Hermite PC basis is optimal only when $f(x,\omega)$ is a Gaussian random field. For more general distributions, a specially constructed set of orthogonal polynomials may be necessary to ensure optimal convergence [75].

- ⋆ Similar element matrices arise in the case of geometric uncertainty and stochastic nonlinear problems. These expressions are revisited in Chapter 4 and Chapter 5.

Assembly of the element matrices and application of the specified boundary conditions result in the following global linear stochastic system of equations:

$$\mathbf{K}(\boldsymbol{\theta})\mathbf{u}(\boldsymbol{\theta}) = \mathbf{f}(\boldsymbol{\theta}), \tag{2.12}$$

where $\mathbf{K}(\boldsymbol{\theta}) \in \mathbb{R}^{n\times n}$ and $\mathbf{f}(\boldsymbol{\theta}) \in \mathbb{R}^n$, n being the number of degrees of freedom. When the conductivity is Gaussian, these terms are of the following form:

$$\begin{aligned} \mathbf{K}(\boldsymbol{\theta}) &= \mathbf{K}_0 + \sum_{i=1}^{d} \mathbf{K}_i \theta_i, \\ \mathbf{f}(\boldsymbol{\theta}) &= \mathbf{f}_0 + \sum_{i=1}^{d} \mathbf{f}_i \theta_i. \end{aligned} \tag{2.13}$$

For the more general case of uncertainty such as non-Gaussian conductivity or geometric uncertainty (these expressions are revisited in Chapter 4), $\mathbf{K}(\boldsymbol{\theta})$ and $\mathbf{f}(\boldsymbol{\theta})$ can be written as:

$$\begin{aligned} \mathbf{K}(\boldsymbol{\theta}) &= \sum_{i=0}^{P_1} \mathbf{K}_i \phi_i(\boldsymbol{\theta}), \\ \mathbf{f}(\boldsymbol{\theta}) &= \sum_{i=0}^{P_1} \mathbf{f}_i \phi_i(\boldsymbol{\theta}), \end{aligned} \tag{2.14}$$

in terms of a PC basis $\{\phi_i\}_{i=0}^{P}$ on $L_2(\Omega, \mathcal{F}, \mathcal{P})$ space.

2.3 The Spectral Stochastic Finite Element Method

The SSFEM is a spectral technique to solve SPDEs employing basis functions from Hermite polynomial chaos. This method was initially proposed by Ghanem and Spanos [39] but a general framework of basis functionals has been proposed by Xiu and Karniadakis [47]. In this section, we discuss the various steps involved in solving a linear stochastic system of equations (Equation 2.12) obtained as a result of discretization of SPDEs.

Given a stochastic system of equations of the form Equation 2.12, the response process is expanded using a gPC basis as follows:

$$\mathbf{u}(\boldsymbol{\theta}) = \sum_{i=0}^{P} \mathbf{u}_i \phi_i.$$

The general expression of the residual error $\boldsymbol{\epsilon}$ due to this approximation is of the form:

$$\boldsymbol{\epsilon} = \Big(\mathbf{K}(\boldsymbol{\theta})\Big)\left(\sum_{j=0}^{P} \mathbf{u}_j \phi_j\right) - \Big(\mathbf{f}(\boldsymbol{\theta})\Big).$$

The unknown coefficients $\mathbf{u}_i$ are obtained by employing an orthogonal projection of the residual onto the PC basis in the Hilbert space $L_2(\Omega, \mathcal{F}, \mathcal{P})$. This projection can be expressed as:

$$\langle \boldsymbol{\epsilon} \phi_k \rangle = 0, \quad \forall\ 0 \leq k \leq P.$$

Equivalently:

$$\sum_{i=0}^{P} \mathbf{u}_j \langle \mathbf{K}(\boldsymbol{\theta}) \phi_j \phi_k \rangle - \langle \mathbf{f}(\boldsymbol{\theta}) \phi_k \rangle = 0, \quad \forall 0 \leq k \leq P. \tag{2.15}$$

The above equation can be easily computed for a given expansion of the random matrices. For the case of Gaussian input uncertainty where $\mathbf{K}(\boldsymbol{\theta}) = \mathbf{K}_0 + \sum_{i=1}^{d} \mathbf{K}_i \theta_i$ and $\mathbf{f}(\boldsymbol{\theta}) = \mathbf{f}_0 + \sum_{i=1}^{d} \mathbf{f}_i \theta_i$, the LHS in Equation 2.15 can be written as $\mathbf{K}_0 \mathbf{u}_k \langle \phi_k^2 \rangle + \sum_{i=1}^{d} \sum_{j=0}^{P} \mathbf{K}_i \mathbf{u}_j \langle \theta_i \phi_j \phi_k \rangle - \sum_{i=1}^{d} \mathbf{f}_i \langle \theta_i \phi_k \rangle,\ \forall 0 \leq k \leq P$. In general when the input uncertainty is non-Gaussian, nonlinear or the geometry is uncertain, $\mathbf{K}(\boldsymbol{\theta})$ and $\mathbf{f}(\boldsymbol{\theta})$ take a more general form given in (2.14). Then the LHS in Equation 2.15 can be written as $\sum_{i=0}^{P_1} \sum_{j=0}^{P} \mathbf{K}_i \mathbf{u}_j \langle \phi_i \phi_j \phi_k \rangle - \sum_{i=0}^{P_1} \mathbf{f}_i \langle \phi_i \phi_k \rangle,\ \forall 0 \leq k \leq P$.

Equation 2.15 represents $(P+1)$ system of equations in $(P+1)$ unknown vectors, namely, $\{\mathbf{u}_0, \mathbf{u}_1, \cdots, \mathbf{u}_P\}$. Note that there are a total of $n(P+1)$ number of unknowns for n degrees of freedom. From Tables 2.1 and 2.2, it can be seen that the number of basis functions $P+1$ grow rapidly with increase in dimensionality of $\boldsymbol{\theta}$. Hence SSFEM involves large computational costs for high dimensional applications. This motivated the development of advanced stochastic solvers which result in a reduced order system of equations.

2.4 Stochastic Reduced Basis Methods

Stochastic Reduced Basis Methods [60, 61] are another class of subspace projection schemes which are provably convergent and efficient for high dimensional problems compared to PC based methods.

Instead of a PC basis, SRBMs approximate the response process of the stochastic system of equations 2.12 using basis vectors spanning the stochastic Krylov subspace defined as

$$\mathcal{K}_N\left(\mathbf{K}(\boldsymbol{\theta}), \mathbf{f}(\boldsymbol{\theta})\right) = \text{span}\left\{\mathbf{f}(\boldsymbol{\theta}), \mathbf{K}(\boldsymbol{\theta})\mathbf{f}(\boldsymbol{\theta}), (\mathbf{K}(\boldsymbol{\theta}))^2\mathbf{f}(\boldsymbol{\theta}), \cdots, (\mathbf{K}(\boldsymbol{\theta}))^{N-1}\mathbf{f}(\boldsymbol{\theta})\right\}.$$

Note that the basis vectors in SRBMs are problem dependent – this is in contrast to gPC expansions where the basis functions are chosen solely depending on the input distribution. We now state an important theorem from [61] which proves the existence of the solution of Equation 2.12 in the stochastic Krylov subspace

Definition: For a random matrix, the minimal polynominal q can be defined as the unique monic random polynomial of smallest degree such that $q(\mathbf{K}(\boldsymbol{\theta}), \boldsymbol{\theta}) = 0$.

Theorem 1. *If the minimal random polynomial of a nonsingular random square matrix* $\mathbf{K}(\boldsymbol{\theta})$ *has a degree* N*, then the solution of the random algebraic system of equations* $\mathbf{K}(\boldsymbol{\theta})\mathbf{u}(\boldsymbol{\theta}) = \mathbf{f}(\boldsymbol{\theta})$ *lies in the stochastic Krylov subspace* $\mathcal{K}_N(\mathbf{K}(\boldsymbol{\theta}), \mathbf{f}(\boldsymbol{\theta}))$*. Thus a stochastic reduced basis representation of the solution process* $\mathbf{u}(\boldsymbol{\theta})$ *can be written as*

$$\mathbf{u}(\boldsymbol{\theta}) = \alpha_0\boldsymbol{\psi}_0(\boldsymbol{\theta}) + \alpha_1\boldsymbol{\psi}_1(\boldsymbol{\theta}) + \cdots + \alpha_{N-1}\boldsymbol{\psi}_{N-1}(\boldsymbol{\theta}) = \boldsymbol{\Psi}(\boldsymbol{\theta})\boldsymbol{\alpha},$$

where $\{\boldsymbol{\psi}_i\}_{i=0}^{N-1}$ *are the basis vectors spanning* $\mathcal{K}_N(\mathbf{K}(\boldsymbol{\theta}), \mathbf{f}(\boldsymbol{\theta}))$*.*

For large scale problems (with large n), the order of the minimal random polynomial may be comparable to n. To address this issue, we solve the random algebraic system of equations using a preconditioned stochastic Krylov subspace. A deterministic matrix $\mathbf{M}$ is called a *preconditioner* of a stochastic matrix $\mathbf{K}(\boldsymbol{\theta})$, if the order of the minimal random polynomial of the transformed stochastic matrix $\mathbf{MK}(\boldsymbol{\theta})$ is lower than that of the original matrix $\mathbf{K}(\boldsymbol{\theta})$. Hence, we observe accelerated convergence rates with basis vectors spanning a preconditioned stochastic Krylov subspace which in turn is defined as

$$\mathcal{K}_N\left(\mathbf{MK}(\boldsymbol{\theta}), \mathbf{Mf}(\boldsymbol{\theta})\right) = \text{span}\left\{\boldsymbol{\psi}_0(\boldsymbol{\theta}), \boldsymbol{\psi}_1(\boldsymbol{\theta}), \boldsymbol{\psi}_2(\boldsymbol{\theta}), \cdots, \boldsymbol{\psi}_{N-1}(\boldsymbol{\theta})\right\},$$

where the stochastic basis vectors $\{\boldsymbol{\psi}_i\}$ can be recursively computed as follows

$$\left.\begin{aligned} \boldsymbol{\psi}_0(\boldsymbol{\theta}) &= \mathbf{Mf}(\boldsymbol{\theta}) \\ \boldsymbol{\psi}_1(\boldsymbol{\theta}) &= \mathbf{MK}(\boldsymbol{\theta})\boldsymbol{\psi}_0(\boldsymbol{\theta}) \\ \boldsymbol{\psi}_2(\boldsymbol{\theta}) &= \mathbf{MK}(\boldsymbol{\theta})\boldsymbol{\psi}_1(\boldsymbol{\theta}) \\ &\vdots \\ \boldsymbol{\psi}_{N-1}(\boldsymbol{\theta}) &= \mathbf{MK}(\boldsymbol{\theta})\boldsymbol{\psi}_{N-2}(\boldsymbol{\theta}) \end{aligned}\right\}. \tag{2.16}$$

In theory, convergence can be guaranteed as long as the preconditioner $\mathbf{M}$ is invertible. In [60, 61], the deterministic matrix $\langle \mathbf{K}(\boldsymbol{\theta}) \rangle^{-1}$ is selected as the preconditioner. For a detailed exposition on the theoretical and computational aspects of SRBMs, see Nair [76].

The residual error $\boldsymbol{\epsilon}(\boldsymbol{\theta})$ due to the truncated reduced basis is:

$$\boldsymbol{\epsilon}(\boldsymbol{\theta}) = \left(\mathbf{K}(\boldsymbol{\theta}) \right) \left(\sum_{i=0}^{N-1} \alpha_i \boldsymbol{\psi}_i(\boldsymbol{\theta}) \right) - \left(\mathbf{f}(\boldsymbol{\theta}) \right).$$

This error can be minimized in a mean square sense by applying a Galerkin projection which in the Hilbert space $L_2(\Omega, \mathcal{F}, \mathcal{P})$ is equivalent to the residual being an orthogonal projection of the space spanned by preconditioned stochastic Krylov subspace i.e.,

$$\langle \boldsymbol{\psi}_k^T(\boldsymbol{\theta}) \boldsymbol{\epsilon}(\boldsymbol{\theta}) \rangle = 0, \ \forall 0 \leq k \leq N-1, \tag{2.17}$$

or equivalently:

$$\sum_{i=0}^{N-1} \alpha_i \langle \boldsymbol{\psi}_k^T(\boldsymbol{\theta}) \mathbf{K}(\boldsymbol{\theta}) \boldsymbol{\psi}_i(\boldsymbol{\theta}) \rangle - \langle \boldsymbol{\psi}_k^T(\boldsymbol{\theta}) \mathbf{f}(\boldsymbol{\theta}) \rangle = 0, \ \forall 0 \leq k \leq N-1. \tag{2.18}$$

The orthogonality condition imposed in equations Equation 2.17 and Equation 2.18 is called a Bubnov-Galerkin projection scheme. Alternatively, the undetermined coefficients in SRBMs can be derived by employing an oblique projection scheme called, the Petrov-Galerkin scheme that essentially enforces the condition that the stochastic residual error vector is orthogonal to the subspace $\mathbf{K}(\boldsymbol{\theta}) \boldsymbol{\psi}_k(\boldsymbol{\theta})$ [61, 76] i.e.,

$$\langle \boldsymbol{\psi}_k^T(\boldsymbol{\theta}) \mathbf{K}^T(\boldsymbol{\theta}) \boldsymbol{\epsilon}(\boldsymbol{\theta}) \rangle = 0, \ \forall 0 \leq k \leq N-1, \tag{2.19}$$

which implies:

$$\sum_{i=0}^{N-1} \alpha_i \langle \boldsymbol{\psi}_k^T(\boldsymbol{\theta}) \mathbf{K}^T(\boldsymbol{\theta}) \mathbf{K}(\boldsymbol{\theta}) \boldsymbol{\psi}_i \rangle - \langle \boldsymbol{\psi}_k^T(\boldsymbol{\theta}) \mathbf{K}^T(\boldsymbol{\theta}) \mathbf{f} \rangle = 0, \ \forall 0 \leq k \leq N-1, \tag{2.20}$$

From Equation 2.17, Equation 2.18, Equation 2.19 and Equation 2.20 one can infer that SRBMs lead to a reduced order $N \times N$ system of equations after Galerkin projection. The order of the equations reduced dramatically when compared to SSFEM.

The Galerkin condition imposed in the afore-mentioned equations is said to be imposed in a *weak* sense as only the ensemble average of the random functions $\boldsymbol{\psi}_k^T(\boldsymbol{\theta}) \boldsymbol{\epsilon}(\boldsymbol{\theta})$ are set to zero. If the orthogonality condition is imposed for *each realization of the random variable* $\boldsymbol{\theta}$, then the projection scheme is called a *strong Galerkin* scheme [76].

The reduced order system of equations Equation 2.18, Equation 2.20 can be simplified by having a PC representation of $\mathbf{K}(\boldsymbol{\theta}), \mathbf{f}(\boldsymbol{\theta})$ and $\boldsymbol{\psi}_k(\boldsymbol{\theta})$ the details of which are covered in section 2.5.

The following result from [61] gives the error norm that is minimized by SRBMs employing the Bubnov-Galerkin projection scheme to compute the undetermined coefficients. This result is later invoked in the context of ME-SRBMs.

Theorem 2. *Let* $\widehat{\mathbf{u}}(\boldsymbol{\theta}) = \boldsymbol{\Psi}(\boldsymbol{\theta})\boldsymbol{\alpha}$ *be a reduced order basis approximation of* $\mathbf{K}(\boldsymbol{\theta})\mathbf{u}(\boldsymbol{\theta}) = \mathbf{f}(\boldsymbol{\theta})$ *in terms of* N *basis vectors. Here* $\mathbf{K}(\boldsymbol{\theta}) \in \mathbb{R}^{n\times n}$ *is a symmetric positive definite matrix,* $\mathbf{u}(\boldsymbol{\theta}), \mathbf{f}(\boldsymbol{\theta}) \in \mathbb{R}^n$ *are random vectors,* $\boldsymbol{\Psi}(\boldsymbol{\theta}) \in \mathbb{R}^{n\times N}$ *is a matrix of stochastic basis vectors and* $\boldsymbol{\alpha} \in \mathbb{R}^N$ *is a vector of undetermined coefficients. If the coefficient vector* $\boldsymbol{\alpha}$ *is computed by imposing the Bubnov-Galerkin condition* $\mathbf{K}(\boldsymbol{\theta})\boldsymbol{\Psi}(\boldsymbol{\theta})\boldsymbol{\alpha} - \mathbf{f}(\boldsymbol{\theta}) \perp \boldsymbol{\Psi}(\boldsymbol{\theta})$ *which in turn implies that* $\left\langle \boldsymbol{\Psi}^T(\boldsymbol{\theta})\{\mathbf{K}(\boldsymbol{\theta})\boldsymbol{\Psi}(\boldsymbol{\theta})\boldsymbol{\alpha} - \mathbf{f}(\boldsymbol{\theta})\}\right\rangle = 0$*, then the* $\mathbf{K}$*-norm of the error defined as*

$$\Delta_N = \langle\{\mathbf{u}(\boldsymbol{\theta}) - \widehat{\mathbf{u}}(\boldsymbol{\theta})\}^T\mathbf{K}(\boldsymbol{\theta})\{\mathbf{u}(\boldsymbol{\theta}) - \widehat{\mathbf{u}}(\boldsymbol{\theta})\}\rangle$$

is minimized.

We present generalized SRBMs to deal with more general forms of uncertainty namely the log-normal random fields (refer to Appendix B for details), geometric uncertainty (Chapter 4) and nonlinear SPDEs (Chapter 5). Generalized SRBMs also simplify the implementation aspects of SRBMs.

2.5 Generalized stochastic reduced basis methods

In the previous section, SRBMs were employed to solve a linear random algebraic system of equations of the form Equation 2.12 where $\mathbf{K}(\boldsymbol{\theta})$ and $\mathbf{f}(\boldsymbol{\theta})$ are given by Equation 2.13. However for a non-Gaussian uncertainty, geometric uncertainty and nonlinearities the coefficient matrices take a more general form given by Equation 2.14. Generalized SRBMs were developed [63] to deal with the aforementioned uncertainties. In addition, hybridization of SRBM and PC approaches simplifies the implementation of the reduced order basis methods. In this scheme, we expand the basis vectors $\{\boldsymbol{\psi}_0(\boldsymbol{\theta}), \boldsymbol{\psi}_1(\boldsymbol{\theta}), \cdots, \boldsymbol{\psi}_{N-1}(\boldsymbol{\theta})\}$ in a PC basis as they are second-order stochastic processes and hence admit mean-square convergent representation in a PC basis. In other words, the basis vector $\boldsymbol{\psi}_p(\boldsymbol{\theta})$ for any $p \geq 0$ is approximated as follows:

$$\boldsymbol{\psi}_p(\boldsymbol{\theta}) \approx \widehat{\boldsymbol{\psi}}_p(\boldsymbol{\theta}) = \sum_{i=0}^{P_p} \boldsymbol{\psi}_i^p \phi_i(\boldsymbol{\theta}). \tag{2.21}$$

Using Equation 2.14, the PC expansion coefficients of $\boldsymbol{\psi}_0(\boldsymbol{\theta}) = \mathbf{M}\mathbf{f}(\boldsymbol{\theta})$ can be written as:

$$\begin{aligned} \boldsymbol{\psi}_k^0 &= \mathbf{M}\mathbf{f}_k, \quad \forall\ 0 \leq k \leq P, \\ &= 0, \qquad k > P. \end{aligned}$$

From Equation 2.16, recall that $\boldsymbol{\psi}_{p+1}(\boldsymbol{\theta})$ can be written in terms of $\boldsymbol{\psi}_p(\boldsymbol{\theta})$ as follows:

$$\begin{aligned}\boldsymbol{\psi}_{p+1}(\boldsymbol{\theta}) &= \mathbf{MK}(\boldsymbol{\theta})\boldsymbol{\psi}_p(\boldsymbol{\theta}) \\ &\approx \sum_{i=0}^{P}\sum_{j=0}^{P_p}\mathbf{MK}_i\boldsymbol{\psi}_j^p\phi_i\phi_j \\ &\approx \sum_{k=0}^{P_{p+1}}\boldsymbol{\psi}_k^{p+1}\phi_k.\end{aligned} \tag{2.22}$$

The unknown coefficients in the PC expansion of $\boldsymbol{\psi}_{p+1}(\boldsymbol{\theta})$, namely $\boldsymbol{\psi}_k^{p+1}$ can be obtained by projecting them onto the PC basis as follows:

$$\boldsymbol{\psi}_k^{p+1} = \frac{\sum_{i=0}^{P}\sum_{j=0}^{P_p}\mathbf{MK}_i\boldsymbol{\psi}_j^p\langle\phi_i\phi_j\phi_k\rangle}{\langle\phi_k^2\rangle}, \forall\ 0 \leq k \leq P_{p+1}\ .$$

Due to the PC expansion of each basis vector, the set of basis vectors that approximately span the preconditioned stochastic Krylov subspace $\widehat{\boldsymbol{\Psi}}(\boldsymbol{\theta}) = \{\widehat{\boldsymbol{\psi}}_0(\boldsymbol{\theta}), \widehat{\boldsymbol{\psi}}_1(\boldsymbol{\theta}), \widehat{\boldsymbol{\psi}}_2(\boldsymbol{\theta}), \cdots, \widehat{\boldsymbol{\psi}}_{N-1}(\boldsymbol{\theta})\}$ can be compactly rewritten in matrix notation as follows

$$\widehat{\boldsymbol{\Psi}}(\boldsymbol{\theta}) = \sum_{i=0}^{P_2}\boldsymbol{\Gamma}_i\phi_i, \tag{2.23}$$

where $\boldsymbol{\Gamma}_i = \left[\boldsymbol{\psi}_i^0, \boldsymbol{\psi}_i^1, \boldsymbol{\psi}_i^2, \cdots, \boldsymbol{\psi}_i^{N-1}\right] \in \mathbb{R}^{n\times N}$ is a deterministic matrix and $P_2 = \max(P_0, P_1, P_2, \cdots, P_{N-1})$.

Thus the stochastic reduced basis representation of the response vector can be written as

$$\widehat{\mathbf{u}}(\boldsymbol{\theta}) = \widehat{\boldsymbol{\Psi}}(\boldsymbol{\theta})\boldsymbol{\alpha} = \left(\sum_{i=0}^{P_2}\boldsymbol{\Gamma}_i\phi_i\right)\boldsymbol{\alpha}, \tag{2.24}$$

where $\boldsymbol{\alpha}^T = \{\alpha_0, \alpha_1, \alpha_2, \cdots, \alpha_{N-1}\}$ is a vector of undetermined deterministic coefficients.

2.5.1 Stochastic Galerkin projection

Substituting Equation 2.24 and Equation 2.14 into the linear random algebraic system of equations 2.12, we have

$$\left(\sum_{i=0}^{P}\mathbf{K}_i\phi_i(\boldsymbol{\theta})\right)\widehat{\boldsymbol{\Psi}}(\boldsymbol{\theta})\boldsymbol{\alpha} = \sum_{i=0}^{P}\mathbf{f}_i\phi_i(\boldsymbol{\theta}). \tag{2.25}$$

The stochastic residual error vector due to the SRBM approximation can be written as

$$\boldsymbol{\epsilon}(\boldsymbol{\theta}) = \left(\sum_{i=0}^{P}\mathbf{K}_i\phi_i(\boldsymbol{\theta})\right)\widehat{\boldsymbol{\Psi}}(\boldsymbol{\theta})\boldsymbol{\alpha} - \sum_{i=0}^{P}\mathbf{f}_i\phi_i(\boldsymbol{\theta}). \tag{2.26}$$

In order to compute the unknown coefficients namely, $\boldsymbol{\alpha}$, we apply a Galerkin projection scheme where the error residual is made orthogonal to the basis vectors $\{\widehat{\boldsymbol{\psi}}_i(\boldsymbol{\theta})\}$, i.e.,

$$\left(\sum_{i=0}^{P}\mathbf{K}_i\phi_i(\boldsymbol{\theta})\right)\widehat{\boldsymbol{\Psi}}(\boldsymbol{\theta})\boldsymbol{\alpha}-\sum_{i=0}^{P}\mathbf{f}_i\phi_i(\boldsymbol{\theta})\perp\widehat{\boldsymbol{\psi}}_i(\boldsymbol{\theta}),\quad\forall\ i\in\{0,1,2,\cdots,N-1\}. \tag{2.27}$$

Imposing orthogonality between the stochastic residual error and the approximating space of basis vectors in the L_2 sense results in the following $N\times N$ reduced-order system of deterministic equations:

$$\left\langle\sum_{i=0}^{P}\phi_i\widehat{\boldsymbol{\Psi}}(\boldsymbol{\theta})^T\mathbf{K}_i\widehat{\boldsymbol{\Psi}}(\boldsymbol{\theta})\right\rangle\boldsymbol{\alpha}=\left\langle\sum_{i=0}^{P}\phi_i\widehat{\boldsymbol{\Psi}}(\boldsymbol{\theta})^T\mathbf{f}_i\right\rangle. \tag{2.28}$$

Substituting the PC expanded set of SRBM basis vectors from Equation 2.23 into the reduced order system of equations Equation 2.28 results in:

$$\left\langle\left(\sum_{i=0}^{P_2}\boldsymbol{\Gamma}_i^T\phi_i\right)\left(\sum_{j=0}^{P}\mathbf{K}_j\phi_j\right)\left(\sum_{k=0}^{P_2}\boldsymbol{\Gamma}_k\phi_k\right)\right\rangle\boldsymbol{\alpha}=\left\langle\left(\sum_{i=0}^{P_2}\boldsymbol{\Gamma}_i^T\phi_i\right)\left(\sum_{j=0}^{P}\mathbf{f}_j\phi_j\right)\right\rangle.$$

Simplifying the preceding equation using the orthogonality relation between the PC basis functions, we have:

$$\left(\sum_{i=0}^{P_2}\sum_{j=0}^{P}\sum_{k=0}^{P_2}\boldsymbol{\Gamma}_i^T\mathbf{K}_j\boldsymbol{\Gamma}_k\langle\phi_i\phi_j\phi_k\rangle\right)\boldsymbol{\alpha}=\sum_{i=0}^{P_1}\boldsymbol{\Gamma}_i^T\mathbf{f}_i\langle\phi_i^2\rangle, \tag{2.29}$$

where $P_1=\min(P,P_2)$. Note that Equation 2.29 is a reduced order $N\times N$ system of deterministic equations. Typically $N<<<n$ and hence the preceding equations can be efficiently solved for the unknown coefficients $\boldsymbol{\alpha}$.

2.5.2 Post-processing

Given the generalized SRBM representation of the response process given by Equation 2.24, the first two statistical moments of the response process have the following simplistic expressions. The mean of the response vector is the expectation operator applied to Equation 2.24, i.e.,

$$\boldsymbol{\mu}_{\mathbf{u}}=\langle\widehat{\mathbf{u}}(\boldsymbol{\theta})\rangle=\left\langle\left(\sum_{i=0}^{P_2}\boldsymbol{\Gamma}_i\phi_i\right)\right\rangle\boldsymbol{\alpha},$$

which reduces to the following simple expression due to the property of PC basis functions namely, $\langle\phi_i\rangle=0,\forall\ i>0$, i.e.,

$$\boldsymbol{\mu}_{\mathbf{u}}=\boldsymbol{\Gamma}_0\boldsymbol{\alpha}.$$

The covariance matrix of the response can be written as

$$\widehat{\mathbf{u}}_{Cov} = \langle \big(\widehat{\mathbf{u}} - \boldsymbol{\mu}_{\mathbf{u}}\big)\big(\widehat{\mathbf{u}} - \boldsymbol{\mu}_{\mathbf{u}}\big)^T \rangle.$$

After some algebraic manipulations, $\widehat{\mathbf{u}}_{Cov}$ can be compactly written as

$$\widehat{\mathbf{u}}_{Cov} = \sum_{i=1}^{P_2} \boldsymbol{\Gamma}_i \boldsymbol{\alpha}\boldsymbol{\alpha}^T \boldsymbol{\Gamma}_i^T \langle \phi_i^2 \rangle$$

We now focus on computing the norm of the residual error given by Equation 2.26. Since $\boldsymbol{\epsilon}(\boldsymbol{\theta})$ is a stochastic function, it admits a PC decomposition of the form

$$\boldsymbol{\epsilon}(\boldsymbol{\theta}) = \left(\sum_{i=0}^{P} \mathbf{K}_i \phi_i(\boldsymbol{\theta}) \right) \widehat{\boldsymbol{\Psi}}(\boldsymbol{\theta})\boldsymbol{\alpha} - \sum_{i=0}^{P} \mathbf{f}_i \phi_i(\boldsymbol{\theta}) = \sum_{i=0}^{P_3} \boldsymbol{\epsilon}_i \phi_i, \tag{2.30}$$

where P_3 is the order of the PC decomposition used. Note that the order of decomposition used here should be greater than the order of expansion of the stochastic basis vectors and the linear algebraic system of equations given by Equation 2.12 and Equation 2.14 i.e., $P_3 > \max(P, P_2)$. Multiplying both sides of the preceding equation by ϕ_k and taking the ensemble average leads to the following simple expression (again due to orthogonality of the PC basis functions):

$$\boldsymbol{\epsilon}_k = \frac{\displaystyle\sum_{i=0}^{P}\sum_{j=0}^{P_2} \mathbf{K}_i \boldsymbol{\Gamma}_j \boldsymbol{\alpha} \big\langle \phi_i \phi_j \phi_k \big\rangle - \mathbf{f}_k \big\langle \phi_k^2 \big\rangle}{\big\langle \phi_k^2 \big\rangle}. \tag{2.31}$$

The L_2-norm of the residual error can now be written as:

$$\| \boldsymbol{\epsilon}(\boldsymbol{\theta}) \| = \big\langle \boldsymbol{\epsilon}(\boldsymbol{\theta})^T \boldsymbol{\epsilon}(\boldsymbol{\theta}) \big\rangle = \sum_{i=0}^{P_3}\sum_{j=0}^{P_3} \boldsymbol{\epsilon}_i^T \boldsymbol{\epsilon}_j \big\langle \phi_i \phi_j \big\rangle. \tag{2.32}$$

In our numerical studies, we use the L_2-norm of the residual error to analyze the convergence trends of SRBMs. In addition to the $\mathbf{K}$-norm error and norm of the residual error, we also employ two other error metrics to study convergence namely the norm of the relative error in mean and standard deviation which are defined as

$$\begin{aligned} \epsilon_\mu &= \frac{\|\boldsymbol{\mu}_{MCS} - \boldsymbol{\mu}_{SRBM}\|}{\|\boldsymbol{\mu}_{MCS}\|}, \\ \epsilon_\sigma &= \frac{\|\boldsymbol{\sigma}_{MCS} - \boldsymbol{\sigma}_{SRBM}\|}{\|\boldsymbol{\sigma}_{MCS}\|}, \end{aligned} \tag{2.33}$$

where the subscripts MCS and $SRBM$ denote the quantities obtained from Monte-Carlo simulation and SRBM approximation. It should be noted that the Galerkin projection (2.27) ensures only the minimization of the $\mathbf{K}$-norm error in light of the Theorem 2 in Section 2.4. Hence $\mathbf{K}$-norm is strictly non-increasing with the increase in the number of basis vectors. But the error metrics ϵ_μ, ϵ_σ and the L_2-norm of the residual error are not strictly non-increasing in theory.

2.6 Summary

In this chapter we introduced the notation followed in the remaining chapters. We reviewed the classical PC leading to gPC and the Karhunen-Loève expansion for random field discretization. Then we have discussed two class of stochastic projection schemes namely SSFEM and SRBM which spectrally decompose the response process using different types of basis vectors. It is understood that SRBMs result in a reduced order system of equations after the Galerkin projection resulting in high efficiency compared to SSFEM for high dimensional problems. Using SRBMs, the accuracy of the solution process can be enhanced by increasing the number of basis vectors or increasing the PC order of the basis vectors. This is p-refinement of the response process. On the other hand, accuracy can also be improved by decomposing the input random space into a number of subdomains. We discuss this strategy called the h-refinement in detail in the next chapter.

Chapter 3

An *h*-refinement version of SRBMs

Traditionally, using SSFEM and SRBMs, the accuracy of the response statistics is improved by increasing the number of basis functionals. This type of refinement is known as *p*-type refinement in algorithms which spectrally decompose the solution process. More recently, Babuška et al [59], Maître et al [58], Xiu and Tartakovsky [77], Wan and Karniadakis [78] came up with the idea of decomposing the input random space (*h*-refinement) in order to decrease the uncertainty in each subdomain, thus resulting in better accuracy in the response statistics. Numerical experiments have shown that *h*-refinement enhances the stability of stochastic projection schemes when applied to non-linear problems, time dependent problems and problems involving point discontinuities [78–80].

In this chapter, we propose multi-element Stochastic Reduced Basis Methods (ME-SRBMs) to achieve *h*-refinement of SRBMs. We note that the desired response statistics are integrals with respect to the input PDFs and hence their accuracy is inversely proportional to the variability in the random space. In addition, as with any Krylov subspace based method, preconditioners have a significant role to play in convergence as can be seen in the following sections. Thus partitioning the space of the random inputs into disjoint elements provides two-pronged benefits, namely, better preconditioners and better cascade of local estimates for the undetermined coefficients. Summing up, the basic idea behind a multi-element formulation is to compare the relative error in variance against a user-defined tolerance and then decompose the random space into a number of random elements or subdomains. The objective of this chapter is to extend this concept of decomposing the input random space to SRBMs and to demonstrate the two fold benefits associated with such a formulation.

3.1 Multi-Element Stochastic Reduced Basis Methods

In this section, we present a multi-element reformulation of SRBMs based on the ideas developed earlier in the context of PC projection schemes [78]. Let $\boldsymbol{\theta}(\omega) = [\theta_1(\omega), \theta_2(\omega), \ldots, \theta_d(\omega)] : \Omega \rightarrow \mathbb{R}^d$ denote a d-dimensional random vector defined on the complete probability space $(\Omega, \mathcal{F}, \mathcal{P})$ where $\theta_i \ \forall \ i \in \{1, 2, \ldots, d\}$ are identical, independently distributed (IID) random variables. We also assume that all the components of the vector $\boldsymbol{\theta} : \Omega \rightarrow [-1, 1]^d$ are uniform random variables with a constant joint PDF $f_{\boldsymbol{\theta}} = \frac{1}{2^d}$. Define B as the decomposition of $[-1, 1]^d$, such that

$$\left.\begin{aligned} B &= \bigcup_{i}^{H} B_i \\ B_i &= [a_1^i, b_1^i) \times [a_2^i, b_2^i) \times \cdots \times [a_d^i, b_d^i) \\ B_i \bigcap B_j &= \emptyset \quad \Leftrightarrow i \neq j, \end{aligned}\right\}$$

where $i, j \in \{1, 2, \ldots, H\}$. Thus B is a partition of $[-1, 1]^d$ into H non-overlapping elements with the property

$$\mathcal{P}(B_i \bigcap B_j) = 0, \tag{3.1}$$

where $\mathcal{P}$ is the probability measure defined on the Hilbert space $L_2(\Omega, \mathcal{F}, \mathcal{P})$. On each random element define an *indicator random variable* I_j such that

$$I_j = \begin{cases} 1 & \text{when } \boldsymbol{\theta} \in B_j, \\ 0 & \text{otherwise.} \end{cases}$$

Thus $I_j^{-1}(1) = \{\boldsymbol{\theta} \mid \boldsymbol{\theta} \in B_j\}$. Then it follows that

$$I_j^{-1}(1) \bigcap I_k^{-1}(1) = \emptyset \quad \Leftrightarrow j \neq k.$$

We define a local random variable on $I_j^{-1}(1)$ as

$$\boldsymbol{\chi}^j = [\chi_1^j, \chi_2^j, \ldots, \chi_d^j] : I_j^{-1}(1) \rightarrow B_j \ ,$$

subject to the conditional PDF

$$f_{\boldsymbol{\chi}^j} = \frac{1}{2^d Pr(I_j = 1)} \ ,$$

where $Pr(I_j = 1)$, the probability of I_j being 1 is given by

$$Pr(I_j = 1) = \prod_{i=1}^{d} \frac{b_i^j - a_i^j}{2} \ .$$

The local random variable $\boldsymbol{\chi}^j$ is mapped to a new random variable $\boldsymbol{\theta}^j = g_j(\boldsymbol{\chi}^j) : I_j^{-1}(1) \rightarrow [-1,1]^d$ with conditional PDF $f_{\boldsymbol{\theta}^j} = \frac{1}{2^d}$ where $g_j(\boldsymbol{\chi}^j)$ is defined such that $\chi_i^j = \frac{b_i^j - a_i^j}{2}\theta_i^j + \frac{b_i^j + a_i^j}{2} \quad \forall i \in \{1, 2, \ldots, d\}$. This random variable transformation is done so that the PDF is the same over all the elements which in turn results in simpler expressions for the moments of the response.

As a consequence of the above decomposition of the input random space, the global stochastic system of equations can be rewritten as a decoupled random algebraic system of equations (defined over a subdomain B_k) as follows:

$$\mathbf{K}(g_k^{-1}(\boldsymbol{\theta}^k))\mathbf{u}(g_k^{-1}(\boldsymbol{\theta}^k)) = \mathbf{f}(g_k^{-1}(\boldsymbol{\theta}^k)) \quad \forall k \in \{1, 2, \cdots H\}. \tag{3.2}$$

These local or elemental systems of equations are solved for the response statistics using SRBMs where the basis is chosen from the preconditioned stochastic Krylov subspace defined by (see Section 2.4):

$$\mathcal{K}_N^k \left(\mathbf{M}^k \mathbf{K}(g_k^{-1}(\boldsymbol{\theta}^k)), \mathbf{M}^k \mathbf{f}(g_k^{-1}(\boldsymbol{\theta}^k)) \right) = \text{span} \left\{ \boldsymbol{\psi}_0^k, \boldsymbol{\psi}_1^k, \boldsymbol{\psi}_2^k, \cdots, \boldsymbol{\psi}_{N-1}^k \right\},$$

where the local stochastic basis vectors $\boldsymbol{\psi}_i^k$ are recursively defined as

$$\begin{aligned}
\boldsymbol{\psi}_0^k(g_k^{-1}(\boldsymbol{\theta}^k)) &= \mathbf{M}^k \mathbf{f}(g_k^{-1}(\boldsymbol{\theta}^k)) \\
\boldsymbol{\psi}_1^k(g_k^{-1}(\boldsymbol{\theta}^k)) &= \mathbf{M}^k \mathbf{K}(g_k^{-1}(\boldsymbol{\theta}^k)) \boldsymbol{\psi}_0^k(g_k^{-1}(\boldsymbol{\theta}^k)) \\
\boldsymbol{\psi}_2^k(g_k^{-1}(\boldsymbol{\theta}^k)) &= \mathbf{M}^k \mathbf{K}(g_k^{-1}(\boldsymbol{\theta}^k)) \boldsymbol{\psi}_1^k(g_k^{-1}(\boldsymbol{\theta}^k)) \\
&\vdots \\
\boldsymbol{\psi}_{N-1}^k(g_k^{-1}(\boldsymbol{\theta}^k)) &= \mathbf{M}^k \mathbf{K}(g_k^{-1}(\boldsymbol{\theta}^k)) \boldsymbol{\psi}_{N-2}^k(g_k^{-1}(\boldsymbol{\theta}^k))
\end{aligned}$$

In the above set of equations $\mathbf{M}^k$ represents a global or a local preconditioner. A global preconditioner is defined as

$$\mathbf{M}^k = \langle \mathbf{K}(\boldsymbol{\theta}) \rangle^{-1} \tag{3.3}$$

and a local preconditioner is defined as

$$\mathbf{M}^k = \langle \mathbf{K}(g_k^{-1}(\boldsymbol{\theta}^k)) \rangle^{-1}. \tag{3.4}$$

Thus the local approximate solution obtained by applying SRBMs to Equation 3.2 can be written as

$$\widehat{\mathbf{u}}_k(g_k(\boldsymbol{\theta})) = \boldsymbol{\Psi}^k \boldsymbol{\alpha}^k, \tag{3.5}$$

where $\boldsymbol{\Psi}^k = [\boldsymbol{\psi}_0^k, \boldsymbol{\psi}_1^k, \cdots, \boldsymbol{\psi}_{N-1}^k]$ is a matrix of stochastic basis vectors and $\boldsymbol{\alpha}^k$ are the undetermined coefficients computed by imposing the Galerkin condition. The Bubnov-Galerkin

condition is enforced as

$$\boldsymbol{\epsilon}(g_k^{-1}(\boldsymbol{\theta}^k)) = \mathbf{K}(g_k^{-1}(\boldsymbol{\theta}^k))\boldsymbol{\Psi}^k\boldsymbol{\alpha}^k - \mathbf{f}(g_k^{-1}(\boldsymbol{\theta}^k)) \perp \boldsymbol{\psi}_j^k, \quad \forall 0 \leq j \leq N-1. \tag{3.6}$$

The above condition results in the following reduced order $N \times N$ system of deterministic equations

$$\langle {\boldsymbol{\psi}_j^k}^T(g_k^{-1}(\boldsymbol{\theta}^k))\boldsymbol{\epsilon}(g_k^{-1}(\boldsymbol{\theta}^k))\rangle = 0, \forall 0 \leq j \leq N-1. \tag{3.7}$$

The undetermined coefficients obtained by solving the above system of equations are substituted into Equation 3.5 to compute the local statistics. These local statistics are assimilated to compute the global statistics as shown in the next section. Absolute continuity on the elemental boundaries is not required as the statistics are integrations with respect to the conditional PDFs. More precisely, the integrals are zero on the elemental boundary region due to Equation 3.1. The approximate global response process $\widehat{\mathbf{u}}(\boldsymbol{\theta})$ defined on $(\Omega, \mathcal{F}, \mathcal{P})$ can be expressed in terms of local approximations $\widehat{\mathbf{u}}_j(\boldsymbol{\theta}^j)$ defined on the elemental random space $(I_j^{-1}(1), \mathcal{F} \bigcap I_j^{-1}(1), P(\cdot|\boldsymbol{\theta} \in I_j^{-1}(1)))$ as

$$\widehat{\mathbf{u}}(\boldsymbol{\theta}) = \sum_{j=1}^{H} \widehat{\mathbf{u}}_j(g_j(\boldsymbol{\theta}))I_j. \tag{3.8}$$

This formulation can also be extended to non-uniform uncertainty models by expanding each of the random components using Legendre-chaos basis functions; see, for example, Wan and Karniadakis [78].

We now present a result on the error norm that is minimized by ME-SRBMs that use the Bubnov-Galerkin projection scheme to evaluate the undetermined coefficients in each random element.

Theorem 3. *Let* $\mathbf{K}(\boldsymbol{\theta})\mathbf{u}(\boldsymbol{\theta}) = \mathbf{f}(\boldsymbol{\theta})$ *be a random algebraic system of equations where* $\boldsymbol{\theta} : \Omega \to [-1, 1]^d$ *is a uniform random vector whose components* $\boldsymbol{\theta}_j$ *are IID random variables,* $\mathbf{K}(\boldsymbol{\theta}) \in \mathbb{R}^{n\times n}$ *is a symmetric positive definite matrix and* $\mathbf{u}(\boldsymbol{\theta}), \mathbf{f}(\boldsymbol{\theta}) \in \mathbb{R}^n$ *are random vectors. The space of the random vector* $\boldsymbol{\theta}$ *is decomposed into* H *disjoint elements where* $\boldsymbol{\theta}^k$ *denotes the local random variable. If SRBMs with* N *basis vectors are employed locally to compute the approximate solution* $\widehat{\mathbf{u}}_k(g_k(\boldsymbol{\theta}))$ *for the above system of equations where in turn a Bubnov-Galerkin projection scheme is used to compute the undetermined coefficients, then the global* $\mathbf{K}$*-norm error given by*

$$\Delta_N = \left\langle \{\mathbf{u}(\boldsymbol{\theta}) - \widehat{\mathbf{u}}(\boldsymbol{\theta})\}^T\mathbf{K}(\boldsymbol{\theta})\{\mathbf{u}(\boldsymbol{\theta}) - \widehat{\mathbf{u}}(\boldsymbol{\theta})\}\right\rangle \tag{3.9}$$

is minimized.

Proof : Let $\widehat{\mathbf{u}}(\boldsymbol{\theta})$ be the approximated solution process. It can be expressed in terms of local approximate solutions as in Equation 3.8. Then the global $\mathbf{K}$-norm error given by Equation 3.9 can be rewritten as

$$\Delta_N = \int_B \{\mathbf{u}(\boldsymbol{\theta}) - \sum_{k=1}^{H} \widehat{\mathbf{u}}_k(g_k(\boldsymbol{\theta}))I_k\}^T \mathbf{K}(\boldsymbol{\theta})\{\mathbf{u}(\boldsymbol{\theta}) - \sum_{k=1}^{H} \widehat{\mathbf{u}}_k(g_k(\boldsymbol{\theta}))I_k\}\Big(\frac{1}{2}\Big)^d \mathrm{d}\boldsymbol{\theta}.$$

After applying Bayes theorem and the law of total probability on the preceding equation, we have

$$\begin{aligned}
\Delta_N &= \sum_{k=1}^{H} Pr(I_k = 1) \int_{B_k} \mathbf{x}^T(\boldsymbol{\chi}^k)\mathbf{K}(\boldsymbol{\chi}^k)\mathbf{x}(\boldsymbol{\chi}^k) f_{\boldsymbol{\chi}^k} \mathrm{d}\boldsymbol{\chi}^k \\
&= \sum_{k=1}^{H} Pr(I_k = 1) \int_{[-1,1]^d} \mathbf{x}^T(g_k^{-1}(\boldsymbol{\theta}^k))\mathbf{K}(g_k^{-1}(\boldsymbol{\theta}^k))\mathbf{x}(g_k^{-1}(\boldsymbol{\theta}^k)) \frac{1}{2^d} \mathrm{d}\boldsymbol{\theta}^k \quad , \qquad (3.10) \\
&= \sum_{k=1}^{H} \Delta_N^k Pr(I_k = 1)
\end{aligned}$$

where $\mathbf{x}(\boldsymbol{\chi}^k) = \mathbf{u}(\boldsymbol{\chi}^k) - \widehat{\mathbf{u}}_k(g_k(\boldsymbol{\chi}^k))$, Δ_N is the global $\mathbf{K}$-norm error and the local $\mathbf{K}$-norm error is defined as

$$\Delta_N^k = \Big\langle \{\mathbf{x}^T(g_k^{-1}(\boldsymbol{\theta}^k))\mathbf{K}(g_k^{-1}(\boldsymbol{\theta}^k))\mathbf{x}(g_k^{-1}(\boldsymbol{\theta}^k))\} \Big\rangle \qquad (3.11)$$

in the k^{th} random element for SRBM expansion with N basis vectors. Note that $\mathbf{K}(g_k^{-1}(\boldsymbol{\theta}^k))$ is a symmetric positive definite matrix. Hence $\mathbf{x}^T(g_k^{-1}(\boldsymbol{\theta}^k))\mathbf{K}(g_k^{-1}(\boldsymbol{\theta}^k))\mathbf{x}(g_k^{-1}(\boldsymbol{\theta}^k)) > 0$ for any nonzero $\mathbf{x}(\boldsymbol{\theta}^k) \in \mathbb{R}^n$, which leads to the conclusion that $\Delta_N^k > 0$ for any $k \in \{1, 2, \cdots, H\}$. Also note that according to Theorem 2 in Chapter 2, if SRBMs in conjunction with the Bubnov-Galerkin projection scheme is applied locally, then the local $\mathbf{K}$-norm error (Δ_N^k, $\forall k \in \{1, 2, \cdots, H\}$) is minimized. Hence from the preceding argument and equation Equation 3.10, it follows that the global $\mathbf{K}$-norm error is also minimized.

□

Theorem 3 implies that the $\mathbf{K}$-norm error is a strictly non-increasing function of the number of subdomains (H). On the other hand if the Petrov-Galerkin scheme is used to evaluate the undetermined coefficients locally, we conjecture that the global L_2 norm of the residual error is minimized – this in turn will imply that the residual error norm is a strictly non-increasing function of the number of random elements.

It is to be noted that the Galerkin condition imposed in Equation 3.7 is said to be a *weak* Galerkin condition because only the ensemble average of the random functions ${\boldsymbol{\psi}_j^k}^T(g_k^{-1}(\boldsymbol{\theta}^k))\epsilon(g_k^{-1}(\boldsymbol{\theta}^k)), \forall j \in \{0, 1, \cdots, N-1\}$ are set to zero. In contrast, the *strong*

Galerkin scheme applied to the global stochastic system of equations, enforces the above condition more stringently, i.e. the orthogonality of the basis and the residual error is enforced for *each realization* of $\boldsymbol{\theta}$. This is accomplished by expanding the undetermined coefficients in a *global* PC basis and subsequently applying a *weak* Galerkin condition; see Nair [76] for details. In the case of ME-SRBMs, a *piecewise* representation of the undetermined coefficients (defined over local partitions of the random space) is employed. Hence ME-SRBMs can be thought of as a projection scheme that implements a relaxed version of the *strong* Galerkin condition.

3.2 Computational aspects

3.2.1 Preconditioners

Preconditioners enhance the convergence characteristics of Krylov subspace methods. A wide variety of preconditioning strategies have been explored in the literature in the context of solving deterministic systems of equations. For a deterministic system of equations $\mathbf{Ku} = \mathbf{f}$, any matrix $\mathbf{M}$ which closely approximates $\mathbf{K}^{-1}$ and is invertible acts as a good preconditioner. In comparison, for random algebraic systems of equations of the form $\mathbf{K}(\boldsymbol{\theta})\mathbf{u}(\boldsymbol{\theta}) = \mathbf{f}(\boldsymbol{\theta})$, it is sought to construct a deterministic preconditioner $\mathbf{M}$ that is a close approximation to the random matrix $\mathbf{K}(\boldsymbol{\theta})^{-1}$. In other words, the degree of the minimal random polynomial of the matrix $\mathbf{MK}(\boldsymbol{\theta})$ must be lower than that of the matrix $\mathbf{K}(\boldsymbol{\theta})$. Thus an incomplete Cholesky factorization or the inverse of the deterministic matrix $\langle \mathbf{K}(\boldsymbol{\theta}) \rangle$ works well in an average sense as a preconditioner for random algebraic systems of equations. In previous studies on SRBMs, the deterministic matrix $\langle \mathbf{K}(\boldsymbol{\theta}) \rangle^{-1}$ has been used as a preconditioner to accelerate stochastic Krylov methods with a great degree of success [60–63, 76].

As discussed in the preceding section, in the case of ME-SRBMs, we can employ two types of preconditioners, namely, the global preconditioner given by Equation 3.3 or the local preconditioner given by Equation 3.4. The motivation behind using a local preconditioner is that it provides a better approximation to $\langle \mathbf{K}(\boldsymbol{\theta}) \rangle^{-1}$ as compared to the global preconditioner in any random element. On the other hand global preconditioning is computationally more efficient than local preconditioning since only a single preconditioner has to be constructed. Both local and global preconditioning strategies admit coarse grained and fine grained parallelization. Using a global preconditioner, a substantial gain in execution speeds can be achieved owing to the fact that the preconditioner is computed only once and

stored in a shared memory space, which can be accessed by other individual nodes. The major advantage with local preconditioning is that the rates of convergence are orders of magnitudes faster than with using global preconditioners.

3.2.2 Post-processing

We now outline how the subdomain response process approximations obtained using ME-SRBMs can be postprocessed to compute the first two statistical moments of the global response. Using Bayes theorem and the law of total probability, the m^{th} moment of the global approximation can be written as

$$\langle \widehat{\mathbf{u}}^m(\boldsymbol{\theta}) \rangle = \int_B \widehat{\mathbf{u}}^m(\boldsymbol{\theta}) \Big(\frac{1}{2}\Big)^d \mathrm{d}\boldsymbol{\theta} = \sum_{j=1}^{H} Pr(I_j = 1) \int_{B_j} \widehat{\mathbf{u}}_j^m(\boldsymbol{\theta}^j) \Big(\frac{1}{2}\Big)^d \mathrm{d}\boldsymbol{\theta}^j. \tag{3.12}$$

From Equation 3.8 and Equation 3.12, the mean of the response process can be written as

$$\boldsymbol{\mu} = \langle \widehat{\mathbf{u}}(\boldsymbol{\theta}) \rangle = \sum_{j=1}^{H} Pr(I_j = 1) \boldsymbol{\mu}^j, \tag{3.13}$$

where $\boldsymbol{\mu}^j$ is the elemental mean given by $\langle \widehat{\mathbf{u}}_j(\boldsymbol{\theta}^j) \rangle$.

The local covariance of the j^{th} element is given by

$$\begin{aligned} \widehat{\mathbf{u}}_{COV}^j &= \langle (\widehat{\mathbf{u}}_j(\boldsymbol{\theta}^j) - \boldsymbol{\mu}^j)(\widehat{\mathbf{u}}_j(\boldsymbol{\theta}^j) - \boldsymbol{\mu}^j)^* \rangle \\ &= \langle \widehat{\mathbf{u}}_j(\boldsymbol{\theta}^j) \widehat{\mathbf{u}}_j^*(\boldsymbol{\theta}^j) \rangle - \boldsymbol{\mu}^j \boldsymbol{\mu}^{j*}. \end{aligned} \tag{3.14}$$

It can be noted that

$$\langle \widehat{\mathbf{u}}(\boldsymbol{\theta}) \widehat{\mathbf{u}}^*(\boldsymbol{\theta}) \rangle = \sum_{j=1}^{H} Pr(I_j = 1) \langle \widehat{\mathbf{u}}_j(\boldsymbol{\theta}^j) \widehat{\mathbf{u}}_j^*(\boldsymbol{\theta}^j) \rangle. \tag{3.15}$$

Hence, the global or the overall response covariance can be computed using Equation 3.14 and Equation 3.15 as shown below

$$\begin{aligned} \widehat{\mathbf{u}}_{COV} &= \langle (\widehat{\mathbf{u}}(\boldsymbol{\theta}) - \boldsymbol{\mu})(\widehat{\mathbf{u}}(\boldsymbol{\theta}) - \boldsymbol{\mu})^* \rangle \\ &= \langle \widehat{\mathbf{u}}(\boldsymbol{\theta}) \widehat{\mathbf{u}}^*(\boldsymbol{\theta}) \rangle - \boldsymbol{\mu} \boldsymbol{\mu}^* \\ &= \sum_{j=1}^{H} Pr(I_j = 1)(\widehat{\mathbf{u}}_{COV}^j + \boldsymbol{\mu}^j \boldsymbol{\mu}^{j*}) - \boldsymbol{\mu} \boldsymbol{\mu}^*. \end{aligned} \tag{3.16}$$

3.3 Numerical Studies

In this chapter we present numerical studies to illustrate the application of ME-SRBMs to model problems in steady state stochastic elasticity problem and stochastic heat transfer

in media with random material properties. Results are presented for uniform uncertainty models which are compared against those obtained using direct MCS. Note that we carry out MCS after Karhunen-Loéve (KL) expansion of the input random fields. This is because our primary focus is on the error from ME-SRBMs and hence it makes sense to eliminate the error introduced by the truncation of KL expansion which is well documented. The convergence trends of the response mean and standard deviation, **K**-norm error, and residual error norm are studied. The variables considered are the number of stochastic basis vectors (p-convergence), the degree of decomposition of the random space (h-convergence) and global/local preconditioning strategies.

Note that in all the subsequent plots, we use the abbreviation ME-SRBM(N, "*type*") to denote the results obtained using N stochastic basis vectors and a given *type* of preconditioning strategy (global or local). The graphs depicting the convergence show the norm relative error in mean and standard deviation which are defined as in Equation 2.33.

3.3.1 Steady state elasticity problem

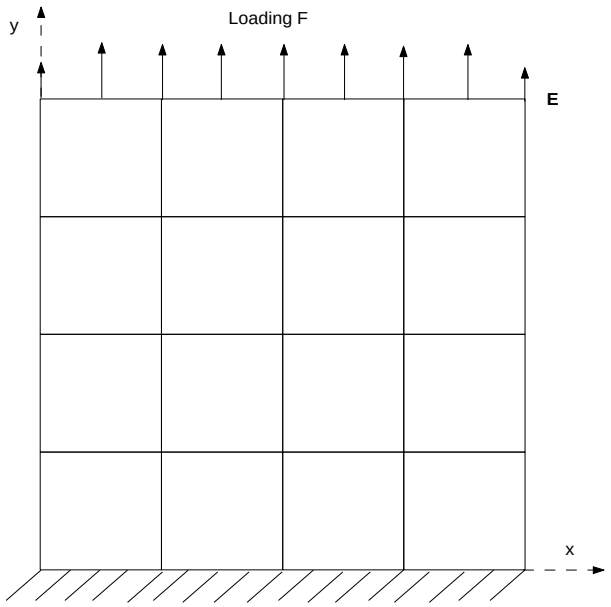

FIGURE 3.1: Schematic of plate problem.

A thin square plate of unit length (i.e. $[0,1] \times [0,1]$) clamped at one edge and subjected to uniform in-plane tension at the opposite edge as shown in Fig. 3.1. This problem has been described in [39] and used in [63] for studying the convergence behavior of PC projection schemes. The random field representing uncertainty in Young's modulus of this structure is

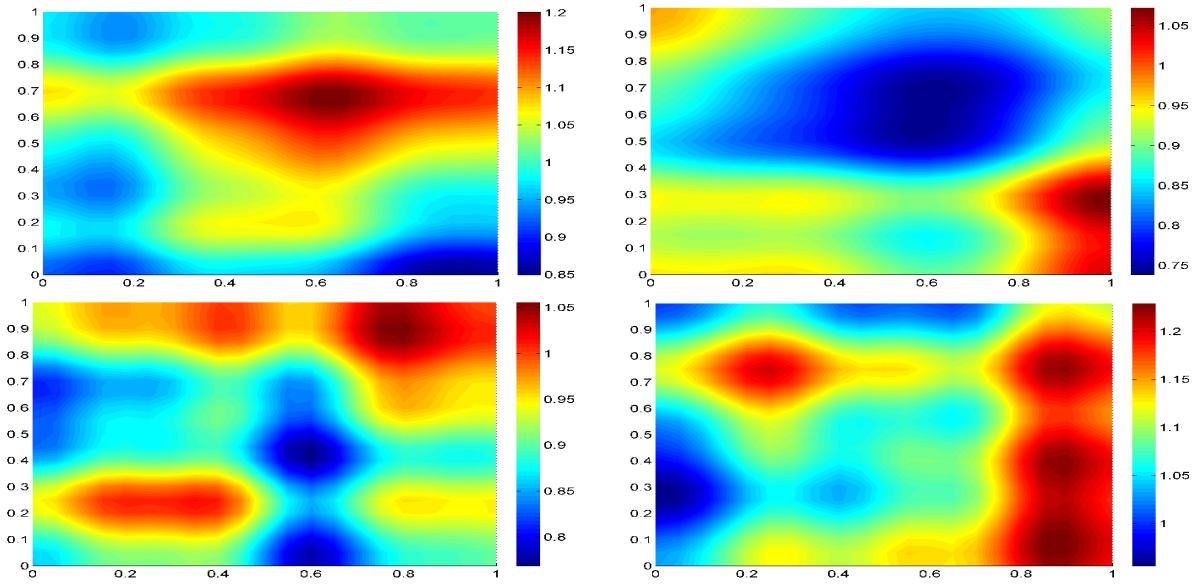

FIGURE 3.2: Four realizations of the Young's modulus field.

discretized using the standard Karhunen-Loéve(KL) expansion. The exponential correlation function shown below is used to represent uncertainty

$$C(\mathbf{x},\mathbf{y}) = \exp\left(-\frac{|x_1 - x_2|}{b_1} - \frac{|y_1 - y_2|}{b_2}\right). \tag{3.17}$$

and the mean of the random field is considered to be unity.

The spatial domain is decomposed into 16 square four noded quadrilateral elements as shown in Fig. 3.1, which leads to a total of 50 DOF considering 2 DOF/node. The external loads are assumed to be deterministic and of unit magnitude. The modulus of the elasticity of the plate is modeled as 2D uniform random field with the exponential correlation model given by Equation 3.17 with $b_1 = b_2 = 1$. The random field is discretized using KL expansion scheme with four and six terms being retained respectively.

ME-SRBMs with up to 2 basis vectors and up to 16 subdomains are applied to compute the first two statistical moments of the displacement. The input standard deviation σ has been set to 0.2 which represents a high degree of input variability in this case. Figure 3.2 shows few realizations of the Young's modulus field.

A Monte-Carlo simulation with a 1 million sample size is used to generate benchmark results against which different metrics are compared. The convergence trends obtained for the case when 2 and 4 terms are retained in the KL expansion of the Young's modulus are shown in Figure 3.3 and Figure 3.4, respectively. It can be seen from the figures that the error in standard deviation decreases (compared to the single element case which corresponds to

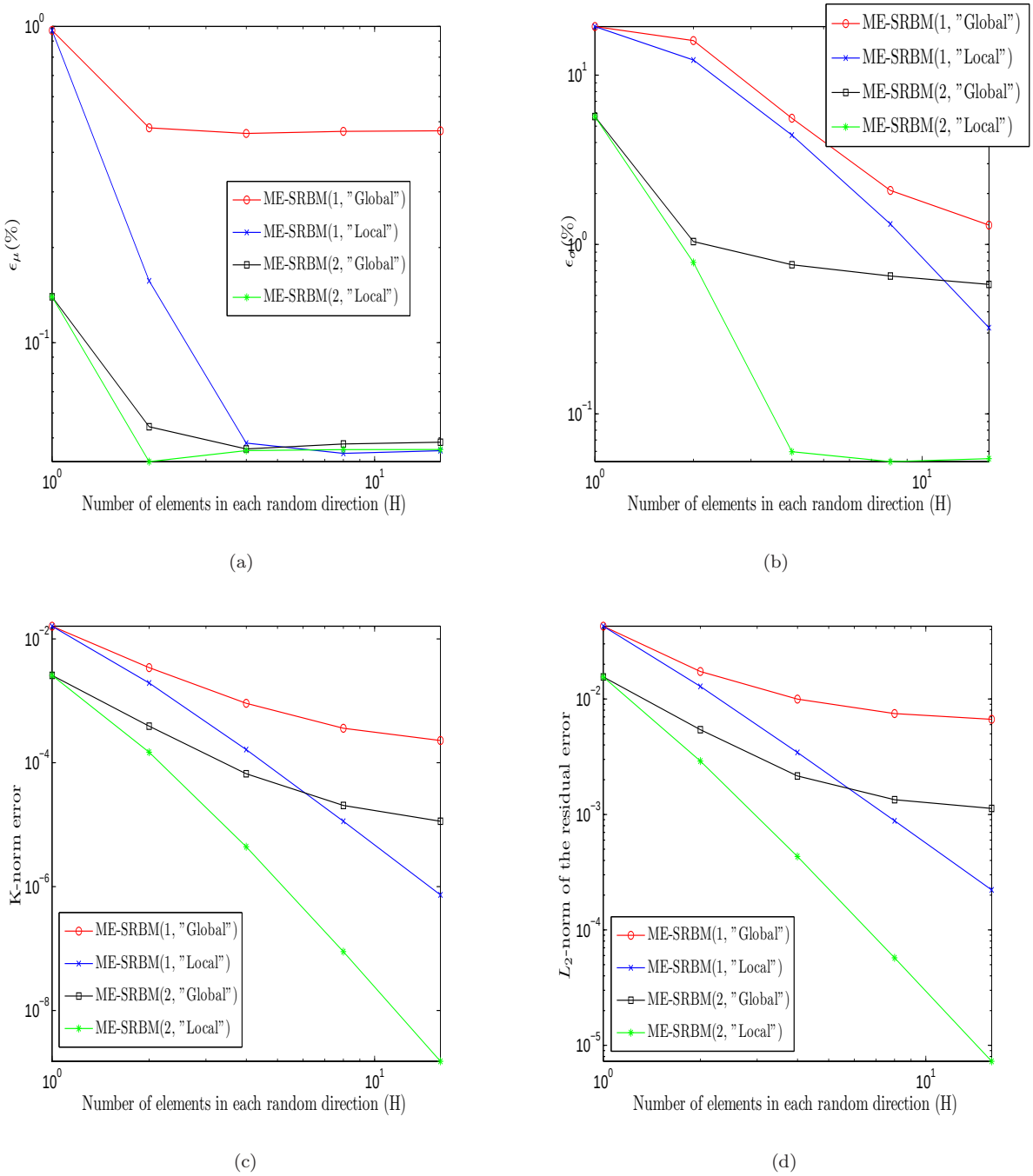

FIGURE 3.3: Convergence trends on the steady state elasticity problem: (a) Percentage norm relative error in mean (ϵ_μ from Equation 2.33) (b) percentage norm relative error in standard deviation (ϵ_σ from Equation 2.33) (c) **K**-norm error (d) norm of residual error using up to 2 basis vectors as a function of number of subdomains and different preconditioners when only two terms are retained in the KL expansion.

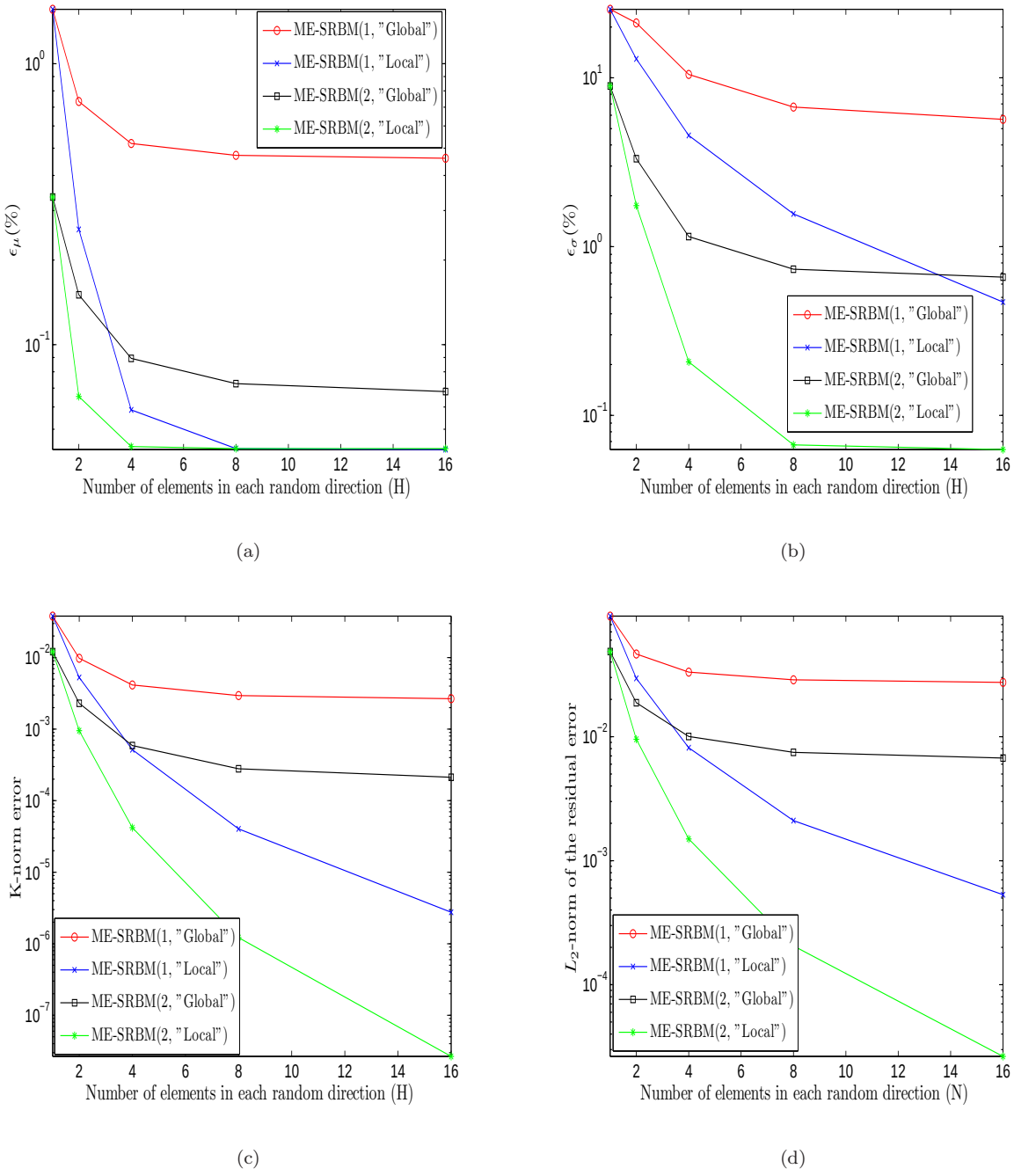

FIGURE 3.4: Convergence trends on the steady state elasticity problem: (a) Percentage norm relative error in mean (ϵ_μ from Equation 2.33) (b) percentage norm relative error in standard deviation (ϵ_σ from Equation 2.33) (c) **K**-norm error (d) norm of residual error using up to 2 basis vectors as a function of number of subdomains and different preconditioners when only four terms are retained in the KL expansion.

the standard SRBM formulation) as the number of random elements is increased. Also local preconditioning results in faster convergence of the error in standard deviation as compared to global preconditioning. The above mentioned figures also show a consistent drop in **K**-norm error and residual error norm as the number of random elements is increased. Accelerated convergence is observed with both metrics for ME-SRBMs with local preconditioning.

3.3.2 Stochastic steady state heat transfer on a square surface

We first consider the stochastic steady state heat equation considered earlier by Xiu and Karniadakis [64]

$$\nabla \cdot [\kappa(x,y;\omega)\nabla u(x,y;\omega)] \quad = \quad 0 \qquad (x,y) \in [-1,1] \times [-1,1]$$

with the boundary conditions

$$u(-1,y;\omega) = 1, \quad \frac{\partial u}{\partial x}(1,y;\omega) = 0, \quad u(x,-1;\omega) = 0, \quad \frac{\partial u}{\partial y}(x,1;\omega) = 0$$

The conductivity $\kappa(x,y;\omega)$ is a stochastic process with certain distribution and a given correlation function with the mean field being $\bar{\kappa}(x,y;\omega) = 1$. Due to the nonhomogeneous Dirichlet boundary conditions, the stochastic system of equations after the imposition of boundary conditions are of the form $\mathbf{K}(\boldsymbol{\theta})\mathbf{u}(\boldsymbol{\theta}) = \mathbf{f}(\boldsymbol{\theta})$, where $\mathbf{K}(\boldsymbol{\theta}) : \mathbb{R}^d \to \mathbb{R}^{n\times n}$, $\mathbf{u}(\boldsymbol{\theta}), \mathbf{f}(\boldsymbol{\theta}) : \mathbb{R}^d \to \mathbb{R}^n$ and n denotes the total number of free degrees of freedom.

The input correlation function we adopt for this numerical example is of the form

$$C(r) = \sigma^2 e^{-r/b}, \quad r \geq 0 \tag{3.18}$$

where r is the Euclidean distance between two points in 2D space, $\sigma = 0.4$ is the input standard deviation and $b = 1$ is the correlation length. In order to reduce the dimensionality of the problem, we apply KL decomposition for random field discretization. Since no analytical eigenvalues and eigenvectors can be obtained for the KL eigenvalue problem for the above mentioned correlation function, we perform numerical KL decomposition. The numerical KL decomposition is based on the finite element approximation of the KL integral eigenvalue problem, proposed by Keese and the reader is referred to [16] for the discretization error introduced by such an approximation.

The convergence trends obtained for the case when 2 and 4 terms are retained in the KL expansion of the conductivity are shown in Figure 3.5 and Figure 3.6, respectively. It can be seen from the figures that the error in standard deviation decreases (compared to the

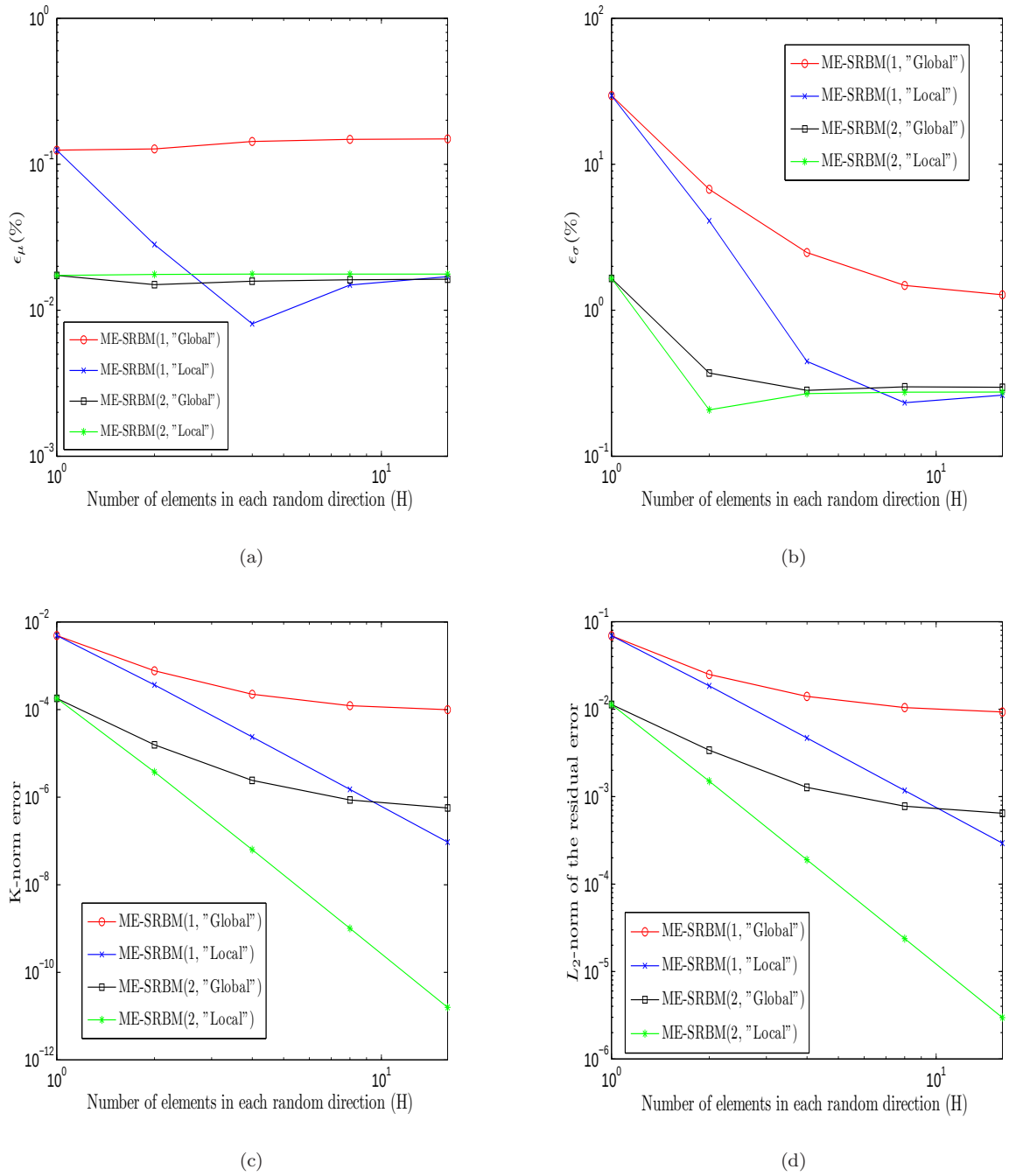

FIGURE 3.5: Convergence trends on the steady state heat transfer problem on a square domain: (a) Percentage norm relative error in mean (ϵ_μ from Equation 2.33) (b) percentage norm relative error in standard deviation (ϵ_σ from Equation 2.33) (c) $\mathbf{K}$-norm error and (d) Norm of residual error using up to 2 basis vectors as a function of number of subdomains (H) and different preconditioners when only two terms are retained in the KL expansion.

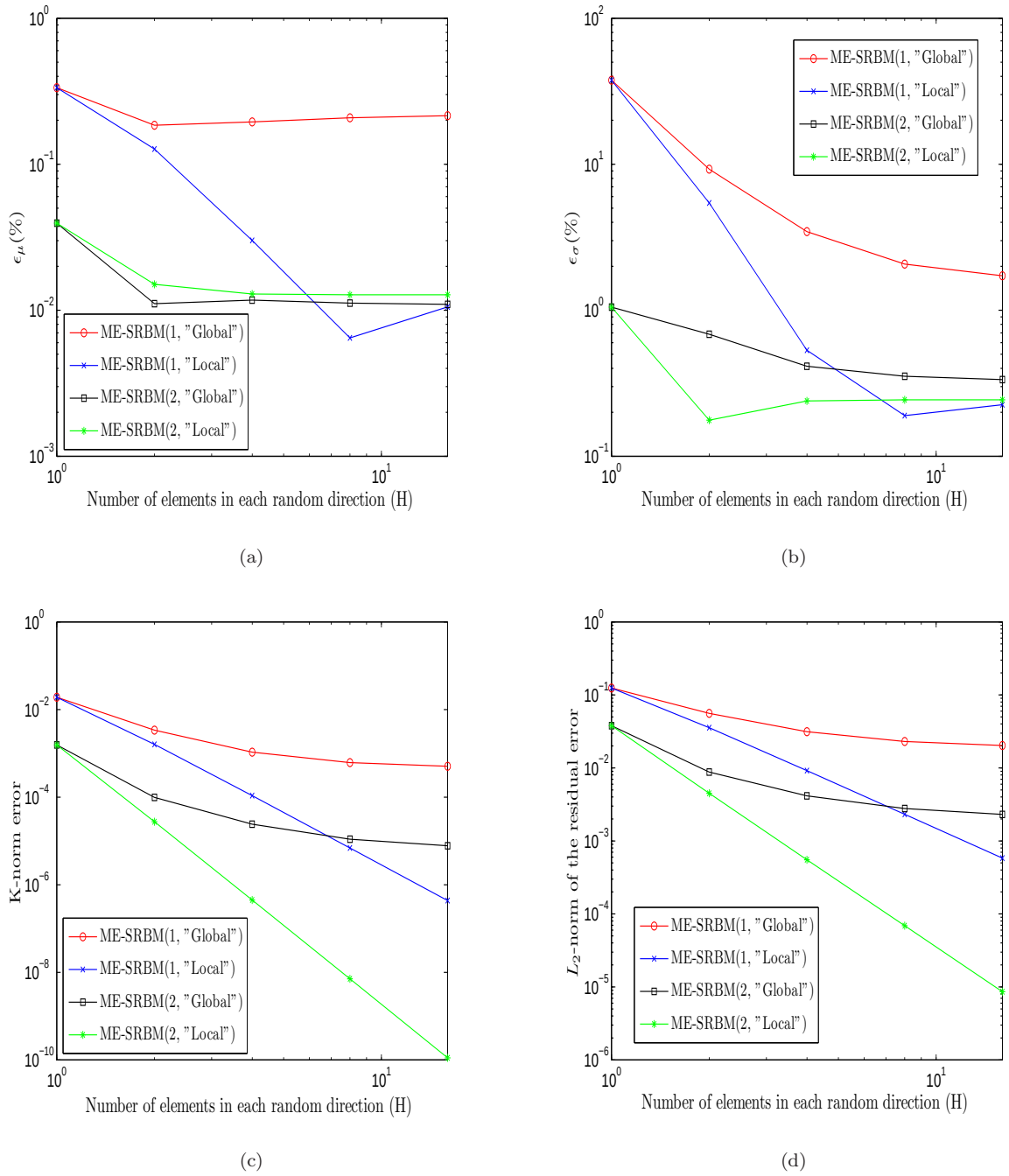

FIGURE 3.6: Convergence trends on the steady state heat transfer problem on a square domain: (a) Percentage norm relative error in mean (ϵ_μ from Equation 2.33) (b) percentage norm relative error in standard deviation (ϵ_σ from Equation 2.33) (c) $\mathbf{K}$-norm error and (d) norm of residual error using up to 2 basis vectors as a function of number of subdomains (H) and different preconditioners when only four terms are retained in the KL expansion.

single element case which corresponds to the standard SRBM formulation) as the number of random elements is increased. Also local preconditioning results in faster convergence of the error in standard deviation as compared to global preconditioning. It is also worth noting that for certain number of random elements (H), the local preconditioning strategy is as good as the strategy employing a higher number of basis vectors with global preconditioning. The above mentioned figures also show a consistent drop in **K**-norm error and residual error norm as the number of random elements is increased. Accelerated convergence is observed with both metrics for ME-SRBMs with local preconditioning. Recall that the Galerkin projection scheme imposed here minimizes an energy norm or the **K**-norm error and its convergence is guaranteed due to Theorem 3. On the other hand, the decrease in residual error may not be strictly monotonic as the number of subdomains is increased for any type of preconditioner used. Similarly no guarantees exist for the strict non-increasing nature of norm relative error in mean and standard deviation. The error metrics ϵ_μ, ϵ_σ and residual error norm have been plotted to demonstrate the accuracy achieved by the formulation at convergence.

Since the method works well for this simple problem, we move onto a more complex geometry with increased number of degrees of freedom. Further, this problem involves convective heat transfer boundary conditions instead of the Dirichlet and Neumann boundary conditions applied earlier.

3.3.3 Stochastic steady state heat transfer on a 2D HP turbine blade

In the high pressure (HP) stage or the first stage of a turbine, the blades are subjected to a high temperature flow due to the hot gases produced by the combustor. To counter the thermal stresses created by this high speed and temperature, the turbine blades are often internally cooled by pumping relatively cool air into the cooling holes. We consider the case when the conductivity of the material of a simplified turbine blade is represented by a random field. Note that this problem has been adapted from reference [81] where thermal analysis over an aerofoil has been performed subject to convective heat transfer boundary conditions.

Finite element mesh on a 2D blade profile is shown in Figure 3.7. We solve the heat transfer equation defined by Equation 5.1 with convective heat transfer boundary conditions. The heat transfer rate is given by

$$\overrightarrow{q} = -\kappa(x, y; \omega)\nabla u(x, y; \omega),$$

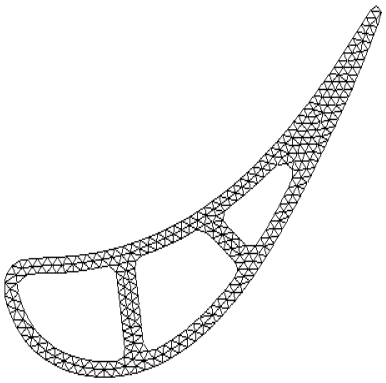

FIGURE 3.7: Finite element mesh on a 2D turbine blade profile.

where $\kappa(x, y; \omega)$ is the thermal conductivity of the blade material which in turn is a stochastic process with a certain probability distribution and the correlation function defined by Equation 3.18 with the mean field being $\bar{\kappa}(x, y; \omega) = 1$ and $u(x, y; \omega)$ is the temperature. The input standard deviation is fixed at $\sigma = 0.2$ and the correlation length (b) is considered to be unity. For the blade surface, the heat flux out of the blade is given by

$$\overrightarrow{q} \cdot \overrightarrow{n} = h_{ext}(u - u_{ext})$$

where $\overrightarrow{q} \cdot \overrightarrow{n}$ is the heat flux out of the blade, $\overrightarrow{n}$ is the unit normal out of the blade surface, h_{ext} is the external convective heat transfer coefficient and u_{ext} is the temperature of the flow external to the blade. Similarly, the heat flux into the cooling passage is given by

$$\overrightarrow{q} \cdot \overrightarrow{n} = h_{int}(u - u_{int})$$

$\overrightarrow{n}$ is still out of the blade i.e., into the cooling passage, h_{int} and u_{int} are the internal convective heat transfer coefficient and the temperature of the flow in the cooling passage respectively. The dimensions of the blade are normalized using chord length (L) during meshing. Hence $\frac{x}{L}$ and $\frac{y}{L}$ are the coordinates of the grid. The temperatures of flow on the boundaries are $u_{ext} = 1300^{\circ}\ C$ and $u_{int} = 200^{\circ}\ C$. The convective heat transfer coefficients in non-dimensional form are given by

$$\frac{h_{ext}L}{\bar{\kappa}(x, y; \omega)} = 14.0 \quad , \frac{h_{int}L}{\bar{\kappa}(x, y; \omega)} = 4.7.$$

The mean and standard deviation of the temperature distribution on the blade obtained using MCS with 50,000 samples are shown in Figure 3.8. The convergence trends for the case when 2 and 4 terms are retained in the KL expansion of the conductivity field are

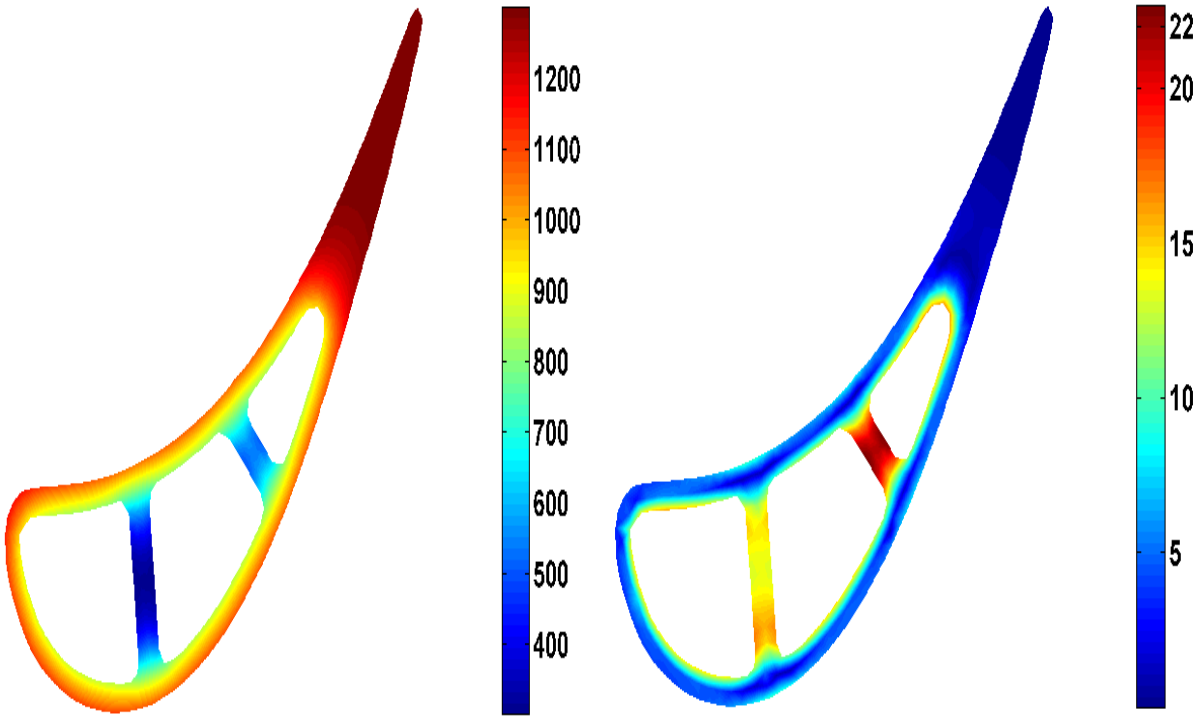

(a) (b)

FIGURE 3.8: (a) Mean and (b) standard deviation of the temperature distribution over the turbine blade.

shown in Figure 3.9 and Figure 3.10, respectively. Similar to the observations made in the preceding numerical example, the figures show that the error in standard deviation decreases (as compared to the single-element case) consistently as the number of random elements is increased. Also local preconditioning results in a faster convergence of the error in standard deviation as compared to global preconditioning. The above mentioned figures also show a consistent drop in **K**-norm error and residual error norm as the number of random elements is increased. Accelerated convergence is observed with both metrics when ME-SRBMs are used with local preconditioners. The **K**-norm error monotonically decreases in agreement with the theory for all the cases.

It has already been pointed out that global preconditioning results in a high degree of parallelization and faster speed of execution than an algorithm using local preconditioning as the former algorithm involves only $O(1)$ matrix inversion operations compared to the $O(H^d)$ inversion operations of the latter. But in general local preconditioners result in faster convergence. At this stage, it is not clear as to what preconditioning strategy is more efficient for a given problem and for a given degree of accuracy. In practice, the global preconditioning

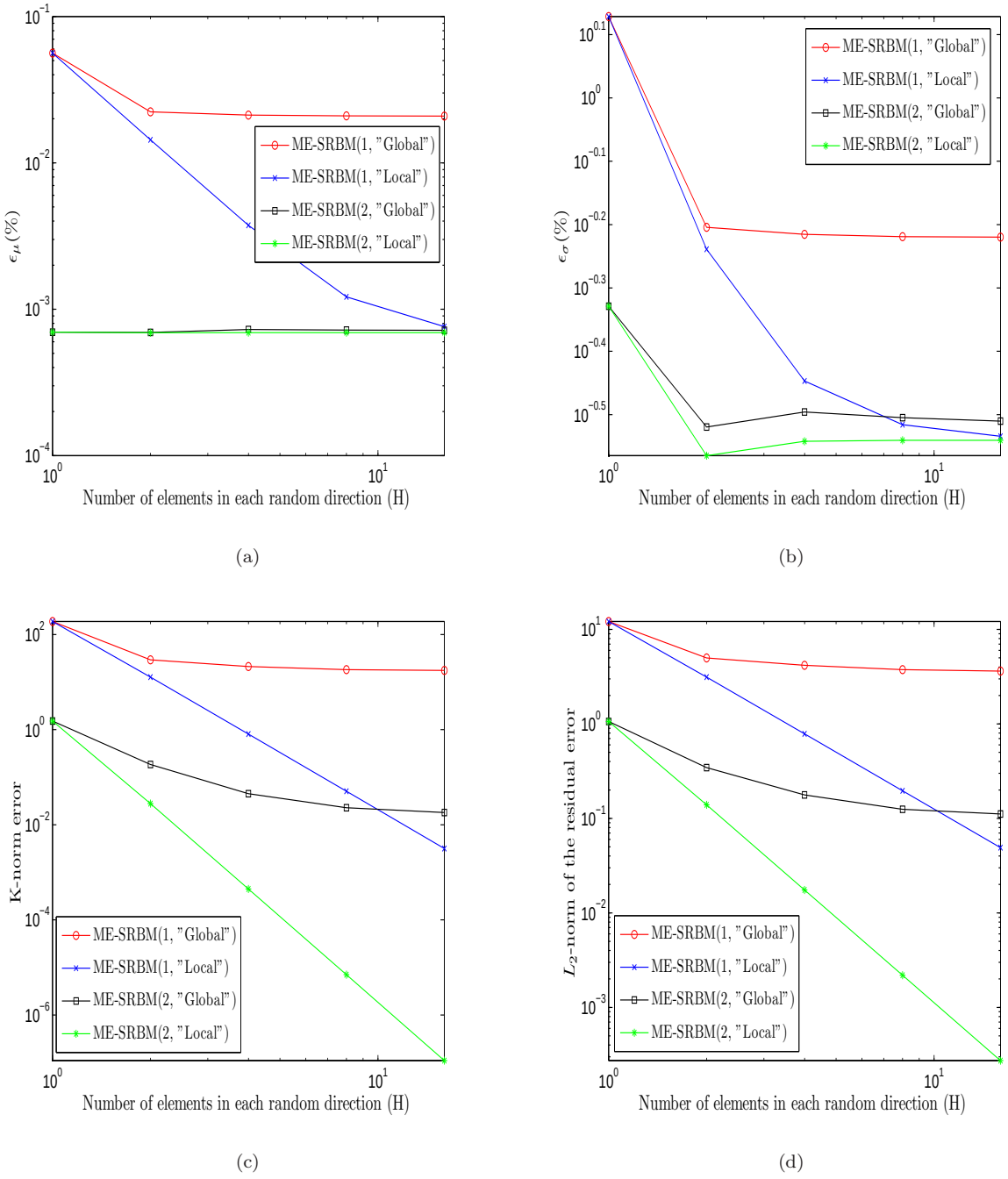

FIGURE 3.9: Convergence trends on the steady state heat transfer problem on the 2D profile of a gas turbine blade: (a) Percentage norm relative error in mean (ϵ_μ from Equation 2.33) (b) percentage norm relative error in standard deviation (ϵ_σ from Equation 2.33) (c) **K**-norm error (d) norm of residual error using up to 2 basis vectors as a function of number of subdomains (H) and different preconditioners when only two terms are retained in the KL expansion.

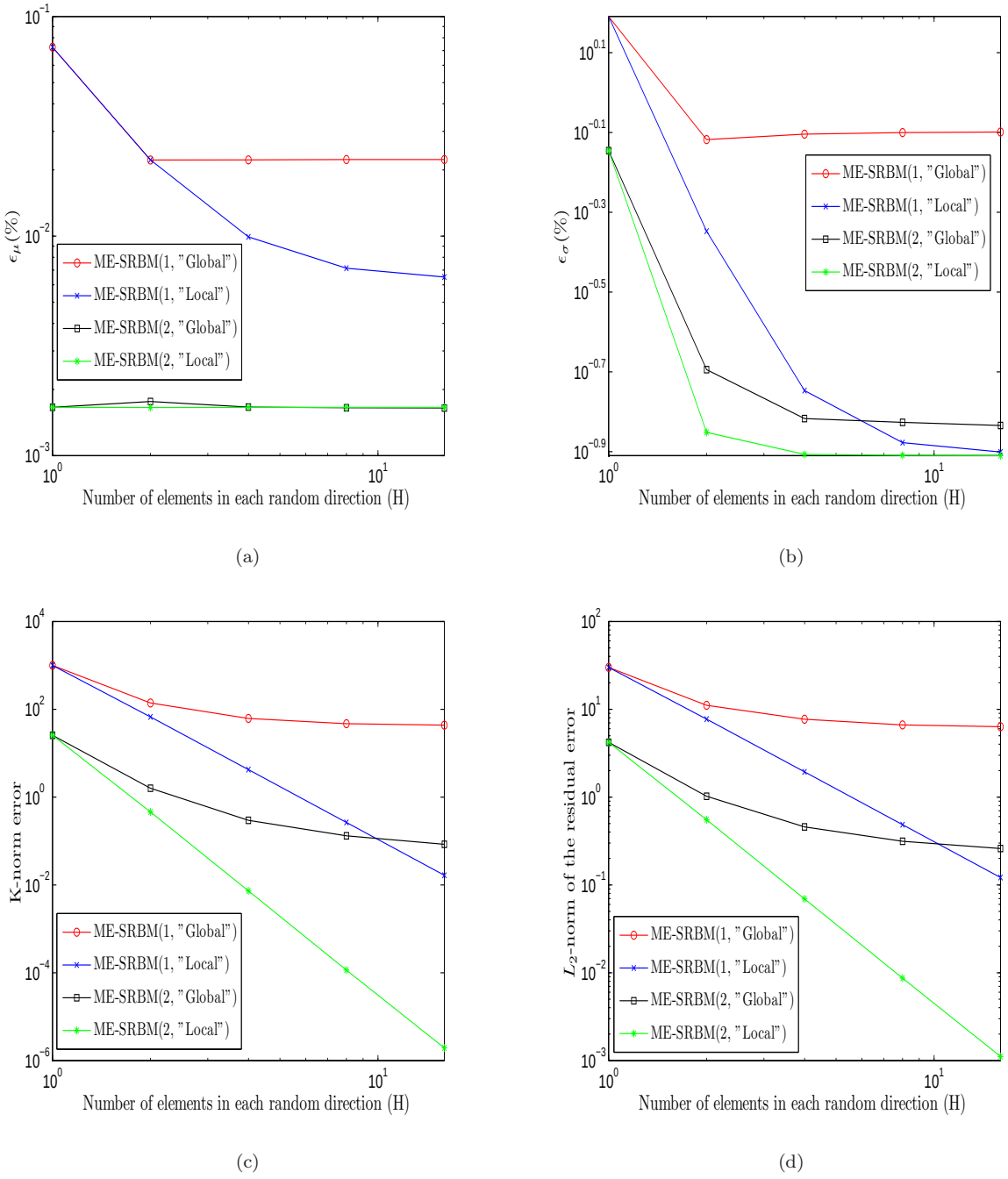

FIGURE 3.10: Convergence trends on the steady state heat transfer problem on the 2D profile of a gas turbine blade: (a) Percentage norm relative error in mean (ϵ_μ from Equation 2.33) (b) percentage norm relative error in standard deviation (ϵ_σ from Equation 2.33) (c) **K**-norm error (d) norm of residual error using up to 2 basis vectors as a function of number of subdomains (H) and different preconditioners when only four terms are retained in the KL expansion.

strategy is computationally efficient for large scale problems with many random variables.

3.4 Summary

In this chapter, we proposed a multi-element formulation of stochastic reduced basis projection schemes for solving linear random algebraic systems of equations arising from discretization of stochastic partial differential equations. The objective of this work is to enhance the accuracy of SRBMs for a given number of basis vectors. This has been achieved by decomposing the random space into multiple subdomains and applying SRBMs to local partitions of the random space. The elemental or local statistics are subsequently assimilated to estimate the global statistics. Numerical studies indicate that ME-SRBMs provide more accurate statistics compared to standard single-element SRBMs. In contrast to p-refinement, the h-refinement strategies proposed here (ME-SRBMs) admit a large degree of parallelization. Although, ME-SRBMs are conceptually simple and offer improved accuracy, they suffer from the *curse of dimensionality* since H^d local decoupled systems of equations need to be solved if a random space of d dimensions is decomposed into H subdomains along each dimension. This number rapidly blows into unrealistic proportions for problems with many uncertain variables. It is expected that the incorporation of adaptive domain decomposition schemes will alleviate this problem to some extent.

ME-SRBMs can be used to improve the accuracy of SRBM approximations for large scale problems with a large degree of input uncertainty where p-refinement may be computationally prohibitive. Adaptive strategies can be formulated based on ME-SRBMs in order to improve the accuracy of solution process for a fixed number of SRBM basis vectors. We discuss possible adaptive strategies employing ME-SRBMs in the remaining chapters.

Chapter 4

Finite element methods for PDEs on random domains

In the previous chapter, reduced order basis methods have been applied to solve SPDEs involving uncertainties in constitutive laws. In this chapter, we propose a novel methodology to tackle deterministic or stochastic PDEs defined on stochastic domains which we refer to as geometrical uncertainty. Geometrical uncertainties arise in natural and engineering systems due to a number of reasons, including measurement errors, lack of information, manufacturing variability, thermal effects or wear occurring in service.

Tackling material uncertainty is relatively straight-forward and simple compared to the multi-fold challenges posed by solving geometrical uncertainty problems especially for multiply connected complex geometries.

Some of the earlier attempts to represent geometric variability were based on simplified, deterministic surface inhomogeneities. Symmetrical aspersions are used in [82, 83] to represent surface indentations while semispheres were used to represent protrusions in [84]. Sinusoidal undulations and periodic non-linearities represent more general forms of surface roughness that have been used in the literature e.g. [85, 86]. Fractal representations of geometrical variability have also been proposed in the literature, e.g., deterministic approaches (Von Koch's [87, 88] fractals, Minkowski's fractals) and their random generalizations. Much of the work on statistical characterization of response in the presence of geometric uncertainty is based on the application of simulation techniques, sensitivity-based approaches and response surface methodology; see, for example, references [89–92].

More recently, some studies have focused on the development of numerical methods for

directly solving the governing PDEs given general statistical descriptions of geometric uncertainty. Such strategies are attractive since they potentially offer better efficiency and faster convergence rates compared to simulation techniques. Canuto and Kozubek [93] proposed a fictitious domain approach where the original PDE is transformed into a saddle point problem in a so-called fictitious domain and the boundary condition on the stochastic boundary is enforced via a Lagrangian multiplier. Honda [94] proposed a spectral stochastic boundary element method to deal with statistical descriptions of geometric uncertainty. This approach employs a Taylor series expansion to express the dependence of the boundary element matrices on the uncertain geometric parameters. The resulting linear random algebraic system of equations are solved using the Ghanem-Spanos polynomial chaos (PC) projection scheme [39]. Harbrecht et al [95] proposed a perturbation based second moment formalism to deal with PDEs on random domains assuming normal perturbations with small amplitudes. Nouy et al [96] employed an extended stochastic finite element method for this class of problems where the random geometries have an explicit representation in terms of random level-set functions. Subsequent analysis is performed by Galerkin projection at stochastic and deterministic levels.

Xiu and Tartakovsky [97, 98] proposed a novel methodology to tackle surface roughness and geometrical uncertainties. The surface roughness was represented by random fields and the original deterministic/stochastic PDE with stochastic boundary transformed into a stochastic PDE (SPDE) over a deterministic domain using stochastic mappings. This transformation enables the use of existing numerical techniques for solving SPDEs on deterministic domains such as stochastic projection schemes based on Weiner-Askey PC expansions [64] or stochastic Krylov methods [76]. However, it is worth noting here that the transformed stochastic equations may be more complicated than the original governing equations and existing analysis codes cannot be directly reused.

In the present chapter, we propose an approach for solving deterministic/stochastic PDEs defined on domains with random boundaries that allows existing *deterministic* finite element formulations (which is henceforth referred to as nonintrusive formulations) to be leveraged. The central idea is to work with mesh-based representations of random geometries, where the connectivity information is deterministic but the coordinates of the mesh nodes are random. This stochastic mesh-based representation of random domains is arrived at by solving an auxiliary PDE with appropriate random boundary conditions. Mesh deformation strategies has been employed previously in the literature [92, 99, 100] to deal with geometric uncertainty

problems in the context of Monte-Carlo simulations and response surface methods. However, the focus of the present work is to propound a theoretical analysis on the conditions that the geometric uncertainty model must satisfy in order to ensure well-posedness. In addition, we prove an equivalence between the proposed approach and the Xiu-Tartakovsky method. The advantages offered by the proposed formulation are outlined below:

- ⋆ The underlying governing equations do not change in contrast to the Xiu-Tartakovsky method thus enabling the reusabililty of existing *deterministic* formulations.
- ⋆ Adaptive sparse quadrature formulations can be efficiently leveraged by employing the element level collocation variant of the current formulation, thereby enabling a high degree of parallelizability.
- ⋆ Admissible boundary perturbations are verifiable apriori.
- ⋆ The wealth of knowledge available on mesh deformation strategies can be leveraged when dealing with high geometric variabilities.
- ⋆ If the statistics on an unperturbed landmark on the nominal geometry is the subject of interest, it can be handled by the method by fixing the particular nodes on the geometry during mesh deformation.

Discretization of the governing SPDE on a random mesh with fixed connectivity and random mesh coordinates subsequently leads to a linear random algebraic system of equations which can be solved for the response statistics using a wide variety of methods such as PC projection schemes [3, 39, 40, 64], reduced-order projection schemes [60, 61, 63], sparse quadrature schemes [18] and generalized spectral decomposition methods [54, 55].

The remainder of the chapter is organized as follows. A model boundary value problem on a random domain is introduced in the next section. Section 4.2 describes the random domain representation in continuum sense employed by the Xiu-Tartakovsky method and discrete sense considered in the current formulation. Section 4.3 deals with spatial discretization of the governing PDEs. Numerical studies on three model problems are presented and the convergence trends of the proposed approach are studied in Section 4.4. We conclude the chapter in the final section and highlight some directions for further work.

4.1 Problem definition

Geometrical uncertainties arise in many biological, geotechnical and engineering applications where the phenomenon under question is defined over random domains bounded by random boundaries. Random boundaries can be represented using level-set functions as in [96] where the boundary is expressed as

$$\partial D(\omega) = \{\mathbf{x}|\ r(\mathbf{x};\omega) = 0, \omega \in \Omega\},$$

where the level-set function $r(\mathbf{x};\omega)$ is generally taken as the signed distance function to the hypersurface: $r(\mathbf{x},\omega) = \pm\ distance(\mathbf{x}, \partial D(\omega))$. Here $(\Omega, \mathcal{F}, \mathcal{P})$ denotes a probability space, where Ω is a set of events, $\mathcal{F}$ is the σ-algebra associated with Ω and $\mathcal{P}$ is a probability measure. However, a level set representation of random boundaries can be readily computed only for simple geometrical entities such as a circle, ellipse, sphere, etc. To model complicated random geometries using level-set representations, more sophisticated schemes such as those proposed in [101] are required. In the present work, we consider a more general model for representing uncertain boundaries which is described in detail below.

Real-life geometric uncertainty applications are complex and arise in a number of engineering and biomedical applications where a finite number of image/measurement samples are available from Coordinate Measurement Machines (CMM), X-ray scans, Computerized Tomography (CT) scans and Magnetic Resonance Imaging data [102–105]. A reduced order model of the boundary variability can be constructed from the boundary ensemble data using Principal Component Analysis (PCA) [106]. The truncated PCA representation of the ensemble data can be written in the general form:

$$\left\{ \begin{array}{c} x_1 \\ x_2 \\ x_3 \end{array} \right\} + \sum_{i=1}^{d} \theta_i(\omega) \boldsymbol{\varphi}_i(x_1, x_2, x_3), \forall \omega \in \Omega \text{ and } (x_1, x_2, x_3) \in \partial D_0. \tag{4.1}$$

where ∂D_0 represents the nominal boundary, $\{\boldsymbol{\varphi}_i(x_1, x_2, x_3)\}$ are the vector-valued PCA eigenfunctions and $\{\theta_i\}_{i=1}^{d}$ are uncorrelated random variables. In the analysis that follows we make the stronger assumption that $\{\theta_i\}_{i=1}^{d}$ are statistically independent. This assumption is not limiting since in practice we can express the original variables in terms of independent random variables using a polynomial chaos expansion in conjunction with the Bayesian estimation approach proposed by Ghanem and Doostan [107].

Henceforth, for simplicity of notation, we use $\mathbf{x} = (x_1, x_2, x_3)$ and $\boldsymbol{\xi} = (\xi_1, \xi_2, \xi_3)$ to denote the coordinate system of the nominal and random domains, respectively. As a result

the random boundary can be compactly rewritten as

$$\partial D(\omega) = \{\mathbf{x} + \boldsymbol{\kappa}(\mathbf{x}, \omega) : \partial D_0 \times \Omega \to \mathbb{R}^3 | \mathbf{x} \in \partial D_0\}, \tag{4.2}$$

where $\boldsymbol{\kappa}(\mathbf{x}, \omega) : \partial D_0 \times \Omega \to \mathbb{R}^3$ is a vector valued random field whose components along the x_1, x_2, x_3 directions κ_{x_1}, κ_{x_2} and κ_{x_3} are zero-mean random fields. This random boundary description is general in scope, tractable and applicable to a number of real-life geometric uncertainty applications.

We illustrate our approach using the Poisson equation defined on a three-dimensional random domain. To begin with, consider the Poisson equation on a deterministic domain D_0 given below:

$$\begin{aligned} \nabla^2_{\mathbf{x}} v(\mathbf{x}) &= a(\mathbf{x}) \quad \text{in } D_0, \\ \mathcal{B}u(\mathbf{x}) &= b(\mathbf{x}) \quad \text{on } \partial D_0, \end{aligned} \tag{4.3}$$

where $\mathcal{B}$ is a boundary operator and the subscript on the ∇ operator denotes derivative with respect to that particular coordinate system. We assume that $a \in C^\infty(D_0)$, $b \in C^\infty(\partial D_0)$ and ∂D_0 is C^∞ which implies $u \in C^\infty(\overline{D_0})$. We assume that the reference domain D_0 is a bounded subdomain of $\mathbb{R}^3$ with sufficiently smooth, closed, orientable manifold as boundary $\partial D_0 \in C^p, p > 2$.

Now the deterministic Poisson equation on a stochastic domain can be posed as

$$\begin{aligned} \nabla^2_{\boldsymbol{\xi}} v(\boldsymbol{\xi}) &= a(\boldsymbol{\xi}) \quad \text{in } D(\omega), \\ \mathcal{B}v(\boldsymbol{\xi}) &= b(\boldsymbol{\xi}) \quad \text{on } \partial D(\omega), \end{aligned} \tag{4.4}$$

subject to $\omega \in L_2(\Omega, \mathcal{F}, \mathcal{P})$. We now state the condition under which the stated boundary uncertainty model (4.2) results in a well-posed problem for the Poisson equation defined on the random domain. For some vector valued stochastic function $\boldsymbol{\kappa}(\mathbf{x}, \omega) \in L^2(\Omega, C^p(\partial D_0))$, we consider the family of surfaces $\partial D = \{\mathbf{x} + \boldsymbol{\kappa}(\mathbf{x}, \omega) : \partial D_0 \times \Omega \to \mathbb{R}^3 | \mathbf{x} \in \partial D_0\} \in C^{p-1}(\partial D_0, \mathbb{R})$ where $\boldsymbol{\kappa}(\mathbf{x}, \omega)$ is a vector valued random field whose components along the x_1, x_2, x_3 directions are zero-mean random fields by construction, i.e., $\langle \kappa_{x_i} \rangle = 0, \forall i = \{1, 2, 3\}$. With the representation of the uncertain boundary in place, we focus on the problem of random domain representation in the next section.

4.2 Random domain representation

Given the random boundary representation (4.2), we now seek an appropriate representation for the stochastic domain D. This is performed by mapping the stochastic domain onto

the deterministic domain (or a nominal domain) denoted by D_0. This step can be either performed in a continuum sense as presented in [97, 98] or in a discrete sense using a stochastic mesh deformation strategy as presented here. We shall show later in this chapter that both approaches are mathematically equivalent.

4.2.1 Mapping in continuum sense

We now briefly outline the Xiu-Tartakovsky method [97, 98] for solving PDEs defined over random domains. We approach the derivation using the notion of covariant and contravariant metric tensors [108]. The random domain $D(\omega) \subset \mathbb{R}^3$ is mapped on to the deterministic domain $D_0 \subset \mathbb{R}^3$ using the bijective mapping function $\mathbf{x} = \mathbf{x}(\boldsymbol{\xi}, \omega)$ whose inverse is defined as $\boldsymbol{\xi} = \boldsymbol{\xi}(\mathbf{x}, \omega)$. Here $\mathbf{x}$ denotes the coordinate system of the deterministic domain D_0. The mapping can be represented as

$$\boldsymbol{\xi} \in D(\omega) \leftrightarrow \mathbf{x} \in D_0 \tag{4.5}$$

The stochastic mapping (4.5) of $D(\omega)$ on to the deterministic domain D_0 can be constructed via solutions of an operator problem (such as the Laplace equation, biharmonic equation or the elasticity equations) with appropriate boundary conditions. In [97], the Laplace equation was solved to compute the mapping function, i.e.,

$$\nabla^2_{\mathbf{x}} \boldsymbol{\xi} = 0 \text{ in } D_0,$$

with appropriate random Dirichlet boundary conditions dictated by the boundary uncertainty model.

The Jacobian of the stochastic to deterministic coordinate transformation can be defined as $\mathbf{J} := \left(\frac{\partial \xi_j}{\partial x_i}\right)_{ij}$. The mapping is bijective if $\mathbf{J}$ is invertible which translates to the determinant of the transformation Jacobian not vanishing anywhere in D_0. The covariant metric tensor of the coordinate transformation can then be defined as [108, 109]

$$\mathbf{G} = \mathbf{J}\mathbf{J}^T. \tag{4.6}$$

The coordinate mapping (4.5) transforms the original Poisson equation defined over a random domain presented in (4.4) into a stochastic Poisson equation on the deterministic domain D_0. The transformed operator problem can be stated as: for $\mathcal{P}$-almost everywhere $\omega \in \Omega, a' \equiv a(\mathbf{x}(\boldsymbol{\xi})) : D_0 \times \Omega \to \mathbb{R}$, find $u : D_0 \times \Omega \to \mathbb{R}$ such that

$$\frac{1}{\sqrt{g}} \sum_{i=1}^{3} \sum_{j=1}^{3} \frac{\partial}{\partial x_i} \left(\sqrt{g} g^{ij} \frac{\partial u}{\partial x_j} \right) = a'(x, \omega), \tag{4.7}$$

with the corresponding transformed boundary conditions. This equation is provably equivalent to the transformed Poisson equation presented in [97] when the Jacobi of transformation is computed as given in [97]. In the preceding equation, g is the determinant of the covariant metric tensor $\mathbf{G}$ defined in (4.6). Here each element of $\mathbf{G}$ is given by g_{ij} and g^{ij} are defined as follows

$$g^{ij} = \frac{G^{ij}}{g},$$

where G^{ij} is the cofactor of the g_{ij} in the determinant g. Note that $g \equiv g(\mathbf{x}, \omega)$ and $g^{ij} \equiv g^{ij}(\mathbf{x}, \omega)$ in (4.7) and we use this dependence in a later section. A detailed derivation of the transformed SPDE is presented for the two-dimensional Poisson equation in Appendix A.

Now we state classical results dealing with the ellipticity and existence of a weak solution of the transformed SPDE model (4.7); the interested reader is referred to [110] for detailed proofs of these results.

Lemma 1: *The transformed PDE* (4.7) *is elliptic iff the following condition is satisfied:*

$$\boldsymbol{\zeta}^T \mathbf{A}(\mathbf{x}, \omega)\boldsymbol{\zeta} > 0, \mathcal{P}-\text{almost surely}, \tag{4.8}$$

where $\mathbf{A}(\mathbf{x}, \omega)$ *is a* 3×3 *matrix with the components* $-\sqrt{g}g^{ij}$, $\forall \mathbf{x} \in D_0, \omega \in \Omega$ *and* $\boldsymbol{\zeta} \neq \mathbf{0} \in \mathbb{R}^3$. *Also a unique weak solution exists for the transformed problem if* $\sqrt{g}g^{ij}$ *and its first order derivatives lie in* $L_\infty(D_0) \times L_2(\Omega)$ $\mathcal{P}$*-almost surely.*

We wish to highlight here that although the continuum mapping approach was illustrated for the Poisson equation, the same principles can be used for more general PDE models.

4.2.2 Mapping in discrete sense

We now focus on constructing a stochastic mesh representation of random domains wherein the connectivity of the mesh is deterministic but the coordinates of the nodes are random variables. The nominal domain of definition D_0 is assumed to be discretized using a good quality mesh. Given a random domain D bounded by a stochastic boundary ∂D, we can map the mesh of the nominal domain onto the random domain $D(\omega)$ using a standard mesh deformation strategy based on the Laplace, biharmonic, linear elasticity or spring analogy based equations; see, for example, [111–117]. The central idea is to solve an auxiliary PDE with appropriate random boundary conditions to establish a relationship between the coordinates of the mesh nodes and the underlying random variable vector $\boldsymbol{\theta}$ defined in equation (4.1).

Mesh perturbation or grid deformation algorithms have been applied to a wide range of applications including shape design optimization, deformation of movable interfaces between

immiscible fluids and aeroelastic simulation of wings. Mesh deformation algorithms fail due to generation of elements with negative areas and volumes [113, 114]. These element reversals or flips are caused when nodes pass other nodes or edges. A target mesh with no element flips is called a *valid mesh*, which can be formally defined as follows [113]:

Definition: A *valid mesh* is a mapping $\eta(\mathbf{x})$ from D_1 to $D_2 = \{\mathbf{y}|\mathbf{y} = \eta(\mathbf{x})\forall \mathbf{x} \in D_1\}$, such that $\eta(\mathbf{x_1}) = \eta(\mathbf{x_2})$ iff $\mathbf{x_1} = \mathbf{x_2}$.

To illustrate, let us consider the case when the Laplace equation based mesh deformation strategy is employed. In the Laplace equation based mesh deformation strategy, we solve the following three (along each spatial dimension) decoupled random Dirichlet problems to deform the baseline mesh

$$\begin{aligned} \nabla^2_{\mathbf{x}}\xi_i &= 0 && \text{in } D_0, \forall i = \{1,2,3\} \\ \xi_i &= (x_i + \kappa_{x_i}(\mathbf{x},\omega)) && \text{on } \partial D_0. \end{aligned} \tag{4.9}$$

It can be noted that given a finite-dimensional representation of the random fields κ_{x_1}, κ_{x_2}, and κ_{x_3} in terms of the random variable vector $\boldsymbol{\theta}$, numerical solution of the preceding equation provides a relationship between the coordinates of the mesh nodes and $\boldsymbol{\theta}$. It is also possible to use other approaches, for example, the Navier-Lamé equations to deform the baseline mesh [117]. We employ the Navier-Lamé equation based mesh deformation approach in the 3D numerical study discussed in Section 4.4.2.2.

In what follows, we present further analysis using the Laplace equation based stochastic mesh deformation strategy, where a finite element (FE) discretization is employed to solve (4.9). It is important to note here that the overall approach and the main theoretical results derived here remain valid for alternative mesh deformation strategies. The nominal domain D_0 is divided into elements with shape functions $\{N_i\}$ defined over the nodes of the elements with the properties $N_j(\mathbf{x}^j) = 1$ and $N_j(\mathbf{x}^k) = 0, \forall j \neq k$ where $\mathbf{x}^j$ represents the coordinates of the j^{th} vertex in the baseline mesh. Define a matrix $\mathbf{A}$ as:

$$\mathbf{A}(i,j) = \int_{D_0} \nabla \mathbf{N}_i \cdot \nabla \mathbf{N}_j \, \mathrm{d}\mathbf{x}.$$

The matrix $\mathbf{A}$ is sparse symmetric positive definite with nonzero entries corresponding to the pairs of neighboring nodes in the finite element mesh. Let $\mathbf{A}_I$ denote the submatrix of $\mathbf{A}$ whose rows and columns are indexed by the interior nodes and let $\mathbf{A}_B$ denote the submatrix of $\mathbf{A}$ whose rows are indexed by the interior nodes and whose columns are indexed by the boundary nodes. Let $\mathbf{z}$ be a vector consisting of the x_i coordinates and $\boldsymbol{\zeta}$ be a vector consisting of the ξ_i coordinates for all the nodes on the nominal mesh and the target perturbed mesh,

respectively, for some $i = \{1, 2, 3\}$.

The interior nodal coordinates along each spatial direction can be obtained as a solution to the following system of equations

$$\begin{aligned} \mathbf{A}_I \boldsymbol{\zeta}_I &= -\mathbf{A}_B \boldsymbol{\zeta}_B \\ &= -\mathbf{A}_B \big(\mathbf{z}_B + \boldsymbol{\kappa}_{x_i}(\boldsymbol{\theta}) \big), \end{aligned}$$

where the subscripts I and B denote the interior and boundary nodes, respectively, and $\boldsymbol{\kappa}_{x_i}$ represents the vector consisting of the function κ_{x_i} (component of the vector valued random field $\boldsymbol{\kappa}(\mathbf{x}, \boldsymbol{\theta})$ along the i^{th} spatial direction) sampled over the boundary nodes $\mathbf{x}_B$. The preceding linear algebraic system of equations with random right hand side can be solved to obtain the coordinates of the interior mesh nodes $\boldsymbol{\zeta}_I$ along each spatial direction as a function of $\boldsymbol{\theta}$.

Note that $\mathbf{A}$ is implicitly dependent on nodal shape functions and hence on the nominal mesh. Further, the mesh deformation is a function of the boundary perturbation $\boldsymbol{\kappa}(\mathbf{x}, \boldsymbol{\theta})$, a d-dimensional random field. For any given realization $\boldsymbol{\theta}^{(k)} \in \mathbb{R}^d$, the deformed grid is a mapping from D_0 to $D(\boldsymbol{\theta}^{(k)})$ such that

$$D(\boldsymbol{\theta}^{(k)}) = \{\boldsymbol{\xi} | \boldsymbol{\xi} = \eta(\mathbf{x}) + \boldsymbol{\gamma}(\eta(\mathbf{x}), \boldsymbol{\theta}^{(k)}) \forall \mathbf{x} \in D_0\},$$

where $\eta(\mathbf{x})$ represents the mesh on the nominal domain D_0 and $\boldsymbol{\gamma}(\eta(\mathbf{x}), \boldsymbol{\theta}^{(k)})$ is the vector-valued deformation field applied to the nominal mesh.

For simplicity of notation, for any random realization $\boldsymbol{\theta}^{(k)} \in \mathbb{R}^d$, let $\mathbf{s}$ denote the grid perturbation direction given by $\frac{\boldsymbol{\gamma}(\eta(\mathbf{x}), \boldsymbol{\theta}^{(k)})}{\|\boldsymbol{\gamma}(\eta(\mathbf{x}), \boldsymbol{\theta}^{(k)})\|}$ where $||\boldsymbol{\gamma}(\eta(\mathbf{x}), \boldsymbol{\theta}^{(k)})||$ denotes the magnitude of perturbation. Thus for any realization, $\boldsymbol{\theta}^{(k)} \in \mathbb{R}^d$, a grid perturbation can be denoted as $\eta(\mathbf{x}) + \mathbf{s}||\boldsymbol{\gamma}(\eta(\mathbf{x}), \boldsymbol{\theta}^{(k)})||$. Note that $\mathbf{s}$ is defined *realization-wise* and hence represents a point-wise deterministic vector. We use $\mathbf{s}$ extensively in the following lemma which establishes the condition under which mesh deformation results in a *valid mesh*. The result presented below uses the analysis of Burg [113] to establish conditions that the boundary uncertainty model must satisfy in order to ensure that all realizations of the stochastic mesh representation are valid meshes.

Lemma 2: *For any realization $\boldsymbol{\theta}^{(k)} \in \mathbb{R}^d$, a randomly deformed mesh is a valid mesh if and only if $\nabla \parallel \boldsymbol{\gamma}(\eta(\mathbf{x}), \boldsymbol{\theta}^{(k)}) \parallel \cdot \mathbf{s} \neq -1, \forall \mathbf{x} \in D_0$, where $\parallel \boldsymbol{\gamma}(\eta(\mathbf{x}), \boldsymbol{\theta}^{(k)}) \parallel$ is the perturbation magnitude and $\mathbf{s}$ is the perturbation direction with $\parallel \mathbf{s} \parallel = 1$.*

Proof: For any realization $\boldsymbol{\theta}^{(k)} \in \mathbb{R}^d$ and any given point $\mathbf{x} \in D_0$ and a deformation direction, $\mathbf{s}$, restrict $\boldsymbol{\xi}$ to the space such that $\eta(\boldsymbol{\xi}) = \eta(\mathbf{x}) + t\mathbf{s}$. Assume that the deformed

mesh is valid which implies that $\eta(\mathbf{x}) + \mathbf{s} \parallel \boldsymbol{\gamma}(\eta(\mathbf{x}), \boldsymbol{\theta}^{(k)}) \parallel = \eta(\boldsymbol{\xi}) + \mathbf{s} \parallel \boldsymbol{\gamma}(\eta(\boldsymbol{\xi}), \boldsymbol{\theta}^{(k)}) \parallel$ iff $\mathbf{x} = \boldsymbol{\xi}$. Hence $\mathbf{x} \neq \boldsymbol{\xi}$ iff $\eta(\mathbf{x}) + \mathbf{s} \parallel \boldsymbol{\gamma}(\eta(\mathbf{x}), \boldsymbol{\theta}^{(k)}) \parallel \neq \eta(\boldsymbol{\xi}) + \mathbf{s} \parallel \boldsymbol{\gamma}(\eta(\boldsymbol{\xi}), \boldsymbol{\theta}^{(k)}) \parallel$. Subtracting both sides with $\eta(\mathbf{x})$ and taking the dot product with $\mathbf{s}$ results in

$$\begin{aligned}
(\eta(\mathbf{x}) + \mathbf{s} \parallel \boldsymbol{\gamma}(\eta(\mathbf{x}), \boldsymbol{\theta}^{(k)}) \parallel - \eta(\mathbf{x})) \cdot \mathbf{s} &\neq (\eta(\boldsymbol{\xi}) + \mathbf{s} \parallel \boldsymbol{\gamma}(\eta(\boldsymbol{\xi}), \boldsymbol{\theta}^{(k)}) \parallel - \eta(\mathbf{x})) \cdot \mathbf{s}, \\
\parallel \boldsymbol{\gamma}(\eta(\mathbf{x}), \boldsymbol{\theta}^{(k)}) \parallel &\neq (\eta(\boldsymbol{\xi}) - \eta(\mathbf{x})) \cdot \mathbf{s} + \parallel \boldsymbol{\gamma}(\eta(\boldsymbol{\xi}), \boldsymbol{\theta}^{(k)}) \parallel, \\
\parallel \boldsymbol{\gamma}(\eta(\mathbf{x}), \boldsymbol{\theta}^{(k)}) \parallel &\neq (\eta(\mathbf{x}) + t\mathbf{s} - \eta(\mathbf{x})) \cdot \mathbf{s} + \parallel \boldsymbol{\gamma}(\eta(\mathbf{x}) + t\mathbf{s}, \boldsymbol{\theta}^{(k)}) \parallel, \\
\parallel \boldsymbol{\gamma}(\eta(\mathbf{x}), \boldsymbol{\theta}^{(k)}) \parallel &\neq t + \parallel \boldsymbol{\gamma}(\eta(\mathbf{x}) + t\mathbf{s}, \boldsymbol{\theta}^{(k)}) \parallel,
\end{aligned}$$

which implies

$$\frac{\parallel \boldsymbol{\gamma}(\eta(\mathbf{x}) + t\mathbf{s}, \boldsymbol{\theta}^{(k)}) \parallel - \parallel \boldsymbol{\gamma}(\eta(\mathbf{x}), \boldsymbol{\theta}^{(k)}) \parallel}{t} \neq -1$$

which by taking the limit $t \to 0$ results in the following condition

$$\nabla \parallel \boldsymbol{\gamma}(\eta(\mathbf{x}), \boldsymbol{\theta}^{(k)}) \parallel \cdot \mathbf{s} \neq -1. \tag{4.10}$$

□

4.2.2.1 Remarks:

- ⋆ If the deformed mesh is valid then mesh deformation is an invertible operation.
- ⋆ This result is valid not just for Laplace based deformation but also for other mesh deformation strategies.
- ⋆ An important consequence of this result is that if the deformation direction is perpendicular to the gradient of deformation function, then an infinite amount of deformation is tolerated.
- ⋆ If a diffusion equation is employed for mesh deformation instead of the Laplace equation where the virtual diffusivity of each element is assumed to be inversely proportional to the element area/volume [116], mesh collapses or element flips can be alleviated to a large extent. There are various alternative strategies [113, 114] that can be adopted in situations where the Laplace equation based mesh deformation approach fails to create valid meshes. Note that Lemma 2 holds irrespective of the type of the mesh deformation strategy employed.

We have presented two strategies so far for mapping the random domain onto a deterministic nominal domain, i.e., in a continuum sense (Xiu-Tartakovsky method [97, 98]) and

in a discrete sense using stochastic mesh deformation algorithms. In the following section, we present details of spatial discretization aspects of the original governing PDEs using a stochastic mesh representation obtained by the discrete mapping approach.

4.3 Spatial discretization employing a stochastic mesh representation

Recall that in our approach we map the stochastic domain onto the deterministic domain by deforming the nominal mesh via the solution of an auxiliary operator equation such as the Laplace or elasticity equations. Thereby, the mesh connectivity remains the same but the mesh coordinates are expressed as functions of the random variable vector $\boldsymbol{\theta}$. If the perturbations are admissible (following Lemma 2) then a weak solution of the original governing equations (4.4) exists due to the Lax-Milgram lemma [110] since $D(\boldsymbol{\theta}) \subset \mathbb{R}^3$ is bounded with a closed, bounded and orientable manifold as a boundary for any realization of $\boldsymbol{\theta}$. As a consequence, the stochastic element stiffness matrix obtained from spatial discretization of the governing equations (4.4) on a stochastic mesh representation can be written in the form

$$\mathbf{K}^e(\boldsymbol{\theta}) = \int_{D^e(\boldsymbol{\theta})} \nabla_{\boldsymbol{\xi}} \mathbf{N}^T \nabla_{\boldsymbol{\xi}} \mathbf{N} \, \mathrm{d}\boldsymbol{\xi},$$

where the integration is performed over an element $D^e(\boldsymbol{\theta})$ whose nodal coordinates are random. This random element can be mapped onto the corresponding deterministic element in the mesh of the nominal domain D_0 using the Jacobian of transformation $\mathbf{J}$ computed as $\left(\frac{\partial \xi_i}{\partial x_j}\right)_{ij}$. Using the Jacobian of transformation, $\nabla_{\boldsymbol{\xi}} \mathbf{N}$ can be written as $\mathbf{J}^{-1} \nabla_{\mathbf{x}} \mathbf{N}$ and $\mathrm{d}\boldsymbol{\xi} = \sqrt{g} \, \mathrm{d}\mathbf{x}$ due to which the stochastic element stiffness matrix can be written as:

$$\begin{aligned} \mathbf{K}^e(\boldsymbol{\theta}) &= \int_{D_0^e} \nabla_{\mathbf{x}} \mathbf{N}^T \, {\mathbf{J}^{-1}}^T \mathbf{J}^{-1} \, \nabla_{\mathbf{x}} \mathbf{N} \, \sqrt{g} \mathrm{d}\mathbf{x} \\ &= \int_{D_0^e} \nabla_{\mathbf{x}} \mathbf{N}^T \, \mathbf{G}^{-1}(\boldsymbol{\theta}) \, \nabla_{\mathbf{x}} \mathbf{N} \, \sqrt{g}(\boldsymbol{\theta}) \mathrm{d}\mathbf{x}. \end{aligned} \tag{4.11}$$

Similarly the force vector can be written as

$$\mathbf{f}^e(\boldsymbol{\theta}) = \int_{D_0^e} a \mathbf{J}^{-1}(\boldsymbol{\theta}) \mathbf{N} \, \sqrt{g}(\boldsymbol{\theta}) \mathrm{d}\mathbf{x}. \tag{4.12}$$

As an aside, it can be shown that the stochastic element matrices obtained via finite element spatial discretization of the transformed SPDE (4.7) derived using the Xiu-Tartakovsky method [97, 98] are of the form given by (4.11) and (4.12) which is proved later in this section.

Now, $\mathbf{K}^e(\boldsymbol{\theta})$ and $\mathbf{f}^e(\boldsymbol{\theta})$ are second order stochastic processes and hence these terms admit PC expansions of the form

$$\mathbf{K}^e(\boldsymbol{\theta}) = \sum_{i=0}^{P_1} \mathbf{K}_i^e \phi_i(\boldsymbol{\theta}) \quad \text{and} \quad \mathbf{f}^e(\boldsymbol{\theta}) = \sum_{i=0}^{P_1} \mathbf{f}_i^e \phi_i(\boldsymbol{\theta}). \tag{4.13}$$

In practice, however, the PC expansion coefficients $\mathbf{K}_i^e$ and $\mathbf{f}_i^e$ are not easy to compute, particularly for complex finite element formulations. We shall return to the issue of efficient computation of the PC coefficients of the element matrices later in Section 4.1.

Assembly of the stochastic element matrices (4.13) and application of appropriate boundary conditions lead to a linear random algebraic system of equations of the form

$$\mathbf{K}(\boldsymbol{\theta})\mathbf{u}(\boldsymbol{\theta}) = \mathbf{f}(\boldsymbol{\theta}), \tag{4.14}$$

where $\mathbf{K}(\boldsymbol{\theta}) \in \mathbb{R}^{n\times n}$ and $\mathbf{f}(\boldsymbol{\theta}) \in \mathbb{R}^n$ are the global coefficient matrix and right hand side, respectively. $\mathbf{u}(\boldsymbol{\theta}) \in \mathbb{R}^n$ represents the solution process whose statistics are to be computed. Here n denotes the total number of degrees of freedom and as a result of finite element assembly $\mathbf{K}(\boldsymbol{\theta})$ and $\mathbf{f}(\boldsymbol{\theta})$ are given in a PC expansion as follows

$$\left.\begin{aligned} \mathbf{K}(\boldsymbol{\theta}) &= \sum_{i=0}^{P_1} \mathbf{K}_i \phi_i(\boldsymbol{\theta}) \\ \mathbf{f}(\boldsymbol{\theta}) &= \sum_{i=0}^{P_1} \mathbf{f}_i \phi_i(\boldsymbol{\theta}) \end{aligned}\right\}, \tag{4.15}$$

where $\{\phi_i(\boldsymbol{\theta})\}_{i=0}^{P_1}$ are PC basis functions and $\mathbf{K}_i$ and $\mathbf{f}_i$ are deterministic PC expansion coefficients. The coefficients in the global matrices given in (4.15) can be alternatively computed nonintrusively, the details of which can be found in the subsection 4.3.2. The linear random algebraic system of equations in a PC basis can be solved to approximate the solution statistics employing one of the methods proposed in [3, 39, 40, 63, 64].

4.3.1 Element-level formulation

The PC coefficients of the element matrices, namely $\mathbf{K}_i^e$ and $\mathbf{f}_i^e$ in (4.13), are not straightforward to compute for complex element formulations. This is because the terms $\mathbf{G}^{-1}(\boldsymbol{\theta})$, $\sqrt{g}(\boldsymbol{\theta})$ and $\mathbf{J}^{-1}(\boldsymbol{\theta})$ tend to be general nonlinear functions of $\boldsymbol{\theta}$. In such cases, the PC expansion coefficients of the element matrices can be computed nonintrusively using a stochastic mesh deformation algorithm and sparse quadrature schemes. For example, by leveraging the orthogonality of the PC basis functions, the PC expansion coefficient $\mathbf{K}_i^e$ can be computed

as

$$\mathbf{K}_i^e = \frac{\langle \mathbf{K}^e(\boldsymbol{\theta})\phi_i(\boldsymbol{\theta})\rangle}{\langle \phi_i^2(\boldsymbol{\theta})\rangle},\ \forall 0 \le i \le P_1.$$

The terms in the numerator can be evaluated using Monte-Carlo methods or sparse quadrature schemes. Sparse quadrature schemes based on Smolyak's construction have been extensively studied in the context of the so called stochastic collocation method [18–24]. Smolyak quadrature requires quadrature formulas $Q_1^{(i)}, Q_2^{(i)}, Q_3^{(i)}, \cdots$ in each dimension i. Assume that every formula $Q_l^{(i)}$ of level l exactly integrates polynomials of degrees not exceeding k_l (independent of i) with respect to the measure $\mathcal{P}$, with $k_{l+1} \ge k_l$. Additionally, assume that each $Q_l^{(i)}$ has the same number of nodes Z_l, where all lowest order methods use only one node, $Z_1 = 1$. The set of nodes used by $Q_l^{(i)}$ will be called $\Xi_l^{(i)} = \{\theta_{l,1}^{(i)}, \theta_{l,2}^{(i)}, \cdots, \theta_{l,Z_l}^{(i)}\}$ and the weights will be denoted by $w_{l,1}^{(i)}, w_{l,2}^{(i)}, \cdots w_{l,Z_l}^{(i)}$. For a function of m random variables $\boldsymbol{\psi}(\theta_1, \theta_2, \cdots, \theta_m)$, a sparse quadrature formula can be constructed as a tensor product of one-dimensional rules as follows:

$$\mathbf{Q_l} = Q_{l_1}^{(1)} \otimes Q_{l_2}^{(2)} \otimes \cdots \otimes Q_{l_m}^{(m)},$$

which can be applied to estimate the term $\langle \mathbf{K}^e(\boldsymbol{\theta})\phi_i(\boldsymbol{\theta})\rangle$ as follows

$$\langle \mathbf{K}^e(\boldsymbol{\theta})\phi_i(\boldsymbol{\theta})\rangle = \sum_{z_1=1}^{Z_{l_1}} \cdots \sum_{z_m=1}^{Z_{l_m}} w_{l_1,k_1}^{(1)} \cdots w_{l_m,z_m}^{(m)} \mathbf{K}^e(\theta_{l_1,z_1}^{(1)} \cdots \theta_{l_m,z_m}^{(m)})\phi_i(\theta_{l_1,z_1}^{(1)} \cdots \theta_{l_m,z_m}^{(m)}).$$

Similarly, $\mathbf{f}_i^e$ can be computed.

A key advantage of the element level formulation is that it allows for the possibility of large scale parallelization since the PC expansion coefficients corresponding to each element can be computed independently of each other. We discuss next a global formulation to compute the unknown coefficients in (4.15).

4.3.2 Global formulation

Instead of computing the element stiffness matrices in a PC basis as discussed in the previous section, we can compute the coefficients of expansion in (4.15) nonintrusively as follows:

$$\begin{aligned} \mathbf{K}_j &= \frac{\langle \mathbf{K}(\boldsymbol{\theta})\phi_j(\boldsymbol{\theta})\rangle}{\langle \phi_j^2(\boldsymbol{\theta})\rangle}, \\ \mathbf{f}_j &= \frac{\langle \mathbf{f}(\boldsymbol{\theta})\phi_j(\boldsymbol{\theta})\rangle}{\langle \phi_j^2(\boldsymbol{\theta})\rangle}. \end{aligned} \tag{4.16}$$

The denominators in the preceding equations can be easily calculated for any PC basis function; see, for example, references [39, 64]. The inner products in the numerators of

equation (4.16) can be approximated using a sparse quadrature rule as follows:

$$\langle \mathbf{K}(\boldsymbol{\theta})\phi_j(\boldsymbol{\theta})\rangle = \sum_{z_1=1}^{Z_{l_1}} \cdots \sum_{z_m=1}^{Z_{l_m}} w_{l_1,k_1}^{(1)} \cdots w_{l_m,z_m}^{(m)} \mathbf{K}(\theta_{l_1,z_1} \cdots \theta_{l_m,z_m})\phi_j(\theta_{l_1,z_1} \cdots \theta_{l_m,z_m}), \quad (4.17)$$

and

$$\langle \mathbf{f}(\boldsymbol{\theta})\phi_j(\boldsymbol{\theta})\rangle = \sum_{z_1=1}^{Z_{l_1}} \cdots \sum_{z_m=1}^{Z_{l_m}} w_{l_1,k_1}^{(1)} \cdots w_{l_m,z_m}^{(m)} \mathbf{f}(\theta_{l_1,z_1} \cdots \theta_{l_m,z_m})\phi_j(\theta_{l_1,z_1} \cdots \theta_{l_m,z_m}), \quad (4.18)$$

where $\boldsymbol{\theta}^{(k)}$ and w_k denote the quadrature points and weights, respectively. The kernel of the summation namely $\mathbf{K}(\theta_{l_1,z_1} \cdots \theta_{l_m,z_m})$ and $\mathbf{f}(\theta_{l_1,z_1} \cdots \theta_{l_m,z_m})$ on the other hand can be computed by repeatedly invoking the deterministic solver on the deformed meshes at the quadrature points. A number of quadrature schemes suitable for evaluating multidimensional integrals of the form considered here can be found in the literature; see Cools [118] for a review and Xiu [119] for an overview of applications to uncertainty analysis. Note that each quadrature point $\boldsymbol{\theta}^{(k)}$ represents a new boundary and hence a new domain of definition of the problem.

4.3.3 Remarks:

Note that while employing the mesh deformation approach, some elements deform to a lesser degree compared to other elements particularly when employing spatially varying diffusivity parameters [116]. This reduction in geometrical variability in a local region implies that fewer number of quadrature points are required to approximate the PC expansion coefficients of the element matrices – this fact can be exploited by adaptive sparse quadrature schemes [20]. The global PC expansion approach on the other hand does not offer this advantage. Therefore, element level formulations are expected to be computationally advantageous in situations where finite element assembly of $\mathbf{K}(\boldsymbol{\theta}^{(k)})$ and $\mathbf{f}(\boldsymbol{\theta}^{(k)})$ (arising out of complicated PDEs and element types) are computationally expensive.

The following lemma proves the equivalence between Xiu-Tartakovsky [97, 98] method with the current approach.

Lemma 3*: Consider a well posed Poisson problem defined on a stochastic domain bounded by a sufficiently regular stochastic boundary given by Equation 4.4. The random domain $D(\omega) \subset \mathbb{R}^3$ is mapped on to a deterministic domain $D_0 \subset \mathbb{R}^3$ using an bijective mapping function $\boldsymbol{\xi} = \boldsymbol{\xi}(\mathbf{x}, \omega)$ whose inverse is defined as $\mathbf{x} = \mathbf{x}(\boldsymbol{\xi}, \omega)$ as described in Section 4.2.1. Then the finite element discretization of the transformed PDE (using a mesh with deterministic*

shape functions $\{N_i(\mathbf{x})\}$ *defined over the nodes) results in an element stiffness matrix of the form Equation 4.11*

Proof: The variational form of the transformed PDE Equation 4.7 can be written as:

$$\mathcal{B}(u,w) = (a',w), \forall w \in H^1(D_0) \times L_2(\Omega),$$

where $\mathcal{B}(u,w)$ is given by

$$\mathcal{B}(u,w) = \int_{D_0} \nabla_{\mathbf{x}} u^T \mathbf{G}^{-1} \nabla_{\mathbf{x}} w \ \sqrt{g} \ \mathrm{d}\mathbf{x}.$$

Substituting the finite element shape functions defined over the nominal domain into the above bilinear form, the element stiffness matrix can be written in the form Equation 4.11. □

The linear random algebraic system of equations Equation 4.14 where $\mathbf{K}(\boldsymbol{\theta})$ and $\mathbf{f}(\boldsymbol{\theta})$ are given by Equation 4.15 can be solved employing a variety of approaches namely PC projection schemes[3, 39, 40, 64], generalized spectral decomposition methods [54–56] or reduced basis projection schemes presented in the Chapter 2. The reader is referred to Chapter 2 for details on stochastic projection schemes and post-processing of the response process obtained from these approaches.

Remark: If statistics on an unperturbed landmark on the nominal geometry are desired, the element nodes on the geometry could be fixed during mesh deformation.

4.4 Numerical studies

In this section we present three numerical studies in two and three dimensions. The first study involves heat transfer on a rough square domain with a random field model describing the rough boundary which has been discretized using the Karhunen-Loéve expansion scheme. The second numerical study deals with heat transfer analysis on a 2D section of a gas turbine blade where the uncertainties namely, the cooling core centers are considered to be stochastic in nature. The large scale numerical study involves a three-dimensional model of the gas turbine blade with a simplified uncertainty model for the cooling holes. Although we have a random field model and a parametric form describing the respective uncertainties in the two numerical studies, the solution methodology is the same for these the studies.

Note that the governing linear random algebraic system of equations are truncated to a finite order of PC basis functions where the truncation order depends on the degree of dependence of the solution process on the geometric uncertainty. Highly nonlinear dependence

of the response process on the input uncertainty warrants a higher order PC expansion of the random algebraic system of equations and vice versa.

The accuracy of the SRBM based approach is compared against benchmark Monte-Carlo simulations. Computing the solution for each realization of the random variable vector $\boldsymbol{\theta}$ involves the following steps: (a) for a given realization of the random vector $\boldsymbol{\theta}$, a geometry is first generated which is followed by (b) deforming the nominal mesh by employing the Laplace based mesh deformation for 2D case studies and a more robust Navier-Lamé equation based scheme for the 3D study. (c) The governing equations are then discretized over this mesh which in turn are solved to obtain the response. The aforementioned steps of generating random realizations of $\boldsymbol{\theta}$ (and the geometry), perturbing the nominal mesh to the new mesh and solving the governing equations is repeated K number of times, where K represents the Monte-Carlo sample size. At any given spatial coordinate on the nominal domain, the true solution is computed by using the shape function approximation and the statistics are computed by post-processing across the samples.

Similarly, employing the SRBM based approach the governing equations can be discretized resulting in a linear random algebraic system of equations in the form Equation 4.14 and Equation 4.15. Here the unknown coefficients in Equation 4.15 can be non-intrusively computed by repeatedly invoking steps (a), (b) outlined above which is followed by discretizing the governing equation on the new random mesh. The resulting random system of equations are subsequently solved by employing reduced order basis projection schemes. Convergence trends are presented with respect to two error metrics, namely, ϵ_μ and ϵ_σ defined as follows:

$$\epsilon_\mu = \frac{\| \boldsymbol{\mu}_{MCS} - \boldsymbol{\mu}_{SRBM} \|_{L_2}}{\| \boldsymbol{\mu}_{MCS} \|_{L_2}} \text{ and } \epsilon_\sigma = \frac{\| \boldsymbol{\sigma}_{MCS} - \boldsymbol{\sigma}_{SRBM} \|_{L_2}}{\| \boldsymbol{\sigma}_{MCS} \|_{L_2}}. \tag{4.19}$$

For the sake of compactness, we use the notation *SRBM(r, N, s)* to denote an approximation to the response process obtained by solving a linear random algebraic system of equations whose coefficient matrix and right hand side are represented in a r^{th} order PC expansion employing N reduced order basis vectors. Here each SRBM basis vector has been truncated to a s^{th} order PC basis. We study the convergence trends of the error metrics as a function of r, N and s.

4.4.1 Diffusion in a square domain with a rough wall

Consider steady-state heat transfer problem defined by Equation 4.4 with $f = 0$, in a two-dimensional domain described by $D(\omega) = \{(x, y)| -1 \leq x \leq 1, -1 + \kappa(x, \omega) \leq y \leq 1\}$.

The bottom boundary is modeled as a rough wall with mean $\langle \kappa(x,\omega) \rangle = 0$ and exponential two-point covariance function

$$C_\kappa(x,\omega) = \exp\big(- \frac{|x-z|}{b} \big), \tag{4.20}$$

where $b > 0$ is the correlation length. Here we set $b = 1$ which corresponds to moderate boundary roughness. Finally we set $u = 1$ on the boundary $x = -1$, $u = 0$ on the rough bottom boundary and homogeneous Neumann boundary conditions elsewhere.

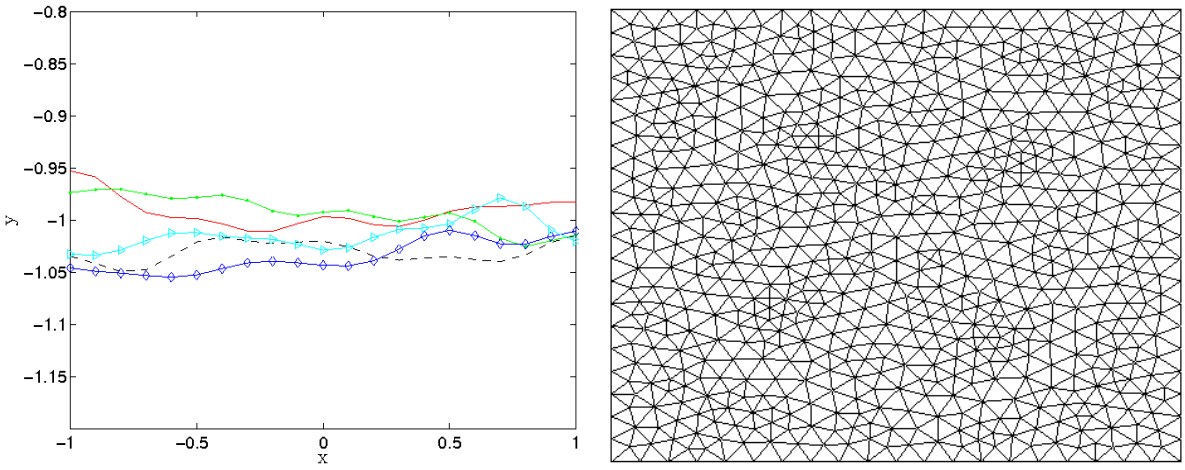

(a) (b)

FIGURE 4.1: (a) Five sample realizations of the rough wall of the plate generated with the ten-term ($d = 10$) KL expansion and (b) mesh on the nominal domain.

Karhunen-Loéve (KL) expansion of $\kappa(x,\omega)$ is performed to decompose the random field governing the rough bottom boundary. This involves the solution of the following Fredholm integral equation of the second kind

$$\int C_\kappa(x,z)\varphi(z)\mathrm{d}z = \lambda\varphi(x), \tag{4.21}$$

where λ and $\zeta(x)$ are the eigenvalues and eigenfunctions of the KL integral eigenvalue problem.

Then the random field $\kappa(x,\omega)$ can be expressed as:

$$\kappa(x,\omega) \approx \sigma \sum_{k=1}^{d} \sqrt{\lambda_k}\zeta_k(x)\theta_k(\omega), \tag{4.22}$$

where the random variables $\{\theta_k(\omega)\}_{k=1}^d$ are considered to be uncorrelated uniform random variables defined on $[-1,1]$. Also the parameter σ is used to control the maximum deviation

of the rough surface. In the current numerical example we set $\sigma = 0.05$ and employ a ten-term KL expansion ($d = 10$) so that more than 95% of the variance is captured and thus limiting the truncation error. A few realizations of the random bottom boundary are shown in Figure 4.1(a). Finite element mesh on the nominal domain is shown in Figure 4.1(b). Using equations 4.15, 4.16, 4.17 and 4.18 with mesh deformation, the problem is spatially discretized resulting in a linear random algebraic system of equations in a Legendre chaos basis. The response process is then approximated using SRBMs.

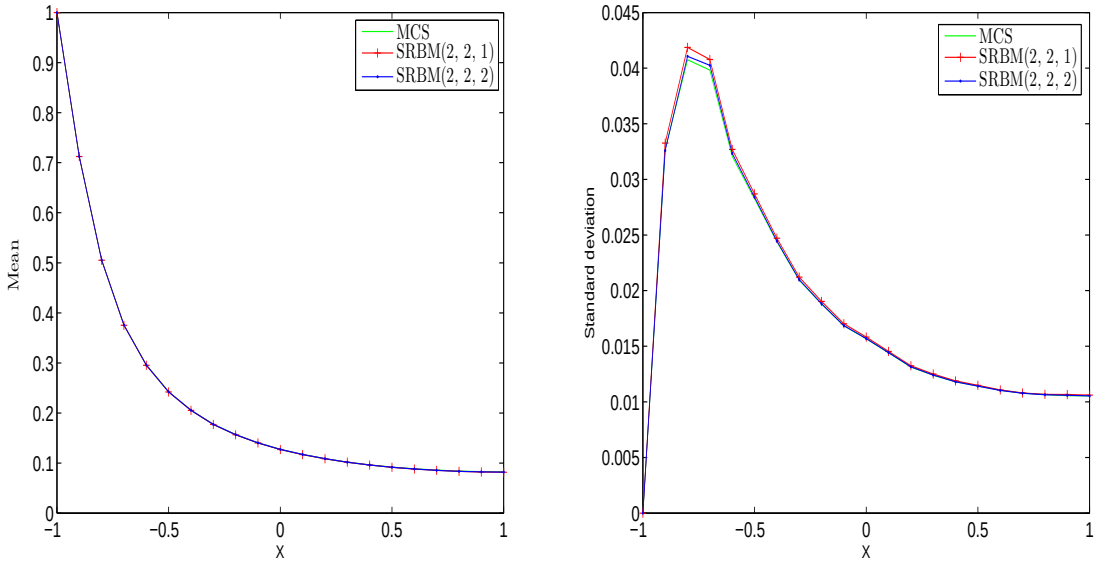

FIGURE 4.2: (a) Mean and (b) standard deviation of temperature profiles on the line $y = -0.8$.

Figure 4.2 shows the mean and standard deviation of the field variable using a benchmark Monte-Carlo simulation and SRBM approximations along the line $y = -0.8$. It can be noted that the mean is approximated with very high accuracy. SRBM approximations with $N = 2$ were computed on the linear random algebraic system of equations in terms of first and second order PC basis functions while the benchmark MCS solution has been computed using 10000 samples. One may notice that the SRBM approximations converge with the increase in order of PC expansions in this figure. Similarly the approximations improve by increasing the number (N) of reduced order basis vectors. The residual error norm given by Equation 2.32 is used to monitor the approximation errors while using SRBMs.

Figure 4.3 shows the trends of the error metric ϵ_σ. It can be observed that this error metric converges as the number of basis vectors is increased. Also, in figure 4.3, it can be

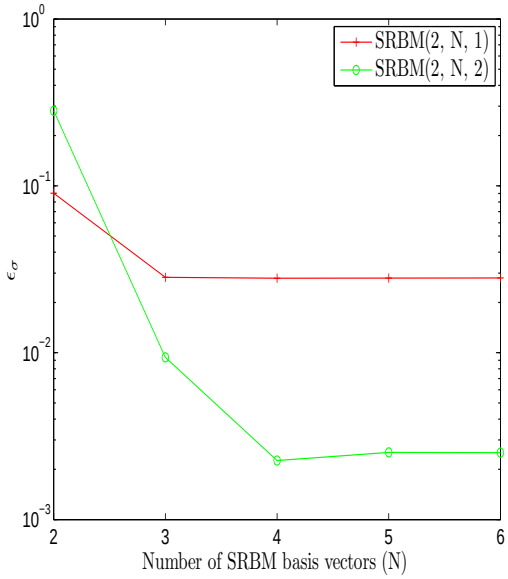

FIGURE 4.3: ϵ_σ for increasing number of basis vectors (N) and a given order of PC expansion (r, s).

observed that higher order PC expansion of each basis vector leads to better accuracy. The error metric ϵ_μ was observed to be very small for all values of r, N and s (of the order of 10^{-4}) and hence the trends of this metric are not shown here. It is worth noting here that the reduced order basis expansion minimizes the **K**-norm error by Theorem 2 in Section 2.4. Hence strictly monotonic convergence can only be guaranteed for the **K**-norm error and not for other error metrics such as the residual error, ϵ_μ and ϵ_σ employing the Galerkin projection. The relative error in mean and standard deviation have been presented to illustrate the level of accuracy that can be attained with a given order of PC expansion.

4.4.2 Heat transfer on a turbine blade model

Now we present numerical studies on complex 2D and 3D geometries involving gas turbine blades. Gas turbine blades in modern aero engines are subjected to tremendous temperatures and pressures. In order to counter the thermal stresses developed due to the high temperature regime, these blades need to be cooled constantly. Hence they are provided with artificial cooling through a series of cooling holes by growing the blades as single crystals over a sacrificial core material which is removed after growth completion, leaving a series of hollow cooling cores in place. Relatively cold air is circulated through these cooling holes resulting in the cooling of the blades. Owing to various factors in the manufacturing process,

the cooling holes vary from blade-to-blade and batch-to-batch due to which the turbine blade geometry varies. These variations may adversely effect the life of the turbine blade necessitating frequent maintenance and replacement. Driven by the need to reduce maintenance and warranty costs, improve product quality and reliability, manufacturers are increasingly inclined to innovate optimal designs which are tolerant to geometrical and material uncertainties. Optimization of the blades [120] is only possible when the optimization goals and constraints are quantified. Quantifying the goals under design constraints in the presence of uncertainties impels probabilistic analysis of the turbine blades. A turbine blade with a set of three cooling holes running through the geometry is shown in Figure 4.4.

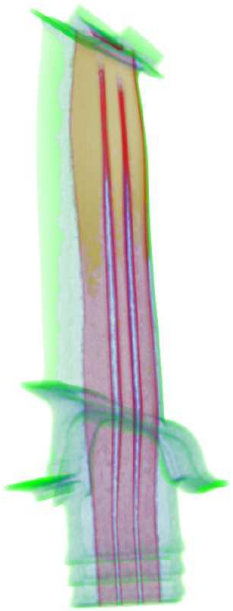

FIGURE 4.4: Turbine blade with cooling holes

Employing a probabilistic approach, the governing equations with uncertainties or the Stochastic Partial Differential Equations (SPDEs) are discretized and subsequently solved to obtain the response statistics. Earlier attempts on probabilistic analysis of turbine blades employed Monte-Carlo simulations and response surface methods [92, 121, 122]. Monte-Carlo simulations can be computationally prohibitive for large scale and high fidelity models with many degrees of freedom. On the other hand response surface methods are not accurate for problems with a high degree of variability. Thus in order to reduce the computational time of the probabilistic thermal analysis of turbine blades, we employed the numerical scheme presented in this chapter.

We present two numerical studies involving heat transfer analysis on a gas turbine blade

in two and three dimensions. Here the governing equations are discretized on a random mesh obtained by perturbing the nominal mesh. The Laplace equation based mesh deformation strategy has been employed for the 2D case study and the Navier-Lamé equation based mesh deformation strategy for the 3D case. Here the random coefficient matrix and the right hand side are nonintrusively computed employing mesh deformation in conjunction with equations 4.17 and 4.18. The resulting linear random algebraic equations are solved employing SRBMs to compute the response statistics. The approach results in highly accurate results at a modest computational cost compared to the benchmark Monte-Carlo simulation. Navier-Lamé operator based mesh deformation strategy has been employed for the 3D case study (in contrast to Laplace operator based strategy applied to 2D case study) in order to demonstrate the ease of employing new mesh deformation strategies in the current computational framework.

Note that we ignore thin film cooling of the blade surface in all our numerical studies. Also note that we ignore material uncertainties in the turbine blade and only deal with geometrical uncertainties.

4.4.2.1 2D case study

Here we deal with a simplistic 2D model of the turbine blade where the moments of the temperature profile are the subject of interest. A typical turbine blade profile with a few possible core positions is shown in Figure 4.5(a). Finite element mesh on the nominal blade geometry is shown in Figure 4.5(b).

The heat equation (4.4) with convective heat transfer boundary conditions is solved on this stochastic domain. The heat transfer rate is given by

$$\overrightarrow{q} = -\nabla u(x, y).$$

The heat flux out of the blade is given by:

$$\overrightarrow{q} \cdot \overrightarrow{n} = h_{ext}(u - u_{ext}),$$

where $\overrightarrow{q} \cdot \overrightarrow{n}$ is the heat flux out of the blade, $\overrightarrow{n}$ is the unit normal out of the blade surface, h_{ext} is the external convective heat transfer coefficient and u_{ext} is the temperature of the flow external to the blade. Similarly, the heat flux into the cooling passage is given by

$$\overrightarrow{q} \cdot \overrightarrow{n} = h_{int}(u - u_{int}),$$

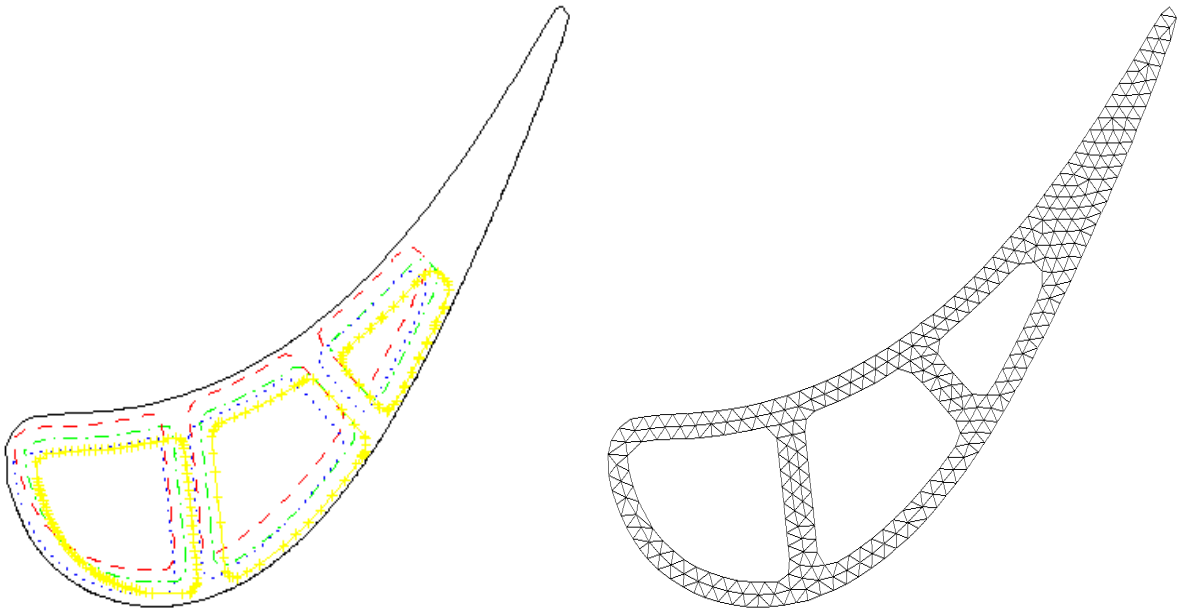

(a) (b)

FIGURE 4.5: (a)Turbine blade geometry with possible core positions and (b) mesh on the nominal blade geometry.

where $\overrightarrow{n}$ is still out of the blade i.e., into the cooling passage, h_{int} and u_{int} are the internal convective heat transfer coefficient and the temperature of the flow in the cooling passage, respectively. The temperatures of flow on the boundaries are $u_{ext} = 1300^{\circ}\ C$ and $u_{int} = 200^{\circ}\ C$. The convective heat transfer coefficients in non-dimensional form are given by $h_{ext} = 14.0$ and $h_{int} = 4.7$.

In the current problem setup, the core centers are assumed to be uncertain. They are varied independently and uniformly along each spatial direction with the limits being $\pm 4\%$ of the nominal core centre location. Also note that all the cores are assumed to move by the same amount in each spatial direction for the sake of simplicity, thus making it a two variable problem.

A Monte-Carlo simulation with 10000 samples has been performed to compute the mean and standard deviation of the temperature profile. The nodal connectivity has been kept consistent across the sample runs by deforming the nominal mesh for various realizations of the core locations. The mesh deformation has been performed employing the Laplace equation where the boundary nodes are perturbed according to the specified deformations and the interior nodes deformed solving the Laplace equation with specified Dirichlet boundary conditions (new boundary coordinates resulting from the perturbations). Here note that

the x and y coordinates are perturbed independently of each other which may result in element reversals or mesh collapses for complicated geometries (as can be seen in the following section).

The mean and standard deviation of the temperature profiles can be seen in Figure 4.6. It can be observed that mean profile remains similar to the mean profile obtained for the case of material uncertainty (refer to Section 3.3.3). As anticipated, the standard deviation profile shows more variations near the cooling cores as compared to the blade outer surface.

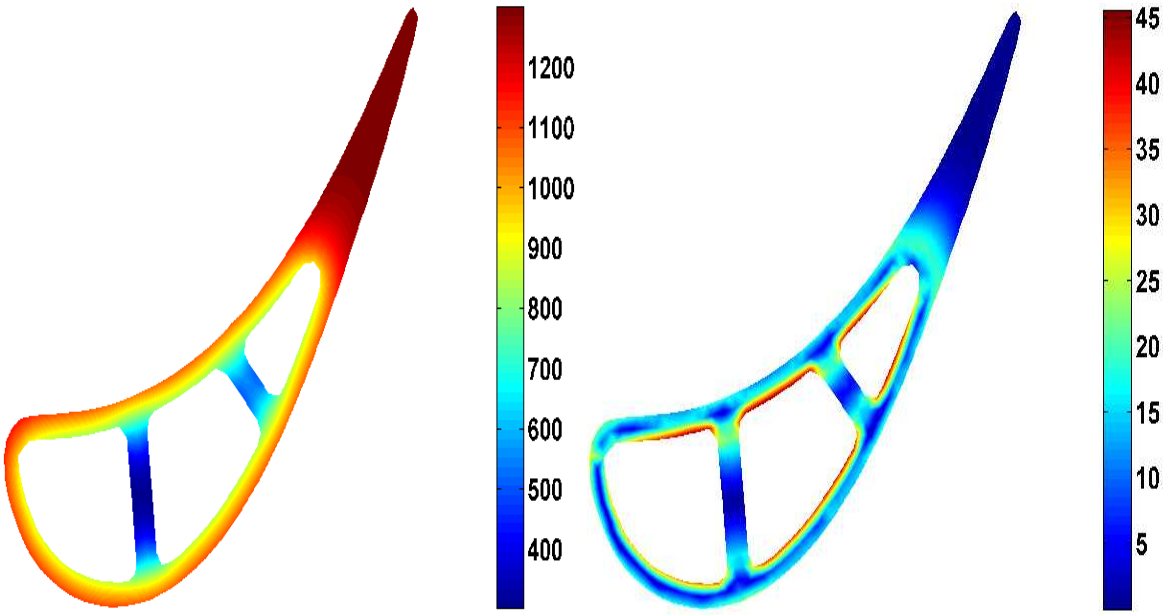

FIGURE 4.6: (a) Mean and (b) standard deviation of temperature profile mapped onto the nominal geometry.

In order to apply SRBMs to the problem, the governing equations are expanded in a second order PC basis which in turn result in a linear random algebraic system of equations given by Equation 4.14 and Equation 4.15. Here the coefficients of expansion are nonintrusively computed (using 2000 samples) following equations (4.16), (4.17) and (4.18). Again mesh deformation strategy has been leveraged for consistency of the connectivity across different expansion terms.

Figure 4.7(a) shows the absolute error in mean which is the absolute difference between the Monte-Carlo and the SRBM estimates on the outer profile of the blade. Reduced order basis methods with varying number of basis vectors have been applied on the linear random algebraic system of equations in terms of second and third order Legendre chaos basis functions. Although, one may observe some errors for lower number of basis vectors, the mean

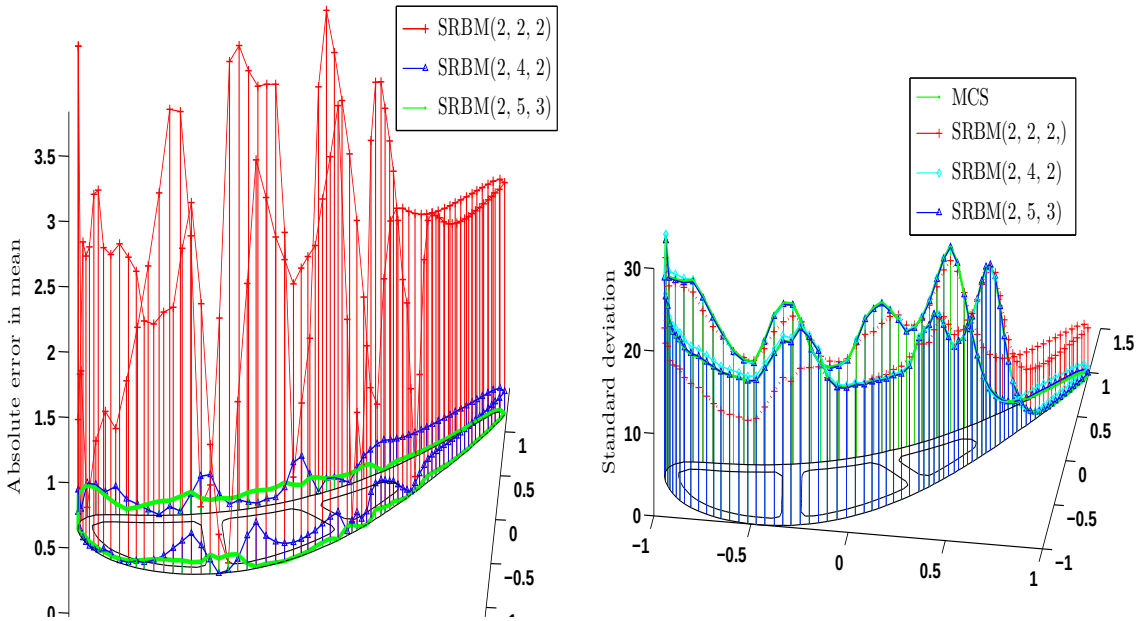

FIGURE 4.7: (a) Absolute error in mean compared to MCS mean and the (b) standard deviation profiles of the temperature on the outer edge of the blade.

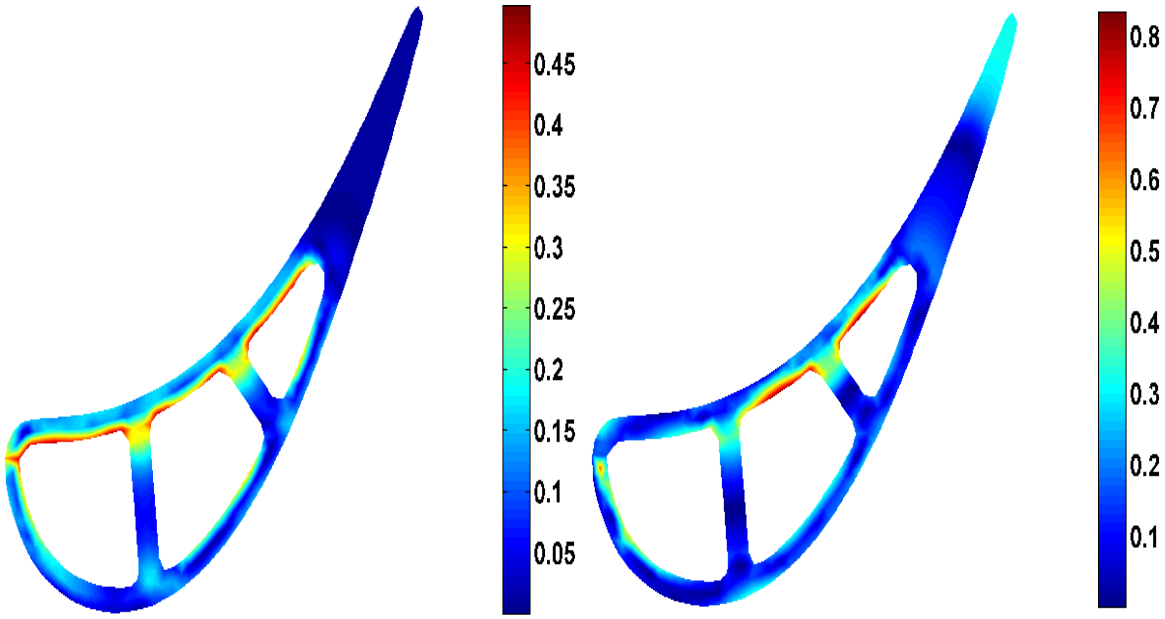

FIGURE 4.8: Absolute error in (a) mean and (b) standard deviation of temperature profile mapped onto the nominal geometry.

converges to the benchmark Monte-Carlo solution as the PC expansion and the number of basis vectors is increased. Similar trends can be observed in Figure 4.7(b) which displays the standard deviation from Monte-Carlo simulations and various orders of PC expansions and the number of SRBM basis vectors. Reduced order basis expansions tend to over-estimate the standard deviation for lower orders of PC expansion. Figure 4.8 shows the approximation error in computing the mean and standard deviation over the blade domain. The maximum absolute error in mean in 0.45 which translates to about 0.001% error and the maximum absolute error in standard deviation is 0.8 which translates to 5% error. Note that SRBMs overestimate the moments at spatial locations where the values are near to zero and hence resulting in high percentage errors. Thus we present the results here in terms of absolute errors as compared to percentage errors. However these inaccuracies at small values can be eliminated by employing higher order PC expansions and higher number of reduced order basis vectors.

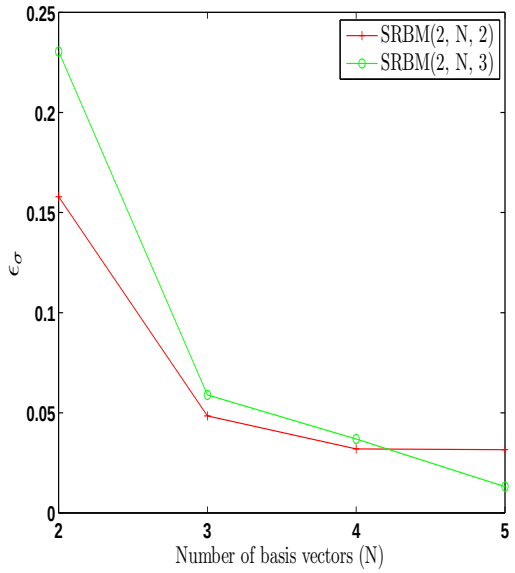

FIGURE 4.9: ϵ_σ for increasing number of basis vectors (N) and a given order of PC expansion (r, s).

Figure 4.9 shows the error metric ϵ_σ when the PC expansion orders of the coefficient matrices in (4.14), (4.15) and the number of basis vectors are increased. It can be observed that this metric converges as the number of basis vectors (N) is increased. In general better accuracy is achieved for higher order Legendre chaos expansion of the coefficient matrices and the basis vectors. As discussed earlier in the context of the preceding numerical study,

monotonic convergence of the error metric ϵ_σ as a function of r, N and s cannot be guaranteed in theory since this error norm is not being minimized by the Galerkin projection scheme. However, we report the trends of this error metric to illustrate the accuracy of the results obtained. The error metric ϵ_μ was observed to be very small for all values of r, N and s (of the order of 10^{-4}) and hence the trends of this metric are not shown here.

In the current numerical study, Monte-Carlo simulations with 10000 samples take about 2.8 hours. While SRBM expansions with five basis vectors employing third order Legendre chaos expansions of the coefficient matrices takes about 34 seconds to achieve the same degree of accuracy. However, note that the nonintrusive simulations (with 2000 samples) for computing the PC coefficients takes about 6 minutes. These nonintrusive computations could be significantly speeded up using sparse quadrature schemes.

4.4.2.2 3D case study

Now we deal with a 3D model of the cooling core uncertainty problem in the turbine blade. Here we consider a simplified uncertainty model for the core uncertainties. The actual statistical uncertainty model could be obtained by employing Coordinate Measurement Machine data or the ultra-sound measurements on a statistical sample of the blades. However as a proof of concept we employ a simplified model where the core coordinates are fixed at the base and upper surface. Perturbations at interior core coordinates are applied as follows

$$\begin{aligned} \kappa_x(\mathbf{x}, \boldsymbol{\theta}) &= \theta_1 \sigma x \sin(\pi z), \\ \kappa_y(\mathbf{x}, \boldsymbol{\theta}) &= \theta_2 \sigma y \sin(\pi z), \\ \kappa_z(\mathbf{x}, \boldsymbol{\theta}) &= 0, \end{aligned} \tag{4.23}$$

along x, y and z directions where θ_1 and θ_2 are chosen to be uniform random variables in the range $[-1, 1]$. The FE mesh nodal coordinates in the nominal mesh have been normalized to fit in a unit cube, due to which the applied perturbations result in zero displacements at the upper and lower surfaces of blade. In addition, the uncertainty model also results in very low perturbations at regions where blade thickness is small. The magnitude of perturbation is limited by σ which in this case has been chosen to be 0.03.

The heat equation (4.4) with convective heat transfer boundary conditions has been solved on the stochastic 3D domain. The problem settings and the convective boundary conditions are exactly similar to the conditions applied to the 2D profile of the blade in the preceding section.

A Monte-Carlo simulation with 2000 samples has been performed to compute the mean

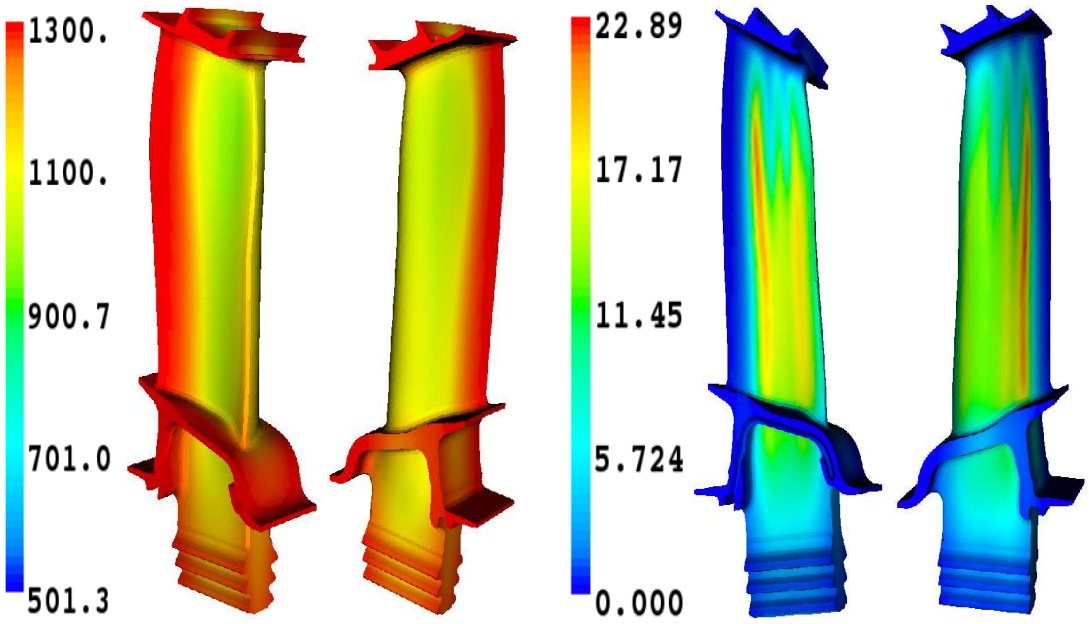

(a) (b)

FIGURE 4.10: (a) Mean and (b) standard deviation of the temperature profile.

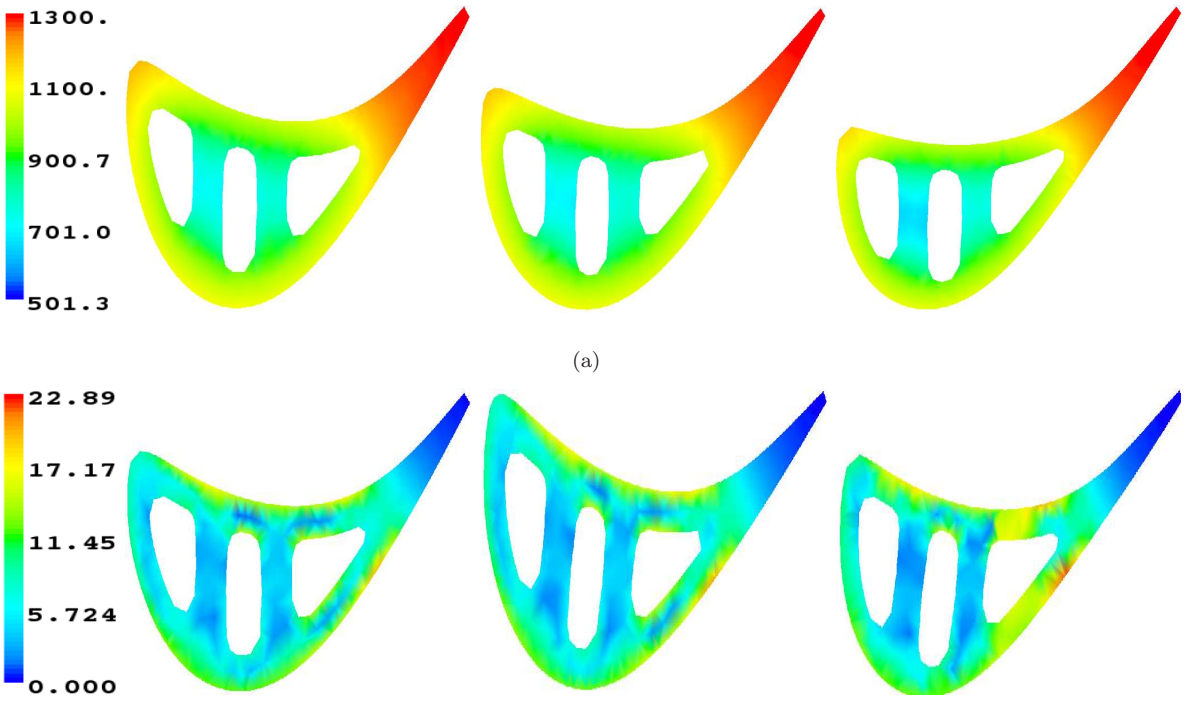

(a)

(b)

FIGURE 4.11: (a) Mean and (b) standard deviations along three different 2D sections (normal to the z-axis).

and standard deviation of the temperature profile. The nodal connectivity has been kept consistent across the sample runs by deforming the nominal mesh for various realization of the core perturbations.

In order to demonstrate the ease of employing alternative mesh deformation strategies, the Navier-Lamé equation based mesh perturbation has been applied here. We present a brief introduction to the governing equations of the Navier-Lamé equation based mesh deformation. Let $D_0 \subset \mathbb{R}^3$ be the nominal domain bounded by a closed, orientable and regular boundary denoted by ∂D_0. The equations governing the displacement of the internal nodes can then be written as

$$\nabla^2 \cdot \boldsymbol{\sigma} + \mathbf{f} = 0, \text{ on } D_0, \tag{4.24}$$

where $\boldsymbol{\sigma}$ is the Cauchy stress tensor and $\mathbf{f}$ is the external force. For linear elasticity, $\boldsymbol{\sigma}$ is defined as

$$\boldsymbol{\sigma} = \rho \, \mathrm{tr}(\boldsymbol{\epsilon}(\mathbf{w}))\mathbf{I} + 2\tau\boldsymbol{\epsilon}(\mathbf{w}),$$

where $\mathbf{w}$ is the displacement, tr() is the trace operator, ρ and τ are the Lamé constants, $\mathbf{I}$ is the identity tensor and $\boldsymbol{\epsilon}(\mathbf{w})$ is the strain tensor

$$\boldsymbol{\epsilon}(\mathbf{w}) = \frac{1}{2}\big(\nabla\mathbf{w} + (\nabla\mathbf{w})^T\big).$$

The Dirichlet boundary conditions are represented as

$$\mathbf{w} = \mathbf{g} \text{ on } \partial D_0.$$

The Navier-Lamé equation with the prescribed perturbations on the core given by Equation 4.23 and zero displacements on the blade surface are applied as Dirichlet boundary conditions. The resulting equations are solved to obtain the displacements of the interior nodal coordinates. Navier-Lamé equation based mesh perturbation strategy is more robust than Laplace based mesh perturbation as a coupled system of equations are solved to obtain the perturbed mesh coordinates in x, y and z directions simultaneously, in contrast to the latter approach. This results in good quality meshes and alleviates element reversals to a large extent.

The mean and standard deviation of the temperature profiles can be seen in Figure 4.10. Figure 4.11 shows the first two moments of the temperature profile on three different 2D sections along the length of the blade. It can be observed from Figure 4.6 that the standard deviation values are high on the airfoil section of the blade due to high geometrical variability imposed by the uncertainty model in that section. An interesting trend that emerges when

comparing the 2D study to 3D study in Figure 4.6(b) and Figure 4.11(b) is that standard deviation is now higher at the blade outer surface compared to near zero standard deviations in 2D case study. The outer sections of the blade are critical to the proper functioning of the blade. Hence the impact of the cooling core location and shape uncertainty on the outer surface is of immense interest. The interesting trend presented above highlights the importance of the 3D study that has been conducted.

In order to apply SRBMs to the problem, the discretized governing equations are expanded in a PC basis which in turn results in a linear random algebraic system of equations given by Equation 4.14 and Equation 4.15. Here the coefficients of expansion are nonintrusively computed (using 500 samples) following equations Equation 4.16, Equation 4.17 and Equation 4.18. Again Navier-Lamé based mesh deformation strategy has been leveraged for consistency of the connectivity across different expansion terms.

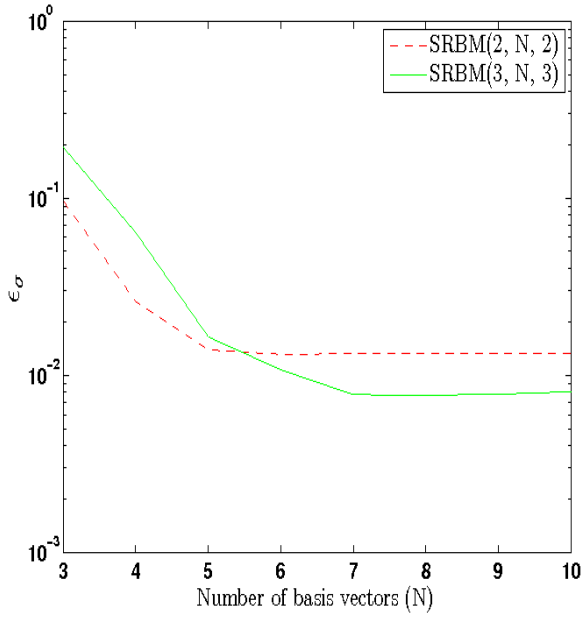

FIGURE 4.12: ϵ_σ for increasing number of basis vectors (N) and a given order of PC expansion (r, s).

Figure 4.12 shows the error metric ϵ_σ when the PC expansion orders of the coefficient matrices in (4.14), (4.15) and the number of basis vectors are increased. It can be observed that this metric converges as the number of basis vectors (N) is increased. In general better accuracy is achieved for higher order Legendre chaos expansion of the coefficient matrices and the basis vectors. As discussed earlier in the context of the two-dimensional problem, monotonic convergence of the error metric ϵ_σ as a function of r, N and s cannot be guaranteed

in theory since this error norm is not being minimized by the Galerkin projection scheme. However, we report the trends of this error metric to illustrate the accuracy of the results obtained. The error metric ϵ_μ was observed to be very small for all values of r, N and s (of the order of 10^{-4}) and hence the trends of this metric are not shown here.

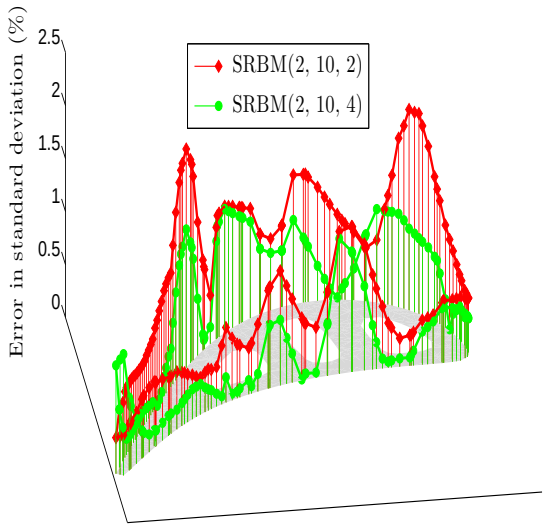

FIGURE 4.13: Percentage error in standard deviation on the blade outer surface for a typical 2D section (normal to the z-axis).

Figure 4.13 shows the percentage error in standard deviation on the outer surface of a typical 2D section of the blade for second order Legendre chaos expansion of the coefficient matrices and varying order of PC expansions of the reduced order basis vectors. It has been observed that the error decreases in general with the increase in the order of the PC basis for expanding SRBM basis vectors in a weighted average sense. Thus the value decreases where the magnitude of deviation is higher and increase at locations where the variation is low. Similar trend has been observed for higher order of PC expansion of the coefficient matrices. Note that highest percentage error in standard deviation is less than 1% showing that the current approach converges to highly accurate results. Similarly the percentage error in mean has been observed to be less than 0.1% over the same 2D section for second and third order expansion of the coefficient matrices.

In the current numerical study, the nominal mesh consists of 32776 nodes and 125209 elements. The surface and volume meshes of the nominal turbine blade are shown in Figure 4.14. A benchmark Monte-Carlo simulation with 2000 samples takes about 10 hours.

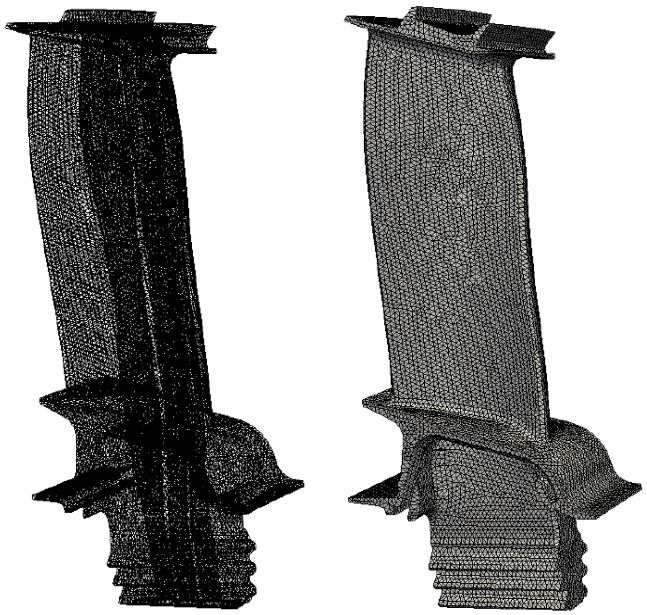

(a) (b)

FIGURE 4.14: (a) Volume mesh and (b) the surface mesh on the nominal turbine blade.

The computational time with the current approach is about 2.5 hours when ten reduced order basis vectors (where each vector is expanded in fourth order Legendre chaos expansion) are employed over linear random algebraic system of equations in third order PC expansion. Reduced order projection scheme with ten basis vectors where each vector is truncated to a fourth order PC expansion takes about 77 seconds. While the bulk of the computational time (about 2.5 hours) is taken by the nonintrusive computation of the coefficient matrices. However, note that the nonintrusive simulations can be sped by employing sparse quadrature schemes.

4.5 Summary

In this chapter, we propose a novel approach for solving linear elliptic partial differential equations on random domains. The central idea underpinning the proposed formulation is to combine finite element discretization with a mesh deformation strategy to enable a finite-dimensional approximation of the original governing equations. A weak condition on the admissible boundary perturbations to ensure the well-posedness of the problem has been proposed. Equivalence has been established with with the Xiu-Tartakovsky method [97, 98]. The proposed approach does not lead to complex SPDEs and it also renders the original

deterministic solvers reusable in contrast to the Xiu-Tartakovsky method. The resulting linear random algebraic system of equations obtained by the current discretization scheme can be subsequently solved using generalized stochastic reduced basis methods to compute the statistics of the solution process. Numerical studies are presented for heat transfer in a square domain with a rough wall and two studies involving gas-turbine blades to demonstrate that the proposed approach converges to highly accurate solutions as the expansion order is increased at significantly lower computational costs compared to simulation techniques. It is anticipated that further computational gains can be achieved by employing more efficient multidimensional sparse quadrature schemes to perform the nonintrusive computations.

Adaptive algorithms based on the ideas presented in Chapter 3 could be developed to tackle problems with high geometric variability. The input random space underlying the random boundary can be decomposed into subdomains reducing the variability in each subdomain where local preconditioners (local nominal meshes in this case) in conjunction with robust mesh deformation algorithms could be employed for improved approximations.

We have only dealt with linear SPDEs so far. In the next chapter, we propose an inexact Picard iterative scheme to solve nonlinear SPDEs.

Chapter 5

Inexact Picard iterative scheme for steady-state nonlinear SPDEs

In the previous chapters, we have analyzed linear stochastic PDEs employing reduced order projection schemes. In this chapter, we develop an inexact Picard iterative scheme to solve nonlinear SPDEs.

Earlier attempts to solve nonlinear SPDEs employed Monte-Carlo simulations [123], response surface methods [124] and perturbation methods [34, 35]. For example Tartakovsky et al. considered nonlinear flow in heterogeneous random media in [34, 35], where the nonlinear SPDEs are linearized employing Kirchoff mapping and are subsequently approximated using a first-order perturbation method. Note that a special form of nonlinearity was considered which admits linearization using Kirchoff mapping and more general forms of nonlinearity do not necessarily admit such a linearization step [125]. Sparse quadrature schemes have been introduced by Matthies et al in [15, 16] in order to analyze nonlinear stochastic PDEs. Also projection schemes based on Polynomial Chaos (PC) expansions have been employed more recently in [48–53]. In the PC based projection schemes, the nonlinear random fields are expanded in a PC basis. The resultant governing equations in PC basis are then spatially discretized and iteratively solved using Newton-Raphson scheme to obtain the response statistics.

Recall from the previous chapters that SRBMs have been found to perform very efficiently for linear SPDEs. Thus SRBMs' efficiency could be leveraged while analyzing nonlinear SPDEs where at each iterative step (irrespective of the iteration scheme) a linear SPDE is being solved after linearizing the original nonlinear governing equations. In this chapter, we

employ Picard iterative step for linearization where we start with an initial guess solution which is assumed to be in a PC basis without loss of generality. This guess is used to linearize the governing equations. Then the SPDE is spatially discretized which results in a linear random algebraic system of equations in a PC basis which in turn can be solved using the generalized SRBMs discussed in Chapter 2. The current guess is now updated with the SRBM approximation of the new solution and is used to again linearize the original governing equations. These iterative steps of linearization of the SPDE, spatial discretization, solving the resultant system of equations and updating the current guess are repeatedly carried out till the desired accuracy is achieved. We present three numerical studies dealing with the heat transfer equation and Burger's equation involving nonlinearities in the constitutive laws. The method is numerically convergent for the heat transfer studies and provides accurate results at significantly lower computational costs compared to MCS methods. But the limitations of the formulation are apparent in the case of Burger's equation where quasi-Newton methods are warranted for better efficiency.

The remainder of this chapter is organized as follows: In the next section, we present some preliminary theoretical context and describe the model nonlinear heat transfer equation studied in the present work. The detailed formulation of the proposed numerical scheme is discussed in Section 5.2. The computational and implementation aspects of the proposed approach are also discussed in Section 5.2. In Section 5.3, numerical studies are presented for three test problems. We summarize the chapter in Section 5.4 and highlight some directions for future research.

5.1 Problem definition

In this section we present the problem definition for a model nonlinear stochastic steady-state heat transfer equation and prove a theoretical result establishing the existence of a fixed point for the nonlinear SPDE under consideration. Under the definitions of the probability space and the inner product (expectation) given in Section 2.1, consider the following nonlinear stochastic steady-state heat transfer equation

$$\left.\begin{array}{lcll} \nabla.[\kappa(x,u,\omega)\nabla u(x,\omega)] & = & f(x,\omega) & \text{in } D\times\Omega \\ \mathcal{B}u(x,\omega) & = & g(x,\omega) & \text{on } \partial D\times\Omega \end{array}\right\} \tag{5.1}$$

where $f(x,\omega)$ is a random field defined on $D\times\Omega$ and $g(x,\omega)$ is a random field defined on $\partial D\times\Omega$. $D\ \subset\ \mathbb{R}^{\ell}, \ell = 1,2,3$ and ∂D denotes the physical domain and its boundary,

respectively. $\mathcal{B}$ is an operator indicating the type of boundary conditions that are imposed, e.g., Dirichlet, Neumann or mixed boundary conditions. $u(x,\omega)$ is the field variable whose spatial statistics are sought to be computed.

Following Matthies and Keese [15, 16] (which was originally adopted in the context of diffusion), we model the nonlinear stochastic conductivity field $\kappa(x,u,\omega)$ as

$$\kappa(x,u,\omega) = \widehat{\kappa}(x,\omega) + \lambda u^2(x,\omega), \tag{5.2}$$

where $\widehat{\kappa}(x,\omega)$ is a random field and λ is a parameter governing the degree of nonlinearity.

Before delving into the numerical algorithms for solving Equation 5.1, it is important to investigate if a solution (fixed point) indeed exists for the SPDE. We define a couple of function spaces which are going to be used extensively in this chapter.

Definition: Let $1 \leq p \leq \infty$. Then $L_p(\Omega)$ space is the set of all measurable functions from Ω to $\mathbb{R}$ whose absolute value raised to the p^{th} power has a finite Lebesgue integral

Definition: For $p \geq 1$, $W_p^k(D)$ refers to the set of all functions $u \in L_p(D)$ such that all derivatives of u of orders lesser than or equal to k belong to $L_p(D)$

We investigate the appropriate function spaces to define u and f for the well-posedness of the problem Equation 5.1. In contrast to the case where the conductivity is linear, we need to define the spatial part in a Sobolev space $W_p^1(D)$ with $p > 2$. Hence $u(x,\omega) \in W_p^1(D) \times L_p(\Omega)$.

On the other hand $f(x,\omega)$ should be in the dual space of $W_p^1(D) \times L_p(\Omega)$, namely, $f \in W^*(D) \times L_q(\Omega)$ where $W^*(D) = W_q^{-1}(D)$ and q is related to p as $1/p + 1/q = 1$.

Since the nonlinearity in Equation 5.2 is quadratic in nature, if $p = 4$, we can define a continuous nonlinear operator [110] on $W_p^1(D) \times L_p(\Omega)$, as follows

$$\mathcal{N} = (\widehat{\kappa}(x,\omega) + \lambda u^2(x,\omega))\nabla u(x,\omega), \ \forall u \in W_p^1(D) \times L_p(\Omega).$$

Define a semi-linear (linear in v) form on $W_p^1(D) \times L_p(\Omega)$ as follows

$$a(u,v) = \left\langle \int_D \nabla v \cdot \mathcal{N}(u) \mathrm{d}x \right\rangle, \forall u, v \in W_p^1(D) \times L_p(\Omega).$$

Now consider the variational formulation given by

$$a(u,v) = \mathscr{L}(v), \forall u, v \in W_p^1(D) \times L_p(\Omega), \tag{5.3}$$

where the linear form $\mathscr{L}$ is defined as

$$\mathscr{L}(v) = \left\langle \int_D f v \mathrm{d}x \right\rangle.$$

The variational formulation Equation 5.3 has a unique solution for all $f \in W^*(D) \times L_q(\Omega)$ by the well-known Lax-Milgram lemma [126], provided $\mathcal{N}(u) > 0$. We ensure the positivity of $\mathcal{N}(u)$ by considering the conductivity to be bounded from below and above, i.e.,

$$0 < \kappa_{min} < \kappa(x, u, \omega) < \kappa_{max} < \infty.$$

The stochastic linear component of the conductivity, i.e., the term $\widehat{\kappa}(x, \omega)$ in (2), can be ensured to be positive-valued by choosing an appropriate random field model (e.g. lognormal random field. Refer to Appendix B for the details on discretizing lognormal random fields.). The term $u^2(x, \omega)$ in the conductivity model (2) is always positive valued everywhere.

To justify the application of the Picard iteration scheme, we prove that the following Dirichlet problem

$$\left.\begin{array}{rcll} \nabla.[\kappa(x, u, \omega)\nabla u(x, \omega)] & = & f(x, \omega) & \text{in } D \times \Omega \\ u(x, \omega) & = & g(x, \omega) & \text{on } \partial D \times \Omega \end{array}\right\}$$

with the nonlinearity model Equation 5.2 and the assumptions listed above has a unique fixed point.

Theorem: *For a given $v \in W_p^1(D) \times L_p(\Omega)$, define an operator $T(\omega)$ by letting $u = Tv$ be the unique solution in $W_p^2(D) \times L_p(\Omega)$ of the linear Dirichlet problem*

$$\left.\begin{array}{rcll} \nabla.[\kappa(x, v, \omega)\nabla u(x, \omega)] & = & f(x, \omega) & \text{in } D \times \Omega \\ u(x, \omega) & = & g(x, \omega) & \text{on } \partial D \times \Omega, \end{array}\right\}, \tag{5.4}$$

where $f \in W^*(D) \times L_q(\Omega)$ and $g \in W_p^1(\partial D) \times L_p(\Omega)$. Then $T(\omega)$ has a fixed point.

Proof: To prove that $T(\omega)$ has a fixed point, we use the well-known Leray-Schauder theorem [126]. This theorem states that T has a fixed point, if it is a compact mapping from a Banach space $W_p^2 \times L_p(\Omega)$ into itself and there exists a constant M such that

$$||u||_{W_p^2 \times L_p(\Omega)} \leq M, \forall u \in W_p^2 \times L_p(\Omega),$$

and $\sigma \in [0, 1]$ satisfying $u = \sigma Tu$.

We now need to show that the operator T defined earlier via the linearized problem (4) is continuous and compact. T maps bounded sets in $W_p^1 \times L_p(\Omega)$ into bounded sets in $W_p^2 \times L_p(\Omega)$ by global Schauder estimate [126] which in turn are precompact in $W_p^2 \times L_p(\Omega)$ by Arzela's theorem. In order to prove the continuity of T, let $\{v_m\}$ be a convergent sequence (converging to v) in $W_p^1 \times L_p(\Omega)$. Then since the sequence $\{Tv_m\}$ is precompact in

$W_p^2 \times L_p(\Omega)$, every subsequence in turn has a convergent subsequence. Let $\{T\bar{v}_m\}$ be such a convergent subsequence with the limit $u \in W_p^2 \times L_p(\Omega)$. Then since

$$\nabla.\left[\kappa(x,v,\omega)\nabla u(x,\omega)\right] - f(x,\omega)$$

$$= \lim_{m\to\infty} \nabla.[\kappa(x,\bar{v}_m,\omega)\nabla T\bar{v}_m(x,\omega)] - f(x,\omega) = 0,$$

we must have $u = Tv$ and hence the original sequence $\{Tv_m\}$ itself converges to u. This concludes our proof that a fixed point indeed exists for the map T which gives the solution of the Dirichlet problem given by Equation 5.1. □

We model the linear component of the conductivity by a lognormal random field, which can be defined by a transformation of a Gaussian random field $Y(x,\omega)$ as

$$\widehat{\kappa}(x,\omega) = \exp(Y(x,\omega)). \tag{5.5}$$

Karhunen-Loève expansion [16, 39, 71] of a lognormal random field results in a set of random variables whose probabilistic structure cannot be easily determined. Ghanem [127] proposed to discretize the underlying Gaussian random field $Y(x,\omega)$ using the Karhunen-Loève expansion scheme and then expand the lognormal field in a Hermite PC basis. Interested reader is referred to Appendix B for details on the lognormal random field discretization. The discretized lognormal random field can be expressed in the form

$$\widehat{\kappa}(x,\omega) \approx \sum_{i=0}^{P_1} \widehat{\kappa}_i(x)\phi_i(\boldsymbol{\theta}). \tag{5.6}$$

Here we use the symbol $\boldsymbol{\theta}$ to denote the vector of uncorrelated random variables arising from Karhunen-Loève discretization of the random fields Y, f and g, and $\{\phi_i\}$ denotes a set of Hermite PC basis functions. We shall henceforth assume that $\widehat{\kappa}(x,\omega)$, $f(x,\omega)$ and $g(x,\omega)$ are statistically independent. Recall from Section 2.2 that this assumption is primarily made for notational convenience and to improve clarity of presentation.

Since we assumed that $f(x,\omega)$ is a random field on $W^* \times L_q(\Omega)$, it can also be represented in the general Hermite PC expansion form[1]

$$f(x,\omega) \approx \sum_{i=0}^{P_f} f_i(x)\phi_i(\boldsymbol{\theta}). \tag{5.7}$$

[1]Recall from Section 2.2 that this representation in a Hermite PC basis is optimal only when $f(x,\omega)$ is a Gaussian random field. For more general distributions, a specially constructed set of orthogonal polynomials may be necessary to ensure optimal convergence [75].

Before moving onto linearization and the spatial discretization of the model nonlinear SPDE described in this section, note that generalized SRBMs (refer to Section 2.5) are employed to solve linear random algebraic systems of equations of the form $\mathbf{K}(\boldsymbol{\theta})\mathbf{u}(\boldsymbol{\theta}) = \mathbf{f}(\boldsymbol{\theta})$ where $\mathbf{K}(\boldsymbol{\theta})$ and $\mathbf{f}(\boldsymbol{\theta})$ are given in a PC expansion of form 2.14. The response process is given as:

$$\mathbf{u}(\boldsymbol{\theta}) = \boldsymbol{\Psi}(\boldsymbol{\theta})\boldsymbol{\alpha} = \left(\sum_{i=0}^{P_u} \boldsymbol{\Gamma}_i \phi_i(\boldsymbol{\theta})\right)\boldsymbol{\alpha} = \sum_{i=0}^{P_u} \mathbf{u}_i \phi_i, \tag{5.8}$$

where $\mathbf{u}_i = \boldsymbol{\Gamma}_i\boldsymbol{\alpha}$, $\boldsymbol{\Psi}(\boldsymbol{\theta}) = \{\boldsymbol{\psi}_0(\boldsymbol{\theta}), \boldsymbol{\psi}_1(\boldsymbol{\theta}), \boldsymbol{\psi}_2(\boldsymbol{\theta}), \cdots, \boldsymbol{\psi}_{N-1}(\boldsymbol{\theta})\}$ are reduced order basis vectors, $\boldsymbol{\Gamma}_i = \left[\boldsymbol{\psi}_i^0, \boldsymbol{\psi}_i^1, \boldsymbol{\psi}_i^2, \cdots, \boldsymbol{\psi}_i^{N-1}\right] \in \mathbb{R}^{n\times N}$ is a deterministic matrix and $\boldsymbol{\alpha}^T = \{\alpha_0, \alpha_1, \alpha_2, \cdots, \alpha_{N-1}\}$ is a vector of undetermined deterministic coefficients which can be computed employing Galerkin projection (refer to Section 2.5.1). Here N denotes the number of SRBM basis vectors employed, n denotes the number of degrees of freedom and $\{\phi_i(\boldsymbol{\theta})\}$ are the PC basis functions.

5.2 Picard iteration scheme

In this section, we present an inexact Picard iteration scheme that employs SRBMs for solving the model nonlinear SPDE presented in Section 5.1. Recall that the linear component of conductivity $\widehat{\kappa}(x,\omega)$ in Equation 5.2 has been represented in a PC basis in Equation B.3. We now discuss linearization of the nonlinear component so that the overall conductivity is in a PC basis which in turn facilitates spatial discretization of the governing equations.

We employ the Picard iteration scheme to linearize the nonlinear governing equations. Let u_0 be an initial guess of the solution which is assumed to be expanded in a PC basis without loss of generality as follows:[2]

$$u_0(x,\boldsymbol{\theta}) = \sum_{i=0}^{P_0} u_{0_i}(x)\phi_i(\boldsymbol{\theta}).$$

The nonlinear conductivity in Equation 5.2 is linearized with u_0 and then the governing equations Equation 5.1 are spatially discretized. The linear algebraic system of equations that arise are solved using generalized SRBMs presented in the earlier section. The approximation to the response thus obtained (which is in a PC basis – see Equation 5.8) is then used to linearize the governing equations. These equations are spatially discretized and this iterative cycle is repeated until convergence.

[2] u_0 is stochastic if an approximate solution to the nonlinear system is known or it can be deterministic in which case only u_{0_0} is nonzero.

Let the solution at any iterative step be written as v. Then the next iterate u is computed by solving the following linearized equation

$$\left.\begin{aligned} \nabla.[\kappa(x,v,\omega)\nabla u(x,\omega)] &= f(x,\omega) \qquad \text{in } D\times\Omega \\ \mathcal{B}u(x,\omega) &= g(x,\omega) \qquad \text{on } \partial D\times\Omega \end{aligned}\right\}. \tag{5.9}$$

It can be seen that the structure of Equation 5.9 is similar to the linear SPDE considered in Chapter 3. Hence SRBMs can be directly applied to approximate u.

In brief, the continuum equations are spatially discretized using finite element approximations resulting in a linear random algebraic system of equations represented in a PC basis. The solution of this system of equations is approximated using basis vectors spanning the preconditioned stochastic Krylov subspace and the current guess is updated to the new response obtained and substituted in Equation 5.9. These steps of updating the current guess and uncertainty propagation are repeated until an appropriate stopping criterion is met.

In the sections that follow, we outline the steps involved in spatial discretization of the linearized governing equations, computing the stochastic reduced basis approximation at each iteration, the stopping criterion and the post-processing steps.

5.2.1 Spatial discretization

A finite element spatial discretization is assumed where the spatial domain $D \subset \mathbb{R}^3$ is divided into subdomains using a finite element mesh. Consider a typical finite element D^e with shape functions $\{N_i^e(x)\} \in W^h \subset W$ defined over its nodes. Here W^h is a finite element space with the maximum element diameter $h > 0$. Then the vector representation of the finite element approximation of the solution over the element D^e can be written as

$$u^e(x,\boldsymbol{\theta}) = \mathbf{N}^e(x)\mathbf{u}^e(\boldsymbol{\theta}). \tag{5.10}$$

Similarly, from the previous iteration, we have the finite element approximation of the current guess solution v over the same discretized spatial domain. Substituting these finite element approximations into the weak form of the governing equations yields the following expressions for the element matrices

$$\begin{aligned} \mathbf{K}^e(\boldsymbol{\theta}) &= \int_{D^e} \nabla\mathbf{N}^e(x)[\widehat{\kappa}(x,\boldsymbol{\theta}) + \lambda v^2(x,\boldsymbol{\theta})](\nabla\mathbf{N}^e(x))^T \mathrm{d}x, \\ \mathbf{f}^e(\boldsymbol{\theta}) &= \int_{D^e} f(x,\boldsymbol{\theta})(\mathbf{N}^e(x))^T \mathrm{d}x. \end{aligned} \tag{5.11}$$

From Equation 5.7 and Equation 5.11, the element force vector can be written as

$$\begin{aligned} \mathbf{f}^e(\boldsymbol{\theta}) &= \int_{D^e} \sum_{i=0}^{P_f} f_i(x)(\mathbf{N}^e(x))^T \phi_i(\boldsymbol{\theta}) \mathrm{d}x, \\ &= \sum_{i=0}^{P_f} \Big(\int_{D^e} f_i(x)(\mathbf{N}^e(x))^T) \mathrm{d}x \Big) \phi_i(\boldsymbol{\theta}). \end{aligned} \tag{5.12}$$

where $f_i(x)$ can be approximated over the element D^e (using centroid[3], shape function, spatial average or other approximations) and the element force vector can be computed using a quadrature rule (e.g., the Gauss quadrature scheme) of appropriate order . Recall that $\widehat{\kappa}(x, \boldsymbol{\theta})$ is already available in a PC expansion (refer to Equation B.3). It can be readily seen from Equation 5.11 that once we represent the nonlinear term $v^2(x, \boldsymbol{\theta})$ in a PC basis, the element stiffness matrix can be readily computed.

From the previous iterative step, we have a stochastic reduced basis approximation of the current guess response $v(x, \boldsymbol{\theta})$ in the form Equation 5.8, i.e.,

$$v(x, \boldsymbol{\theta}) = \sum_{i=0}^{P_v} v_i(x) \phi_i(\boldsymbol{\theta}). \tag{5.13}$$

With $v(x, \boldsymbol{\theta})$ expressed in a PC basis, the term $v^2(x, \boldsymbol{\theta})$ can also be readily written in a PC basis as

$$v^2(x, \boldsymbol{\theta}) = \sum_{i=0}^{P_{v^2}} \eta_i(x) \phi_i(\boldsymbol{\theta}), \tag{5.14}$$

where $\eta_k(x) = \langle v^2(x, \boldsymbol{\theta}) \phi_k \rangle / \langle \phi_k^2 \rangle$. Hence from Equation B.3 and Equation 5.14 the conductivity can be written as

$$\begin{aligned} \kappa(x, v(x, \boldsymbol{\theta}), \boldsymbol{\theta}) &= \widehat{\kappa}(x, \boldsymbol{\theta}) + \lambda v^2(x, \boldsymbol{\theta}), \\ &= \sum_{i=0}^{P_k} \big(\widehat{\kappa}_i(x) + \lambda \eta_i(x) \big) \phi_i(\boldsymbol{\theta}), \end{aligned} \tag{5.15}$$

where $P_k = \max(P_1, P_{v^2})$. Now substituting Equation 5.15 into the expression for the element stiffness matrix Equation 5.11 leads to

$$\mathbf{K}^e(\boldsymbol{\theta}) = \sum_{i=0}^{P_k} \mathbf{K}_i^e \phi_i(\boldsymbol{\theta}),$$

where

$$\mathbf{K}_i^e = \int_{D^e} \nabla \mathbf{N}^e(x) [\widehat{\kappa}_i(x) + \lambda \eta_i(x)] (\nabla \mathbf{N}^e(x))^T \mathrm{d}x. \tag{5.16}$$

[3]The value of $f_i(x)$ over an element is approximated by its value at the centroid of the element.

The structure of equations Equation 5.16 and Equation 5.12 is similar to equations for the element matrices that arise when spatially discretizing linear SPDEs. The functions $(f_i(x), \widehat{\kappa}_i(x), \eta_i(x))$ can be approximated over each element using various approximation techniques, for example, centroid, spatial average or shape function based approximations. Assembly of the element matrices and incorporation of appropriate boundary conditions thus leads to a linear random algebraic system of equations of the form Equation 2.12, where the global stiffness and force matrices are given by Equation 2.14 (here $P \geq \max(P_k, P_f)$). The resulting equations Equation 2.12 are iteratively solved to approximate the response statistics.

5.2.2 Convergence criterion and numerical issues

We terminate the iterations when the L_2-norm of the difference between the consecutive solutions $\mathbf{v}(\boldsymbol{\theta})$ and $\mathbf{u}(\boldsymbol{\theta})$ is less than or equal to the user specified tolerance ϵ_{tol}, i.e.,

$$||\mathbf{u}(\boldsymbol{\theta}) - \mathbf{v}(\boldsymbol{\theta})|| < \epsilon_{tol}. \tag{5.17}$$

The L_2-norm in the preceding equation can be simplified (using orthogonality of PC basis functions) as

$$\begin{aligned} ||\mathbf{u}(\boldsymbol{\theta}) - \mathbf{v}(\boldsymbol{\theta})|| &= \left\langle \big(\mathbf{u}(\boldsymbol{\theta}) - \mathbf{v}(\boldsymbol{\theta})\big)^T \big(\mathbf{u}(\boldsymbol{\theta}) - \mathbf{v}(\boldsymbol{\theta})\big) \right\rangle^{\frac{1}{2}}, \\ &= \left(\sum_{i=1}^{P'} \big(\mathbf{u}_i - \mathbf{v}_i\big)^T \big(\mathbf{u}_i - \mathbf{v}_i\big) \langle \phi_i^2 \rangle \right)^{\frac{1}{2}}, \end{aligned}$$

where $P' \geq \max(P_u, P_v)$

In Equation 2.12, when the conductivity is nonlinear, note that both the current guess and updated solutions namely, $\mathbf{v}(\boldsymbol{\theta})$ and $\mathbf{u}(\boldsymbol{\theta})$ are expanded using SRBMs (and PC basis). Ideally, $\mathbf{u}(\boldsymbol{\theta})$ should be expanded in a higher order SRBM basis (and hence a higher order PC basis) compared to $\mathbf{v}(\boldsymbol{\theta})$ for numerical stability. But increasing the order of the basis at each iterative step is not computationally feasible. Hence the basis is truncated in real-world applications which may adversely effect the stability of the iterative scheme in certain cases. This problem can be alleviated by using an adaptive approach wherein the number of stochastic basis vectors is chosen based on the residual norm (which can be readily estimated, for example, using the approximation given in Equation 2.32) in the numerical approximation of Equation 2.12. Alternatively, h-refinement strategies [128] can be employed to refine the approximation locally in the probability space so that lower order global basis vectors can

provide better accuracy. We shall later demonstrate numerically in Section 5.3 that the inexact Picard iteration scheme converges satisfactorily for the model problem considered for various strengths of nonlinearity.

The converged response process given in the form Equation 5.8 can be post-processed to obtain the statistical moments of the response process and error metrics such as the L_2-norm of the residual error, K-norm error which we use in the numerical studies to analyze the convergence trends. Computation of the statistical moments and error metrics can be found in Section 2.5.2. In the following section, we outline the steps to deal with other forms of nonlinearities in the context of inexact Picard iteration schemes employing PC/SRBM projection methods.

5.2.3 Treating other types of nonlinearities

In the previous sections, we focused on additive type of nonlinearities. SPDEs with more general forms of nonlinearities can also be tackled using the proposed numerical scheme. For example, consider a multiplicative uncertainty model [34, 35, 125] where the conductivity is written in the form

$$\kappa(x, u, \boldsymbol{\theta}) = \widehat{\kappa}(x, \boldsymbol{\theta})u(x, \boldsymbol{\theta}).$$

Although, the above nonlinearity can be linearized by transforming the field variable using the Kirchoff transformation [34, 35], it can be alternatively treated using the proposed stochastic Picard iterative scheme. Given a PC basis representation of both the linear random conductivity and the response process as Equation B.3 and Equation 5.13, the nonlinear conductivity can be expanded in a higher order PC basis as follows:

$$\begin{aligned} \kappa(x, u, \boldsymbol{\theta}) &= \sum_{k=0}^{P'} \kappa_k(x)\phi_k, \\ \kappa_k(x) &= \sum_{i=0}^{P_1}\sum_{j=0}^{P_u} \widehat{\kappa}_i(x)u_j(x)\frac{\langle \phi_i\phi_j\phi_k \rangle}{\langle \phi_k^2 \rangle}, \end{aligned}$$

where $P' \geq \max(P_1, P_u)$.

The above equation when substituted into the variational formulation gives rise to a linearized system of equations from where the procedure follows according to the steps described in the preceding sections. We wish to highlight here that the present approach can be readily applied to a wide range of nonlinear stochastic heat transfer problems, provided we have an accurate PC representation of the constitutive laws.

5.3 Numerical studies

In this section, three numerical studies are presented to show the merits and de-merits of the formulation. Two studies are on heat transfer over two different spatial domains with nonlinear coefficients. The first study is a simple nonlinear heat equation defined on a L-shaped domain where the uncertainties are random variables in the conductivity, forcing and boundary conditions. The second study employs a random field model for the conductivity. The present formulation works well for both these studies where one can observe significant speed-up compared to MCS. The final study deals with one-dimensional Burger equation with the viscosity considered as a random variable.

For the sake of compactness, we use the notation *SRBM(r, N, s)* to denote an approximation to the response process obtained by solving a linear random algebraic system of equations whose coefficient matrix and right hand side are represented in a r^{th} order PC expansion employing N reduced order basis vectors. Here each SRBM basis vector has been truncated to a s^{th} order PC basis. We study the convergence trends of the error metrics as a function of r, N and s.

5.3.1 Steady-state heat transfer in an L-shaped channel

We consider a stationary heat transfer problem defined (originally studied in the context of diffusion in [56]) on a L-shaped channel $D \subset \mathbb{R}^2$ represented in Figure 5.1 where $D = ((-1,0)\times(-1,1))\bigcup((0,1)\times(0,1))$. Homogeneous Dirichlet boundary conditions have been applied on the boundary Γ_1. A normal flux g is imposed on the boundary Γ_2. Zero flux conditions have been applied on the other boundaries represented by Γ_0. A source term f is imposed on $D_1 = (0,1)\times(0,1)$ portion of the domain.

The stochastic solution, $u(x,\omega) \in \mathbb{R}, \forall x \in D$ and $\omega \in \Omega$ must satisfy almost surely,

$$\begin{aligned} -\nabla\cdot((\kappa_0+\kappa_1 u^2)\nabla u) &= \begin{cases} 0 & \text{in } D - D_1 \\ f & \text{in } D_1 \end{cases} \\ -(\kappa_0+\kappa_1 u^2)\tfrac{\partial u}{\partial n} &= \begin{cases} 0 & \text{on } \Gamma_0 \\ g & \text{on } \Gamma_2 \end{cases} \\ u &= 0 \text{ on } \Gamma_1, \end{aligned} \tag{5.18}$$

where κ_0 and κ_1 are conductivity parameters. The conductivity parameters and source terms are parametrized in terms of uniform random variables $\theta_1, \theta_2, \theta_3$ and θ_4 each distributed on

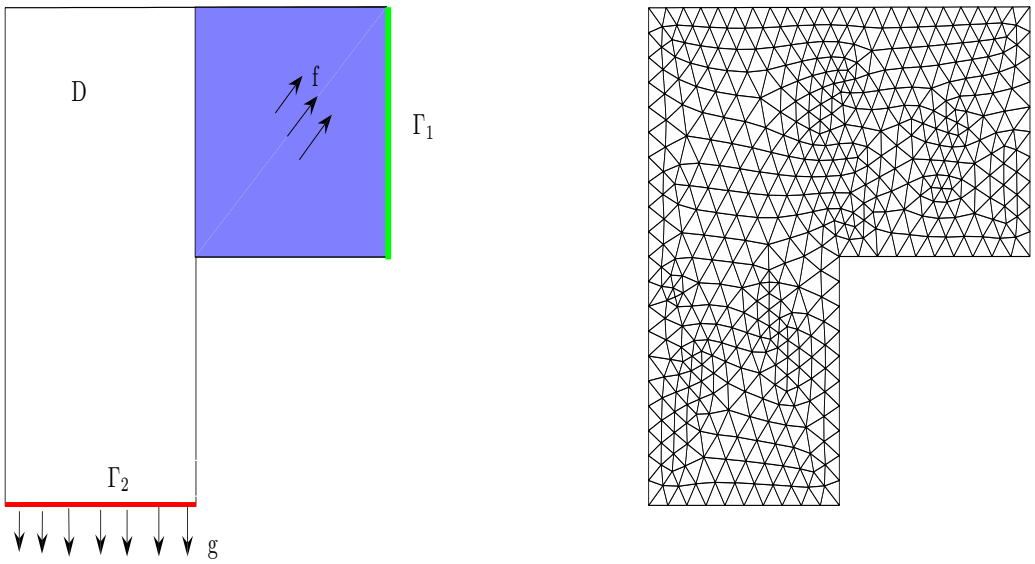

FIGURE 5.1: (a) Schematic of the problem statement (b) Finite element mesh on the problem domain.

$[-1, 1]$ given as:

$$\begin{aligned} \kappa_0 &= \mu_{\kappa_0}(1 + c_{\kappa_0}\sqrt{3}\theta_1), \\ \kappa_1 &= \mu_{\kappa_1}(1 + c_{\kappa_1}\sqrt{3}\theta_2), \\ f &= \mu_f(1 + c_f\sqrt{3}\theta_3), \\ g &= \mu_g(1 + c_g\sqrt{3}\theta_4). \end{aligned} \tag{5.19}$$

The deterministic parameters in the above equation are set to the following values:

$$\begin{aligned} &\mu_{\kappa_0} = 3, \quad \mu_{\kappa_1} = 1.5, \quad \mu_f = 6, \quad \mu_g = 2.25, \\ &C_{\kappa_0} = 0.2, \quad C_{\kappa_1} = 0.2, \quad C_f = 0.2, \quad C_g = 0.2, \end{aligned} \tag{5.20}$$

The spatial domain is discretized using a finite element mesh with 504 nodes and 924 triangular elements (refer to Figure 5.1(b)). A benchmark Monte-Carlo simulation with 100000 samples in four dimensions has been performed. Figure 5.2 shows the mean and standard deviations of the field variable u. Inexact Picard iteration scheme has been implemented where the response process has been truncated to either second or third order PC expansions. Varying number of reduced order basis vectors have been employed to study convergence. From Figure 5.3 it can be observed that the numerical approach results in highly accurate results where the maximum percentage errors in mean is less than 0.1% and less than 1% in the case of standard deviation. The maximum percentage errors in mean and

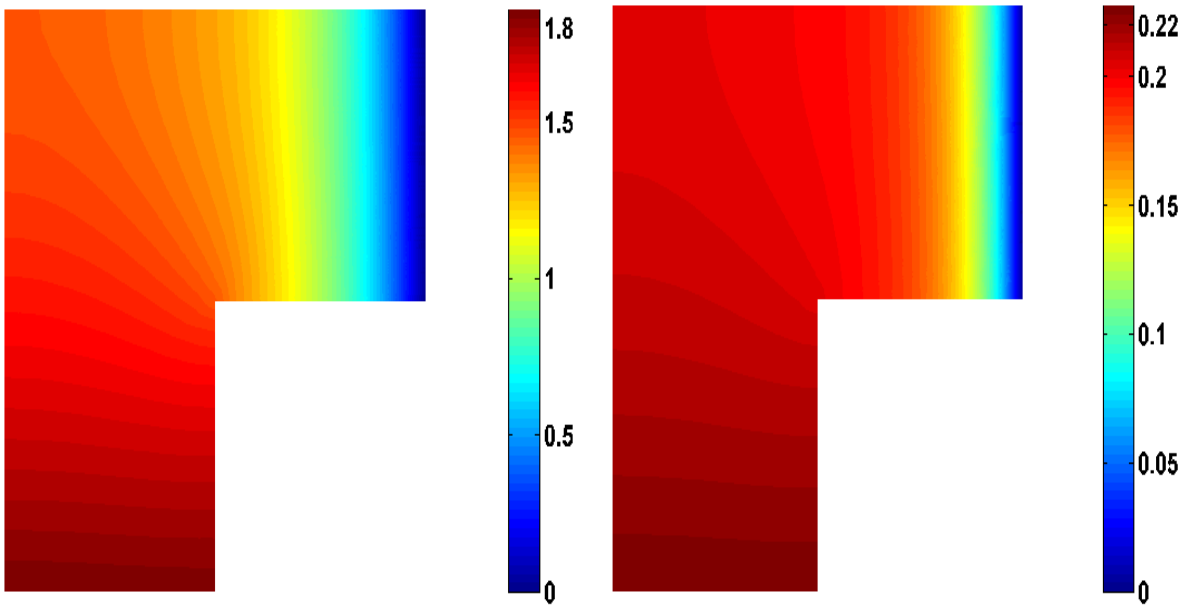

(a) (b)

FIGURE 5.2: (a) Mean and (b) standard deviation of the temperature profile.

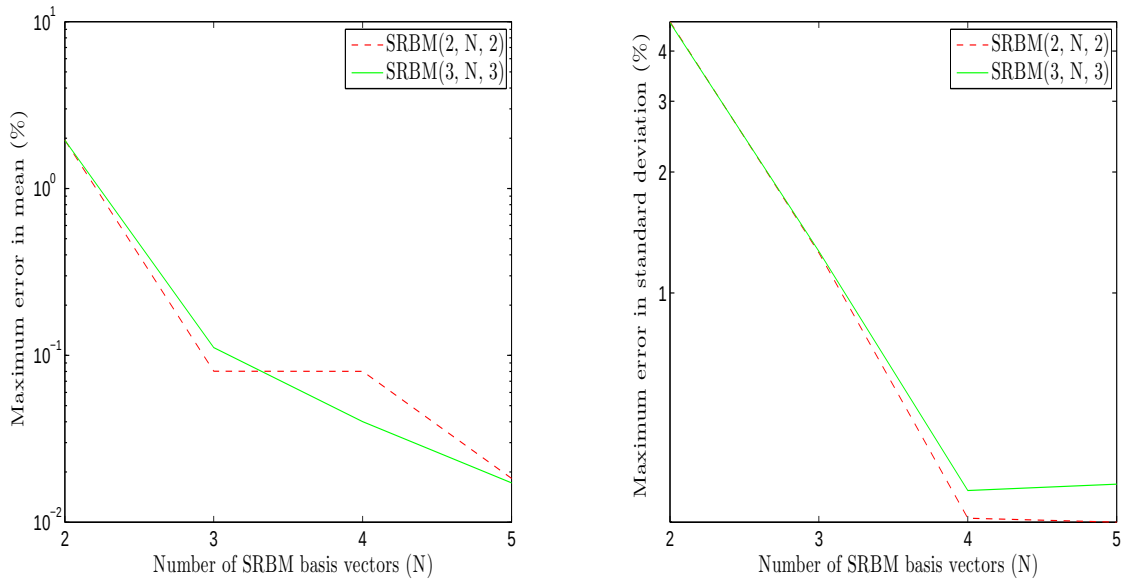

(a) (b)

FIGURE 5.3: (a) Maximum absolute percentage error in mean and (b) maximum absolute percentage error in standard deviation for varying orders of PC expansion (r, s) and number of basis vectors (N).

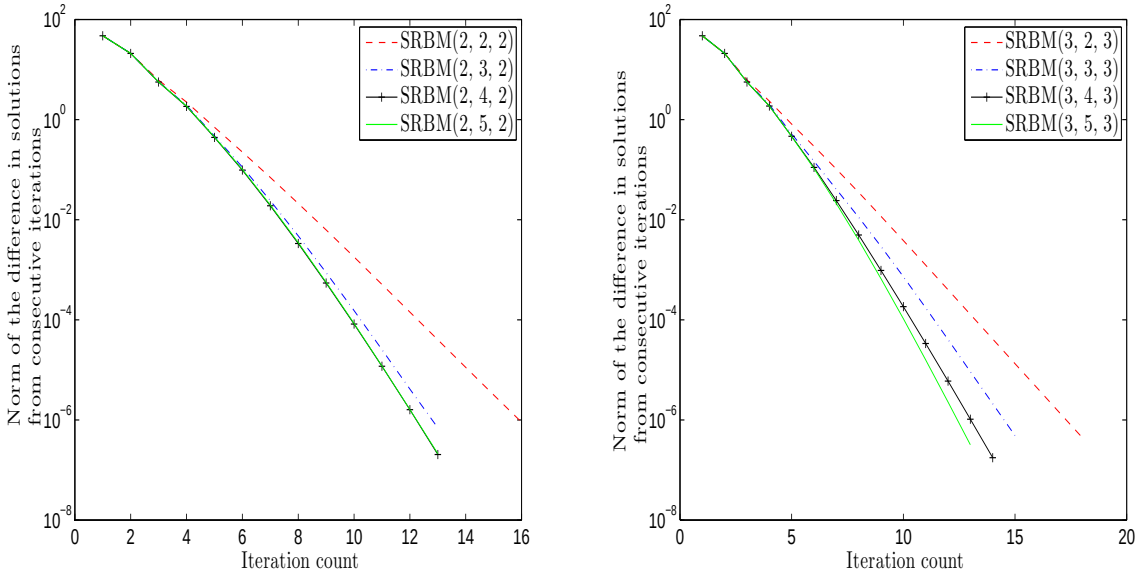

(a) (b)

FIGURE 5.4: Convergence trends of the inexact Picard iteration scheme: L_2-norm of the difference in solutions from successive iterations employing (a) second order PC and (b) third order PC.

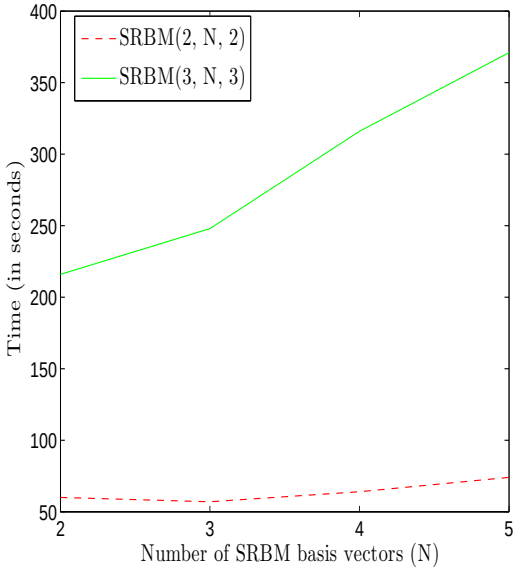

FIGURE 5.5: Time in seconds for convergence employing varying orders of PC expansion (r, s) and number of basis vectors (N)

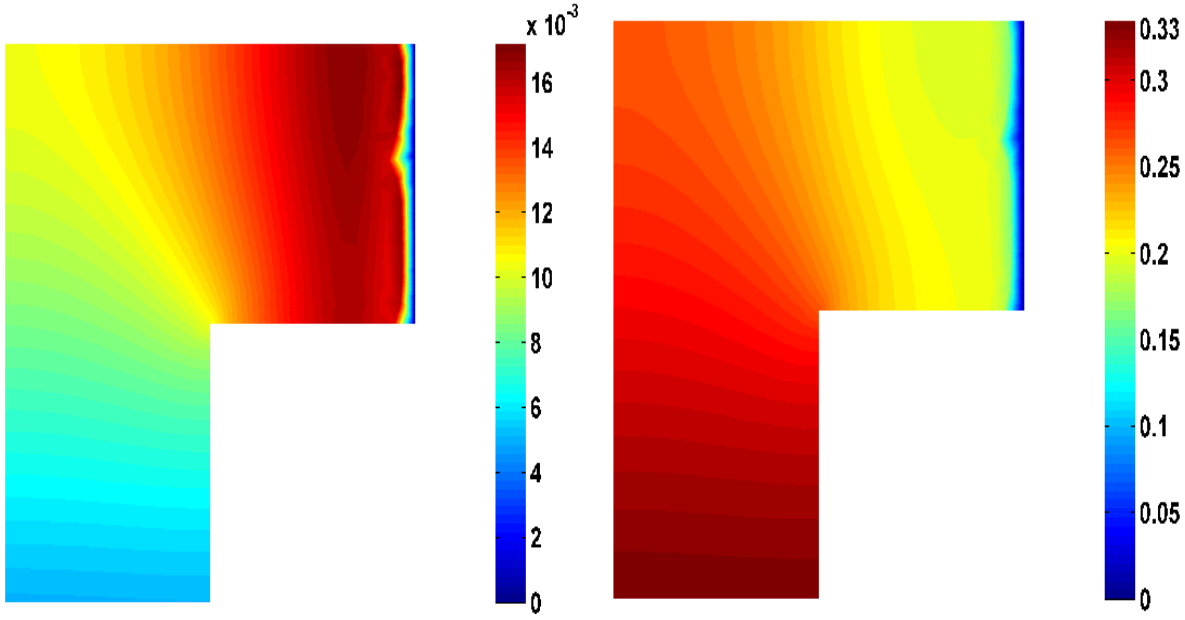

(a) (b)

FIGURE 5.6: Absolute percentage error profiles in (a) mean and (b) standard deviation employing five reduced order basis vectors in conjunction with third order PC expansions of the coefficient matrices, the right hand side and the basis vectors ($SRBM(3,5,3)$).

standard deviation tend to increase slightly after four basis vectors which may be attributed to Monte-Carlo errors. Figure 5.4 shows the convergence metric namely the L_2-norm of the difference in the consecutive response guesses for second and third order PC truncation of the response process. It can be clearly observed that the iteration count decreases when the accuarcy of approximation is increased at each iterative step by increasing the number of SRBM basis vectors. Figure 5.5 shows the time (in seconds) required for convergence employing varying orders of PC expansion and number of reduced order basis vectors. As expected, the computational time increases for higher order PC expansions when the number of SRBM basis vectors is increased. From figures 5.3 and 5.4 it may be concluded that the case $SRBM(3,5,3)$ leads to the most accurate solution which takes about 400 seconds for convergence. This is significantly faster compared to the 9 days required for the MCS with 100000 samples.

Figure 5.6 shows the absolute percentage error in mean and standard deviation over the L-shaped domain for the case when the response process is truncated in a third order PC expansion and five SRBM basis vectors have been employed. It shows that the approach leads to highly accurate results everywhere in the problem domain where the maximum percentage

errors in mean and standard deviation are 0.01% and 0.33% respectively.

This numerical study has been originally presented in [56] in the context of diffusion where it was analyzed employing generalized spectral decomposition method. We compare the results obtained by GSD and the current approach in the following section.

5.3.1.1 Comparison with generalized spectral decomposition method

Here we compare the inexact Picard iteration scheme with the generalized spectral decomposition method presented in [56]. The generalized spectral decomposition (GSD) method consists in searching an optimal decomposition of the solution to a stochastic problem under the form $\sum_{i=1}^{M} u_i \varphi_i(\boldsymbol{\theta})$, where the u_i are deterministic functions while $\varphi_i(\boldsymbol{\theta})$ are functions of the input random variables. In this context, the set of $\{\varphi_i\}$ are understood as a reduced basis.

Optimal decompositions could be easily defined if the solution u were known (by employing KL expansion or other spectral decomposition methods). In the case of linear symmetric elliptic coercive problems, by defining an optimal decomposition with respect to the underlying optimization problem, the functions u_i were shown to be solutions of an eigen-like problem. Nouy and Maître [56] presented ad-hoc algorithms based on classical (which they call Algorithm 1) and improved (called Algorithm 2) power method for classical eigenproblems for the resolution of the eigen-like problem in nonlinear SPDEs. We now define two metrics given as

$$\begin{aligned} \boldsymbol{\rho}_{\mu} &= \frac{|\boldsymbol{\mu}_{MCS} - \boldsymbol{\mu}_{SRBM}|}{sup(\boldsymbol{\mu}_{MCS})}, \\ \boldsymbol{\rho}_{\sigma} &= \frac{|\boldsymbol{\sigma}_{MCS} - \boldsymbol{\sigma}_{SRBM}|}{sup(\boldsymbol{\sigma}_{MCS})}, \end{aligned} \tag{5.21}$$

for the comparison study.

Here we consider the results generated using inexact Picard scheme when five SRBM basis vectors in terms of third order PC expansions which in turn have been employed on the stationary heat transfer equation defined on the L-shaped domain. The error metrics $\boldsymbol{\rho}_{\mu}$ and $\boldsymbol{\rho}_{\sigma}$ have been computed for the above mentioned problem settings. These metrics have been compared against $\boldsymbol{\rho}_{\mu}$ and $\boldsymbol{\rho}_{\sigma}$ in [56] where a seventh order expansion, namely $M = 7$ has been employed. Figure 5.7 shows the new relative errors in mean and standard deviation computed using Equation 5.21. Comparing these results with [56], we conclude that the maximum error in mean obtained employing inexact Picard iteration scheme is at least a 20 times lower than the results obtained employing GSD method. In addition, note that the inexact Picard scheme employs a lower PC expansion as compared to the GSD method.

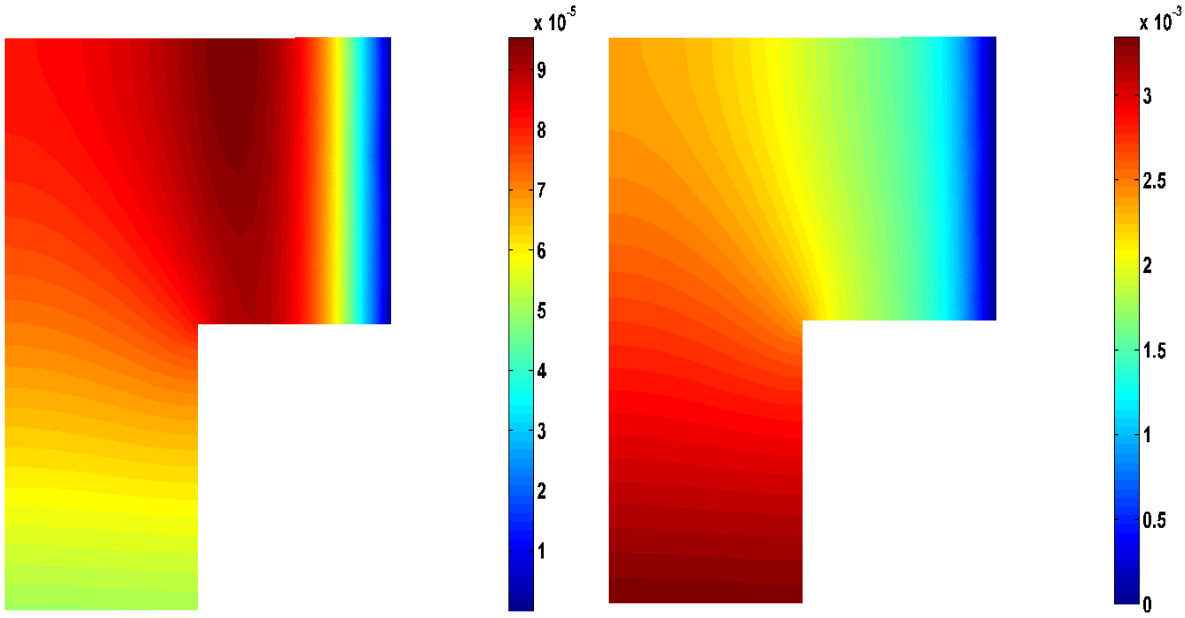

(a) (b)

FIGURE 5.7: (a) $\boldsymbol{\rho}_{\mu}$ and (b) $\boldsymbol{\rho}_{\sigma}$ employing five reduced order basis vectors in conjunction with third order PC expansions ($SRBM(3,5,3)$).

On the other hand maximum error in standard deviation are slightly higher(less than 0.0035 compared to less than 0.003) compared to the results generated by GSD method employing Algorithm 1 and Algorithm 2. This can be attributable to the higher order expansions employed in GSD method. The spatial variation in the relative error in standard deviation generated using the SRBM based approach is more comparable to the trend generated by Algorithm 1. Algorithm 2 on the other hand, seems to generate results with very small errors ($<<$ 0.003) everywhere spatially. It is anticipated that similar accuracy could be achieved employing higher order PC expansions in the Picard iterative scheme.

In this study, the randomness in the PDE is only present through random variables in the conductivity, forcing and boundary conditions. In the following numerical study, we deal with a random field representation of the stochastic conductivity.

5.3.2 Heat transfer on a square domain

Consider a square domain defined by $D = [0,1]^2$ with homogeneous Neumann boundary conditions on the walls ($x = 0, x = 1$) and Dirichlet boundary conditions $u = 0$ and $u = 1$ on the lower and upper boundaries respectively. The stochastic conductivity given by

Equation 5.2 is nonlinear on the domain with no sources or sinks. The linear stochastic component of the conductivity given by $\widehat{k}(x,\omega)$ is modeled as a statistically homogeneous lognormal random field with an isotropic exponential covariance function,

$$C_Y(r) = \sigma_Y^2 \exp(-r/b),$$

where $r = |\mathbf{x} - \mathbf{y}|$ and b is the correlation length. We have set the correlation length $b = 0.2$ and the mean of the lognormal random field $\langle \widehat{k}(x,\omega) \rangle = 1$ and variance $\sigma_Y^2 = 1$. Refer to Appendix B for details on the lognormal random field discretization. The parameter that controls the degree of nonlinearity namely λ in Equation 5.2 is set to $\lambda = 0, 0.1, 0.5, 1$ to represent linear, weak, moderate and strong nonlinear conductivities, respectively. A finite element spatial discretization was performed using a mesh of triangular elements with 2763 degrees of freedom and 5528 elements; see Figure 5.8.

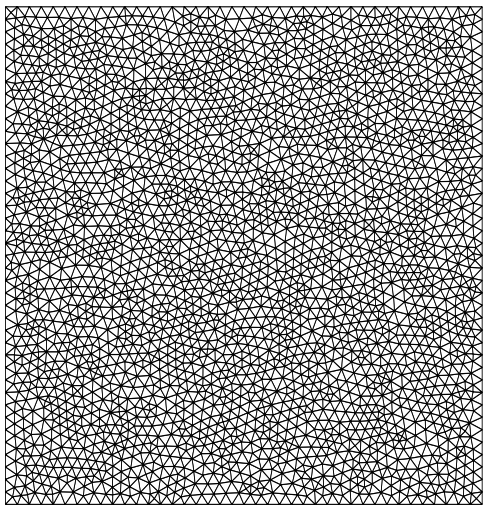

FIGURE 5.8: Finite element mesh on the square domain.

A Monte-Carlo simulation with 100000 samples is first conducted to generate a set of benchmark results against which the performance of the inexact stochastic Picard iteration scheme is compared. The underlying Gaussian random field $Y(x,\omega)$ of the lognormal model for the linear conductivity term $\widehat{\kappa}(x,\omega)$ is discretized using the Karhunen-Loève expansion scheme [39] and ten random variables are retained in the expansion. $\widehat{\kappa}(x,\boldsymbol{\theta})$ is then expanded in a second order Hermite PC basis in terms of ten Gaussian random variables. For all the numerical studies, we start with an initial guess of zero and the iterations are terminated

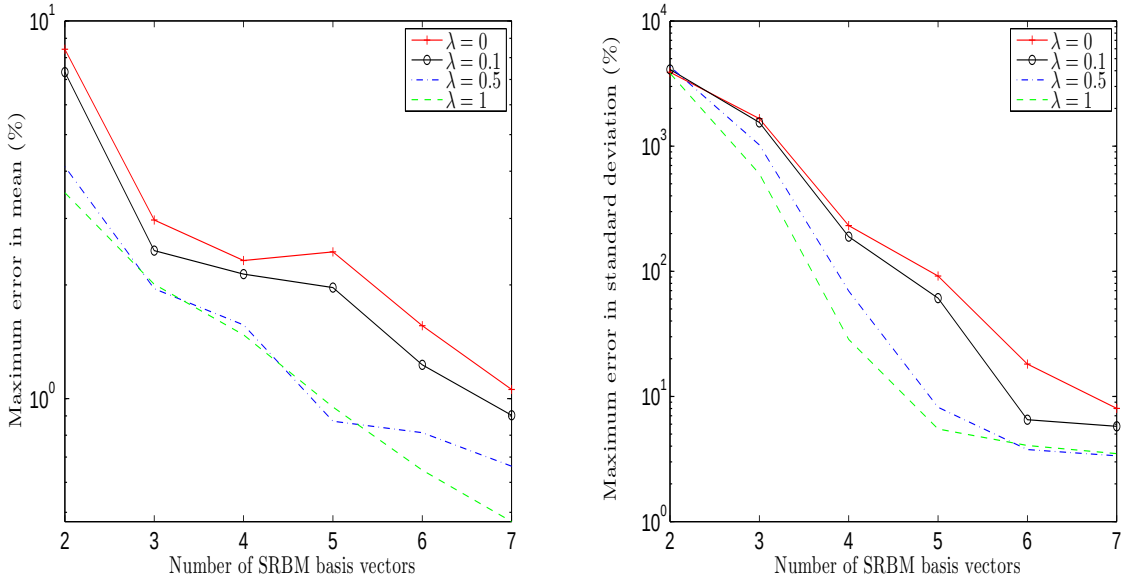

(a) (b)

FIGURE 5.9: (a) Maximum percentage error in mean (b) and maximum percentage error in standard deviation for different strengths of nonlinearities for the case $SRBM(2, N, 2)$.

when the norm given in Equation 5.17 is less than or equal to 10^{-6}. The Monte-Carlo mean and standard deviation are computed from the solutions of these simulations. Note that errors involved in these simulations are only due to truncated representation of $\widehat{\kappa}(x, \omega)$ and not due to the truncation of PC expansions of the response process.

We now present some error metrics computed by comparing the results generated by MCS and the proposed numerical approach that employs the Picard iterative scheme in conjunction with SRBMs. We restrict the expansion of $\widehat{\kappa}(x, \boldsymbol{\theta})$ to a second order PC basis in terms of ten Gaussian random variables for all the strengths of nonlinearities (λ). The initial guess is considered to be zero over the entire spatial domain and the iterations are terminated when the L_2-norm of the difference between successive solutions is less than or equal to 10^{-6}. Convergence is studied for varying number of SRBM basis vectors where each stochastic basis vector is truncated to a second order PC expansion. For each case, the inexact Picard scheme takes around 12 iterations to meet the stopping criterion in Equation 5.17 with $\epsilon_{tol} = 10^{-6}$.

Figure 5.9 shows two error metrics namely maximum errors in mean and standard deviation respectively. This figure shows that the numerical scheme provides good approximations for the response statistics as the number of basis vectors is increased. The linear problem ($\lambda = 0$) is similar to the one dealt in [36] – the errors obtained by employing SRBMs are

considerably small compared to those obtained using perturbation-based moment methods in that study. Our results also suggest that the errors in the mean and standard deviation tend to decrease when the strength of nonlinearity is increased. This trend can be attributed to the fact that the standard deviation of the response decreases with increase in the value of λ due to the chosen structure for the nonlinearity model. As a consequence, the proposed stochastic Picard iteration scheme converges to improved approximations for the mean and standard deviation of the response.

Figure 5.10 shows the spatial distribution of the percentage error in standard deviation for the strongly nonlinear case ($\lambda = 1$) when 7 basis vectors are employed to approximate the solution process. It can be seen that the maximum error in the standard deviation is 3.4% which is remarkable considering that we set the variance of the conductivity field $\sigma_Y^2 = 1$.

Theoretically, higher order PC expansion of basis vectors would lead to improved approximations at the expense of a significant increase in computational complexity. In our numerical studies, we did not find any significant increase in the accuracy of the solutions using higher order PC representation of the basis vectors. Hence, we have presented the results only with second order PC expansions which agree well with the benchmark results.

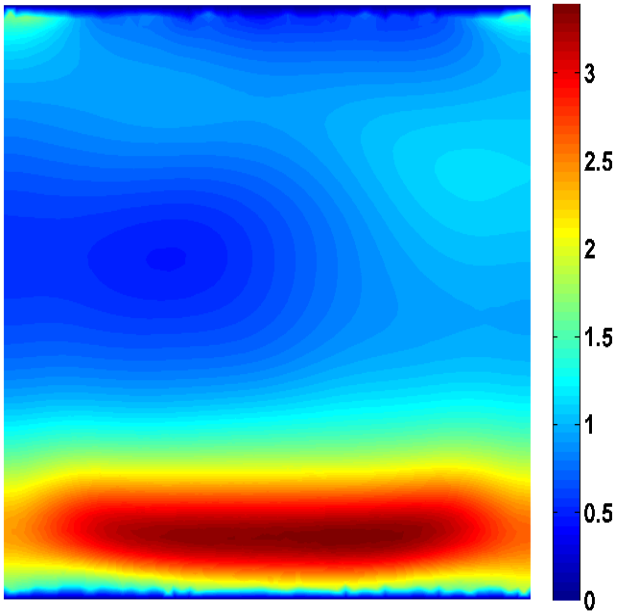

FIGURE 5.10: Spatial distribution of percentage error in standard deviation for $\lambda = 1$ using 7 basis vectors namely $SRBM(2, 7, 2)$.

In addition to converging to good approximations, our approach is orders of magnitude faster than the benchmark Monte-Carlo simulation when the number PC basis functions is

order of magnitudes lower in comparison to the number of degrees of freedom. To illustrate, we consider the number of floating point operations required by MCS and SRBM for a two-dimensional elliptic SPDE spatially discretized on a structured mesh. It can be shown that MCS will take $N_s N_{iter} O(n^2)$ floating point operations, where N_s is the sample size, N_{iter} is the average number of Picard iterations conducted for each realization of the input random variables, and n is the total number of degrees of freedom. On the other hand, SRBMs require $N_{iter} O(n^{1.5})$ to compute the preconditioner at each inexact Picard iteration and an additional $O(PP_u + PP_u^2)$ matrix-vector operations for Galerkin projection (see Equation 2.29). In practice if $P, P_u <<< n$, it is expected that the computational cost of SRBMs will be orders of magnitude lower than MCS. For this problem (with $n = 2763$), SRBM based approach is about 800 times faster compared to MCS to obtain the first two moments with same level of accuracy which translates to about 125 *deterministic* evaluations compared to 100000 evaluations taken by MCS. We expect the computational advantages offered by SRBMs to be more dramatic for problems with more degrees of freedom.

The numerical studies discussed so far demonstrated the applicability of the current formulation to simple problems. In the following study dealing with 1D Burger's equation, we discuss the limitations of the inexact fixed point scheme and motivate the need for more sophisticated schemes.

5.3.3 1D Burger's equation

We now consider the Burger's equation in one dimension where the viscosity is considered to be random. The stochastic Burger's equation is given by:

$$\frac{\partial f(\omega)}{\partial x} - \mu(\omega)\frac{\partial^2 u(\omega)}{\partial x^2} = 0, \text{ on } x = [-3, 3], \omega \in L_2(\Omega, \mathcal{F}, \mathcal{P}) \tag{5.22}$$

with the Dirichlet boundary conditions $u = 0$ and $u = 1$ imposed at $x = -3$ and $x = 3$ respectively. The viscosity, μ, has been taken to be a Gaussian random variable with a mean $\bar{\mu} = 0.25$ and a coefficient of variation $COV(\mu) \equiv \frac{\sigma}{\mu} = 10\%$ where σ refers to the standard deviation. Here $f(\omega)$ is chosen to be $u(\omega)(\frac{1}{2} - u(\omega))$ in which case the PDF of the PDE has an analytical solution given by [129]

$$\mathcal{P}(u) = \frac{\exp\left(-\left(\frac{x}{4\tanh^{-1}\left(1-2u\right)} + \bar{\mu} \right)^2 / 2\sigma^2 \right) \left| \frac{x}{\left(u-1\right)u\tanh^{-1}\left(1-2u\right)^2} \right|}{8\sqrt{2\pi}\sigma}. \tag{5.23}$$

Finite difference spatial discretization of the stochastic Burger's equation where the interval $[-3, 3]$ is divided into $N + 2$ sections each with a step length h using an upwinding

scheme results in the following discretized set of equations:

$$\frac{1}{2}\left(\frac{u_i - u_{i-1}}{h}\right) - \frac{u_i^2 - u_{i-1}^2}{2h} - \frac{\mu}{h^2}\left(u_{i-1} - 2u_i + u_{i+1}\right) = 0, \tag{5.24}$$

where u_i refers to the solution at the i^{th} grid point $\forall i \in \{0, 1, 2, 3, \cdots, N+1\}$.

The viscosity can be expressed in terms of a standard normal random variable θ as follows:

$$\mu = \bar{\mu} + \sigma\theta. \tag{5.25}$$

Employing the stochastic inexact fixed-point scheme discussed in the preceding sections we can linearize Equation 5.24 as follows:

$$\frac{1}{2}\left(\frac{u_i^{(k)} - u_{i-1}^{(k)}}{h}\right) - \frac{u_i^{(k-1)}u_i^{(k)} - u_{i-1}^{(k-1)}u_{i-1}^{(k)}}{2h} - \frac{\mu}{h^2}\left(u_{i-1}^{(k)} - 2u_i^{(k)} + u_{i+1}^{(k)}\right) = 0, \tag{5.26}$$

where $u_i^{(k)}$ refers to the solution computed at the i^{th} grid point on k^{th} iteration. Equation 5.26 can be equivalently expressed as:

$$u_{i-1}^{(k)}\left(-\frac{1 - u_i^{(k-1)} - u_{i-1}^{(k-1)}}{2h} - \frac{\mu}{h^2}\right) + u_i^{(k)}\left(\frac{1 - u_i^{(k-1)} - u_{i-1}^{(k-1)}}{2h} + \frac{2\mu}{h^2}\right) - u_{i+1}^{(k)}\frac{\mu}{h^2} = 0, \forall k \geq 1 \tag{5.27}$$

We start with the iterative process with an initial guess $\mathbf{u}^{(0)}$ in a PC basis and using Equation 5.27 iterate until the convergence criterion given in Equation 5.17 is met. Let $\mathbf{u}^{(k-1)}$ expanded in a PC basis (as in Equation 5.13) be the current guess after $k-1$ iterations. From Equation 5.13, the solution at the i^{th} grid point can be expressed as:

$$u_i^{(k-1)} = \sum_{j=0}^{P} u_i^j \phi_j(\theta), \tag{5.28}$$

where $\{\phi_j(\theta)\}$ are Hermite polynomials in terms of the standard normal random variable θ. Substituting Equation 5.28 and the expansion of μ from Equation 5.25 in Equation 5.27 we obtain a linear random algebraic system of equations of the form Equation 4.14 where $\mathbf{K}$ and $\mathbf{f}$ are given by Equation 4.15, $\mathbf{K}_j \in \mathbb{R}^{N\times N}$ and $\mathbf{f}_j \in \mathbb{R}^N, \forall 0 \leq j \leq P$. The expressions for $\{\mathbf{K}_j\}$ and $\{\mathbf{f}_j\}$ are given as follows:

$$\begin{aligned}
\mathbf{K}_0 &= \begin{pmatrix} s_0 & t_0 & 0 & \cdots \\ r_0 & s_0 & t_0 & 0\cdots \\ 0 & \cdots & r_0 & s_0 \end{pmatrix} \quad \mathbf{K}_1 = \begin{pmatrix} s_1 & t_1 & 0 & \cdots \\ r_1 & s_1 & t_1 & 0\cdots \\ 0 & \cdots & r_1 & s_1 \end{pmatrix} \\
\mathbf{K}_j &= \begin{pmatrix} s_j & 0 & 0 & \cdots \\ r_j & s_j & 0 & 0\cdots \\ 0 & \cdots & r_j & s_j \end{pmatrix}, \quad \forall 1 \geq j \leq P \\
f_N^0 &= -t_0 \qquad\qquad f_N^1 = -t_1 \\
f_i^j &= 0 \qquad\qquad \text{elsewhere}
\end{aligned} \tag{5.29}$$

$$\begin{aligned} r_0 &= -\frac{1-u_i^0-u_{i-1}^0}{2h} - \frac{\bar{\mu}}{h^2}, \quad s_0 = \frac{1-u_i^0-u_{i-1}^0}{2h} + \frac{2\bar{\mu}}{h^2}, \quad t_0 = -\frac{\bar{\mu}}{h^2}, \\ r_1 &= -\frac{-u_i^1-u_{i-1}^1}{2h} - \frac{\sigma}{h^2}, \quad s_1 = \frac{-u_i^1-u_{i-1}^1}{2h} + \frac{2\sigma}{h^2}, \quad t_1 = -\frac{\sigma}{h^2}, \\ r_j &= -\frac{-u_i^j-u_{i-1}^j}{2h}, \qquad\qquad s_j = \frac{-u_i^j-u_{i-1}^j}{2h}, \end{aligned} \tag{5.30}$$

Here we set $\bar{\mu}$ to 0.25 and the coefficient of variation of μ i.e $\frac{\sigma}{\bar{\mu}}$ to 10%. A Monte-Carlo simulation has been performed over the linear algebraic system of equation given above which forms the benchmark solution for the SPDE. This simulation has been performed by employing 100000 samples on a uniform grid with $h = 0.001$ which took about 12 hours to compute the first two moments of the response. The mean and standard deviation profiles of the solution are given in Figure 5.11. It may observed that at $x = 0$, the solution is deterministic in nature i.e. the variance of the solution is zero. If the viscosity parameter is a random field in contrast to the random variable model considered here, the centerline solution may be stochastic in nature.

The proposed inexact Picard scheme has been employed to obtain the response statistics by truncating the solution process at each iteration to a second order PC expansion. The initial guess is set to the deterministic response with viscosity set as $\mu = \bar{\mu}$. Convergence trends are studied by incrementing the number of reduced order basis vectors. The percentage error in computing mean and standard deviation along with the approximate mean and standard deviation profiles along x using different number of SRBM vectors are shown in 5.11. It can be observed that the approximate moments converge to Monte-Carlo solutions when the number of SRBM basis vectors are increased. It can be inferred from 5.11 (c) that maximum percentage error in approximating the mean is a little over 1% at a location where the mean is very close to zero. Thus it can be concluded that the proposed scheme results in good approximations of the mean. Similarly, it has been observed that percentage errors in standard deviation (refer 5.11) are less than 1% everywhere except in the small neighbourhood of the centerline where true standard deviation is close to zero. This trend can be alleviated by further refining the grid.

The computational times required for inexact Picard iteration scheme employing three, four and five SRBM basis vectors in terms of second order truncated PC representation of each basis vectors are 291s, 495s and 396s respectively which are considerably faster compared to the 12 hours taken by Monte-Carlo simulations.

Figure 5.12 shows the L_2-norm of the difference in the PC expansion of the solutions from successive iterations. Here, it can be inferred that the convergence albeit slow is monotonic

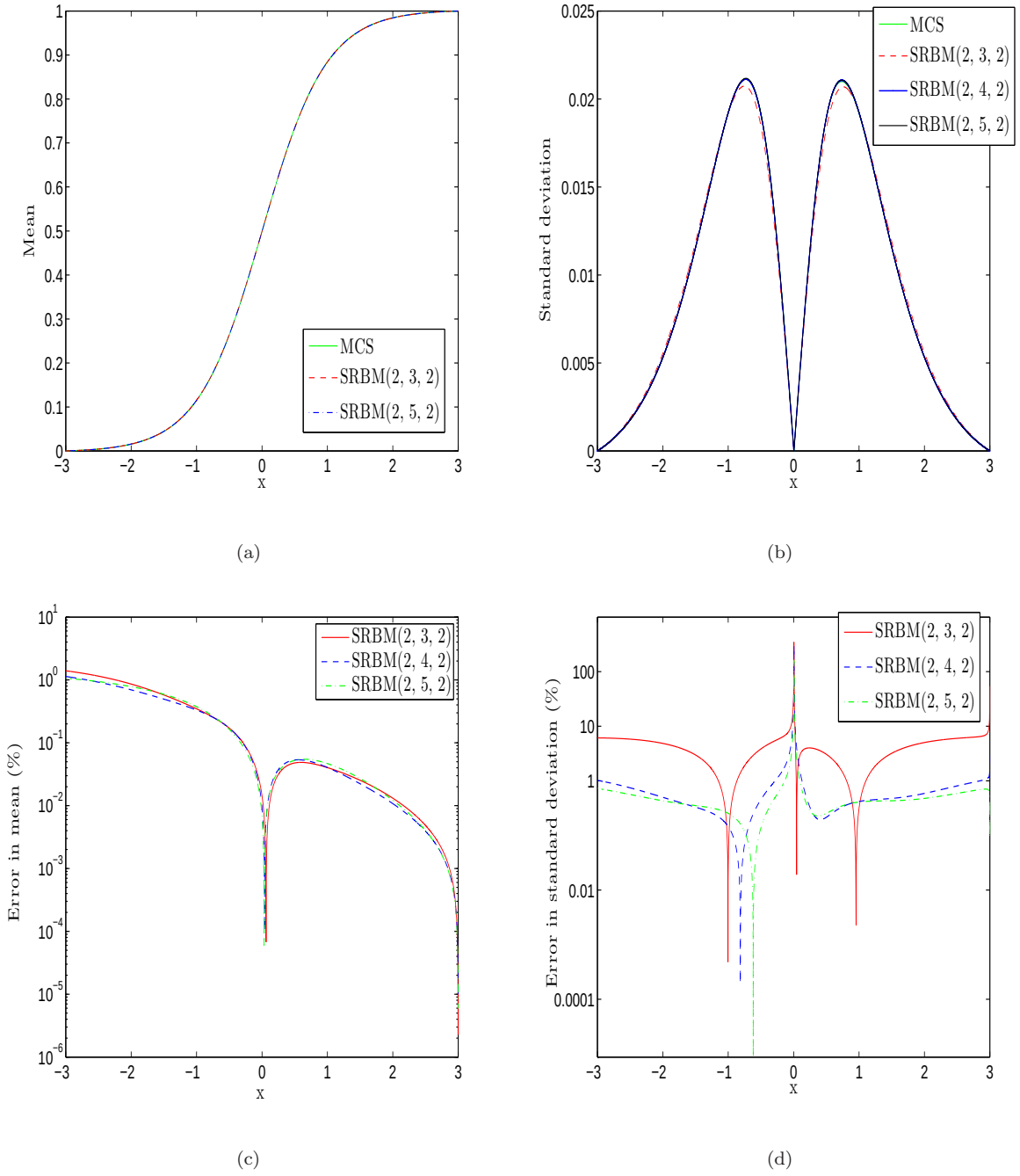

FIGURE 5.11: (a) Mean profile (b) Standard deviation of the profile (c) absolute percentage error in mean at each spatial location and (d) absolute percentage error in standard deviation for varying number of SRBM basis vectors employing second order PC expansions.

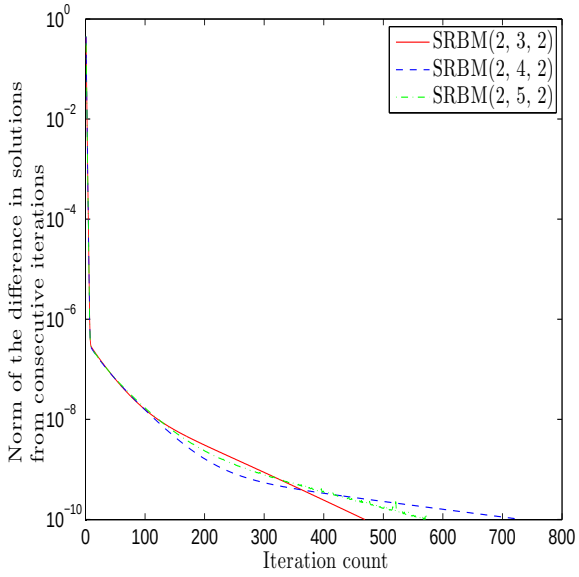

FIGURE 5.12: The convergence criteria namely the norm in the difference of the successive solutions with each iteration for varying number of SRBM basis vectors employing second order PC expansions

in nature with a dramatic decrease observed in the first few iterations. The tolerance is set to 10^{-5} for both the inexact Picard scheme and Monte-Carlo simulations. The convergence slows down significantly after 10^{-4}. The number of iterations for the convergence of the stochastic problem is still comparable to that of the convergence of deterministic solution.

It has been observed that the norm of the difference of the solution between successive iterations oscillates wildly towards the end when higher order PC expansions are employed to represent each SRBM basis vector. Thus Picard iterative in conjunction with the upwind finite difference scheme does not present a stable iterative scheme for the stochastic problem. Even when the convergence is monotonic in the case of second order PC expansions, it is very slow. Also the convergence is highly sensitive to the initial guess. Newton scheme [129] works well for the determinstic case where the convergence is obtained in about 20 iterations for the same tolerance level. This motivates the development of stochastic Newton iterative schemes with line search to tackle the Burger's equation with randomly parametrized viscosity.

5.4 Summary

In this chapter, we propose an inexact Picard iteration scheme for analysis of nonlinear stochastic PDEs. The central idea underpinning the proposed formulation is to combine the Picard iteration scheme with generalized stochastic reduced basis methods that employs basis vectors spanning a preconditioned stochastic Krylov subspace. We show the existence of a fixed point for a specific nonlinear stochastic heat equation. Numerical studies were presented for heat equation on an L-shaped and square domains with stochastic conductivity. Comparison studies have been conducted for linear and weakly/strongly nonlinear conductivity models. The results on heat equation show that the present numerical scheme provides good approximations for the response statistics as the expansion order is increased while taking significantly less computational time compared to standard Monte Carlo simulation. We then present a numerical study on 1D Burger equation where the method does not work well. The proposed formulation is not stable for this problem when higher order PC expansions have been employed to expand the SRBM basis vectors. For low order PC expansion the convergence is monotonic but very slow. In addition convergence is highly sensitive to the initial guess.

The proposed approach can be enhanced further by employing adaptive multi-element generalizations discussed in Chapter 3 or by adaptively increasing the number of stochastic basis vectors using estimates of the residual norm. It is also of interest to develop Newton-Raphson-SRBM formulations based on the ideas presented here since this may provide faster convergence rates. The proposed approach is general in scope and can be applied to simple nonlinear stochastic elliptic partial differential equations such as the numerical studies presented on heat transfer. A general rule-of-thumb for the applicability of this formulation is the stability of the determinstic fixed point iterative scheme on the deterministic version of the PDE. If the deterministic Picard scheme is unconditionally stable, then the inexact Picard iterative scheme can be employed to tackle the stochastic problem. A theoretical analysis of the convergence of the proposed iterative numerical scheme would be useful to gain further insights into the convergence characteristics of the stochastic Picard iteration scheme.

Chapter 6

Concluding remarks and future work

6.1 Conclusions

The focus of this thesis is to employ SRBMs to solve a class of linear and nonlinear elliptic SPDEs arising in heat transfer analysis of engineering and natural systems. The contributions of the research are as follows:

1 In Chapter 3, h-refinement strategy of stochastic reduced basis methods (multi-element SRBMs or ME-SRBMs) has been presented for solving linear random algebraic systems of equations which enhance the accuracy of SRBMs for a given number of basis vectors. Here the random space is decomposed into multiple subdomains and then SRBMs are applied on the local partitions of the random space. The elemental or local statistics are subsequently assimilated to estimate the global statistics. Theoretical result on the convergence of the $\mathbf{K}$-norm error has been presented. Two preconditioning strategies namely global and local preconditioning strategies have been presented. Local preconditioning results in better approximations compared to global preconditioning strategy. But the computational costs employing local preconditioning strategy are higher. Hence for large scale problems with many degrees of freedom, global preconditioning strategy should be employed for efficiency. Numerical studies indicate that ME-SRBMs provide more accurate statistics compared to standard single-element SRBMs. In contrast to p-refinement, the h-refinement strategies (ME-SRBMs) admit a large degree of parallelization. The method presented in the current form however suffers from the

curse of dimensionality for large scale problems with large number of random variables. However, adaptive spatial decomposition algorithms could be developed based on the ideas presented in this chapter.

2 A novel approach to solve linear elliptic PDEs on random domains has been proposed in Chapter 4. The governing PDEs are spatially discretized (using finite elements) by employing mesh deformation strategy resulting in a linear random algebraic system of equations in a PC basis. Mesh deformation facilitates the consistency in local-global connectivity across the different coefficients of PC expansion which are in turn computed non-intrusively using PC projection schemes. We have proved the equivalence of the method with a state-of-the-art technique to tackle geometric uncertainty where the domain mapping is performed in continuum contrary to the mapping in discrete sense performed in this chapter. Also, a weak condition on the degree of perturbation for the well-posedness of the problem has been established. Numerical studies involving heat transfer studies on two-dimensional domains indicate that the proposed approach converges to highly accurate solutions at modest computational costs. We have also presented a large scale numerical study involving three-dimensional gas turbine blade model where the cooling core geometries are uncertain. This study also shows that the method converges to highly accurate solutions at significantly lower computational costs compared to simulation techniques. Moreover the method is very general scope and can be applied to wide class of PDEs defined on random domains. Various mesh deformation techniques could be easily incorporated into the presented framework and the existing deterministic solvers could be easily employed to analyze the stochastic problem.

3 SRBMs in combination with the Picard iterative scheme have been applied to nonlinear SPDEs in Chapter 5. The important steps that are central to this new formulation are to linearize the governing equations using the response process from the last iterative step and subsequently discretizing the governing equations which results in a linear random algebraic systems of equations. This system of equations are then solved using SRBM projection schemes to obtain the response process which acts as the next solution guess. This iterative procedure is continued till a desired accuracy is achieved. Two numerical studies involving heat transfer on an L-shaped channel and square domain have been presented which show convergence for varying degree of nonlinearities on

increasing the number of SRBM basis vectors. The technique provided highly accurate results and the computational gains are orders of magnitude compared to Monte-Carlo simulations. These numerical studies suggest that the stochastic inexact Picard scheme could be employed to problems where the deterministic setting of the problem has a solution via the deterministic Picard iterative scheme. Finally, a numerical study involving the 1D Burger equation has been presented where the method is not stable for higher orders of PC expansions. It has also been observed that for some settings convergence can be very slow, motivating the need to develop more sophisticated techniques such as stochastic inexact Newton schemes based on SRBMs.

6.2 Future work

Further research should primarily focus on improving the computational efficiency and robustness of the aforementioned formulations, the details of which are as follows:

⋆ **ME-SRBMs :** In Chapter 3 the random space has been divided into a fixed number of subdomains where SRBM approximations of the response process have been obtained. However for large scale complex problems with a large number of variables, this approach suffers from the *curse of dimensionality*. In such a case, the notion of adaptive spatial decomposition can be efficiently leveraged. The input random space could be adaptively decomposed based on the residual error norm or other error metric and highly accurate solutions could be thus be obtained employing relatively smaller number of reduced order basis vectors in a local region. Numerical approaches employing adaptive h-refinement strategies could be developed to tackle geometrical uncertainties and nonlinearities in the governing equations in addition to solving SPDEs where the uncertain constitutive laws exhibit a high degree of variability.

⋆ **Geometric Uncertainty:**

1. **Efficient computation of stochastic coefficient matrices:** In Chapter 4, we have employed Monte-Carlo method to compute the coefficients of PC expansion in the numerical studies. Alternative strategies should be investigated for efficiently computing the stochastic coefficient matrices. This will involve the development of sparse quadrature schemes and intrusive formulations.

2. **Adaptivity:** Adaptive strategies employing ME-SRBMs could be investigated in the context of the global and element level formulations. In the global-level formulation, the random space underlying the stochastic domain can be decomposed into subdomains thus reducing the variability in each subdomain. Then a robust mesh deformation strategy could be applied in conjunction with local preconditioning (in this context refers to a local nominal mesh) can be applied to obtain robust deformed meshes thus eliminating element reversals or mesh collapses. SRBM approximation with smaller number of basis vectors could then be employed to obtain the response process in each random element. The statistics from the local response processes could then be assimilated to compute the global statistics.

   Adaptivity could also be studied in the context of the element-level formulation where assigning variable material properties during mesh deformation based on the elemental area/volume alleviates element reversals or mesh collapses. Lower order PC expansions of the matrices can be performed for elements which undergo smaller deformations during the mesh deformation process. Higher order PC expansions can be employed on the other hand for elements undergoing large deformations. This notion of adaptivity could be leveraged to improve the efficiency of the element-level formulations for tackling geometric uncertainty.

⋆ **Nonlinearities:**

1. **Faster iterative schemes:** The inexact Picard scheme is shown to be slow and not unconditionally convergent for the 1D Burger's equation study in Chapter 5. Faster iterative schemes like the Newton-Raphson scheme could be investigated to tackle more complex nonlinear problems where the Picard scheme is not unconditionally convergent or sluggish.

2. **Theoretical analysis:** It is also anticipated that some theoretical results may be established on the convergence of stochastic Newton and Picard iteration schemes employing SRBMs.

3. **Adaptivity:** Adaptive schemes could be explored in order to improve the convergence and stability characteristics of the SRBMs used in combination with Picard iteration scheme. There can be two possible adaptive strategies based on monitoring the residual error norm and employing ME-SRBMs. Firstly, the residual error

norm which is indicative of the errors due to PC truncation can be monitored and used to determine the desired order of PC expansion of SRBM basis vectors.

Adaptive strategies employing ME-SRBMs can alternatively be used for large scale problems (with a large number of degrees of freedoms) where increasing the order of SRBM expansion may not be feasible. The response process can be refined adaptively in a region in the input probability space where the approximations are error-prone. Thus the convergence characteristics can be improved.

⋆ **Orthonormalization of the basis :** SRBMs can be implemented as Arnoldi process to orthonormalize the basis vectors. This will lead to improved numerical stability when large number of basis vectors are employed.

⋆ **Transient analysis :** SRBMs have been employed for dealing with only steady state systems so far. Transient stochastic systems could also be investigated in the future.

Appendix A

A 2D case study for the domain transformed heat equation

Here we present a 2D case study to derive the transformed Equation 4.7 when the coordinates are mapped from stochastic to deterministic domain in continuum. The Jacobian of the coordinate transformation can be written as:

$$\mathbf{J} = \begin{pmatrix} \frac{\partial \xi_1}{\partial x_1} & \frac{\partial \xi_2}{\partial x_1} \\ \frac{\partial \xi_1}{\partial x_2} & \frac{\partial \xi_2}{\partial x_2} \end{pmatrix}$$

where $x = \{x_1, x_2\} \in D_0$ and $\xi = \{\xi_1, \xi_2\} \in D(\omega)$. Then, the covariant metric tensor $\mathbf{G}$ is given by:

$$\mathbf{G} = \mathbf{J}\mathbf{J}^T = \begin{pmatrix} g_{11} & g_{12} \\ g_{21} & g_{22} \end{pmatrix}$$

where $\{g_{ij}\}$ are given as:

$$\begin{aligned} g_{11} &= \left(\frac{\partial \xi_1}{\partial x_1}\right)^2 + \left(\frac{\partial \xi_2}{\partial x_1}\right)^2 \\ g_{12} &= \frac{\partial \xi_1}{\partial x_1}\frac{\partial \xi_1}{\partial x_2} + \frac{\partial \xi_2}{\partial x_1}\frac{\partial \xi_2}{\partial x_2} \\ g_{21} &= g_{12} \\ g_{22} &= \left(\frac{\partial \xi_1}{\partial x_2}\right)^2 + \left(\frac{\partial \xi_2}{\partial x_2}\right)^2. \end{aligned}$$

Now $\mathbf{G}^{-1} = (g^{ij})$ where g^{ij} are given as:

$$\begin{aligned} g^{11} &= g_{22}/g \\ g^{12} &= -g_{21}/g \\ g^{21} &= -g_{12}/g \\ g^{22} &= g_{11}/g, \end{aligned} \tag{A.1}$$

here g is the determinant of G and we denote the determinant of $\mathbf{J}$ as $\sqrt{g}$. Partial derivatives in the nominal and target domains are connected through $\mathbf{J}$ as follows:

$$\begin{pmatrix} \frac{\partial}{\partial \xi_1} \\ \frac{\partial}{\partial \xi_2} \end{pmatrix} = \mathbf{J}^{-1} \begin{pmatrix} \frac{\partial}{\partial x_1} \\ \frac{\partial}{\partial x_2} \end{pmatrix}, \tag{A.2}$$

due to which the partial derivatives of u in the domain $D(\omega)$ can be written as:

$$\begin{aligned} \frac{\partial u}{\partial \xi_1} &= \frac{1}{\sqrt{g}} \left(\frac{\partial \xi_2}{\partial x_2} \frac{\partial u}{\partial x_1} - \frac{\partial \xi_2}{\partial x_1} \frac{\partial u}{\partial x_2} \right) \\ \frac{\partial u}{\partial \xi_2} &= \frac{1}{\sqrt{g}} \left(\frac{\partial \xi_1}{\partial x_1} \frac{\partial u}{\partial x_2} - \frac{\partial \xi_1}{\partial x_2} \frac{\partial u}{\partial x_1} \right). \end{aligned} \tag{A.3}$$

From the above equations Equation A.2 and Equation A.3, the left hand side of the Poisson equation can be obtained as follows:

$$\begin{aligned} \frac{\partial}{\partial \xi_1}\left(\frac{\partial u}{\partial \xi_1}\right) + \frac{\partial}{\partial \xi_2}\left(\frac{\partial u}{\partial \xi_2}\right) = \frac{1}{\sqrt{g}} \Bigg(& \underbrace{\left[\frac{\partial \xi_1}{\partial x_2} \frac{\partial}{\partial x_1} \left(\frac{1}{\sqrt{g}} \frac{\partial \xi_1}{\partial x_2} \frac{\partial u}{\partial x_1} \right) + \frac{\partial \xi_2}{\partial x_2} \frac{\partial}{\partial x_1} \left(\frac{1}{\sqrt{g}} \frac{\partial \xi_2}{\partial x_2} \frac{\partial u}{\partial x_1} \right) \right]}_{\text{a}} \\ & \underbrace{- \left[\frac{\partial \xi_1}{\partial x_2} \frac{\partial}{\partial x_1} \left(\frac{1}{\sqrt{g}} \frac{\partial \xi_1}{\partial x_1} \frac{\partial u}{\partial x_2} \right) + \frac{\partial \xi_2}{\partial x_2} \frac{\partial}{\partial x_1} \left(\frac{1}{\sqrt{g}} \frac{\partial \xi_2}{\partial x_1} \frac{\partial u}{\partial x_2} \right) \right]}_{\text{b}} \\ & \underbrace{- \left[\frac{\partial \xi_1}{\partial x_1} \frac{\partial}{\partial x_2} \left(\frac{1}{\sqrt{g}} \frac{\partial \xi_1}{\partial x_2} \frac{\partial u}{\partial x_1} \right) + \frac{\partial \xi_2}{\partial x_1} \frac{\partial}{\partial x_2} \left(\frac{1}{\sqrt{g}} \frac{\partial \xi_2}{\partial x_2} \frac{\partial u}{\partial x_1} \right) \right]}_{\text{c}} \\ & + \underbrace{\left[\frac{\partial \xi_1}{\partial x_1} \frac{\partial}{\partial x_2} \left(\frac{1}{\sqrt{g}} \frac{\partial \xi_1}{\partial x_1} \frac{\partial u}{\partial x_2} \right) + \frac{\partial \xi_2}{\partial x_1} \frac{\partial}{\partial x_2} \left(\frac{1}{\sqrt{g}} \frac{\partial \xi_2}{\partial x_1} \frac{\partial u}{\partial x_2} \right) \right]}_{\text{d}} \Bigg). \end{aligned} \tag{A.4}$$

Now the terms (a), (b), (c), (d) in Equation A.4 can be written as:

$$\begin{aligned} a &= \frac{\partial}{\partial x_1} \left(\frac{1}{\sqrt{g}} \left[\left(\frac{\partial \xi_1}{\partial x_2} \right)^2 + \left(\frac{\partial \xi_2}{\partial x_2} \right)^2 \right] \frac{\partial u}{\partial x_1} \right) - \left\{ \frac{\partial \xi_1}{\partial x_2} \frac{\partial^2 \xi_1}{\partial x_1 \partial x_2} \frac{1}{\sqrt{g}} \frac{\partial u}{\partial x_1} + \frac{\partial \xi_2}{\partial x_2} \frac{\partial^2 \xi_2}{\partial x_1 \partial x_2} \frac{1}{\sqrt{g}} \frac{\partial u}{\partial x_1} \right\} \\ &= \frac{\partial}{\partial x_1} \left(\sqrt{g} g^{11} \frac{\partial u}{\partial x_1} \right) - \left\{ \cdots \right\} \\ b &= -\frac{\partial}{\partial x_1} \left(\frac{1}{\sqrt{g}} \left[\frac{\partial \xi_1}{\partial x_1} \frac{\partial \xi_1}{\partial x_2} + \frac{\partial \xi_2}{\partial x_1} \frac{\partial \xi_2}{\partial x_2} \right] \frac{\partial u}{\partial x_2} \right) + \left\{ \frac{\partial \xi_1}{\partial x_1} \frac{\partial^2 \xi_1}{\partial x_1 \partial x_2} \frac{1}{\sqrt{g}} \frac{\partial u}{\partial x_2} + \frac{\partial \xi_2}{\partial x_1} \frac{\partial^2 \xi_2}{\partial x_1 \partial x_2} \frac{1}{\sqrt{g}} \frac{\partial u}{\partial x_2} \right\} \\ &= \frac{\partial}{\partial x_1} \left(\sqrt{g} g^{12} \frac{\partial u}{\partial x_2} \right) + \left\{ \cdots \right\} \\ c &= -\frac{\partial}{\partial x_2} \left(\frac{1}{\sqrt{g}} \left[\frac{\partial \xi_1}{\partial x_1} \frac{\partial \xi_1}{\partial x_2} + \frac{\partial \xi_2}{\partial x_1} \frac{\partial \xi_2}{\partial x_2} \right] \frac{\partial u}{\partial x_1} \right) + \left\{ \frac{\partial \xi_1}{\partial x_2} \frac{\partial^2 \xi_1}{\partial x_2 \partial x_1} \frac{1}{\sqrt{g}} \frac{\partial u}{\partial x_1} + \frac{\partial \xi_2}{\partial x_2} \frac{\partial^2 \xi_2}{\partial x_2 \partial x_1} \frac{1}{\sqrt{g}} \frac{\partial u}{\partial x_1} \right\} \\ &= \frac{\partial}{\partial x_2} \left(\sqrt{g} g^{21} \frac{\partial u}{\partial x_1} \right) + \left\{ \cdots \right\} \\ d &= \frac{\partial}{\partial x_2} \left(\frac{1}{\sqrt{g}} \left[\left(\frac{\partial \xi_1}{\partial x_1} \right)^2 + \left(\frac{\partial \xi_2}{\partial x_1} \right)^2 \right] \frac{\partial u}{\partial x_2} \right) - \left\{ \frac{\partial \xi_1}{\partial x_1} \frac{\partial^2 \xi_1}{\partial x_2 \partial x_1} \frac{1}{\sqrt{g}} \frac{\partial u}{\partial x_2} + \frac{\partial \xi_2}{\partial x_1} \frac{\partial^2 \xi_2}{\partial x_2 \partial x_1} \frac{1}{\sqrt{g}} \frac{\partial u}{\partial x_2} \right\} \\ &= \frac{\partial}{\partial x_2} \left(\sqrt{g} g^{22} \frac{\partial u}{\partial x_2} \right) - \left\{ \cdots \right\} \end{aligned} \tag{A.5}$$

Recall from Section 4.1 that $\partial D_0 \in C^\infty$ due to which the mixed derivatives $\partial^2/\partial x_1 x_2$, $\partial^2/\partial x_2 x_1$ are equal. Thus summation of the terms (a), (b), (c) and (d) from Equation A.4 and Equation A.5 results in a compact expression for the transformed PDE in the form of Equation 4.7 as the $\{\cdots\}$ terms cancel each other.

Appendix B

Discretization of lognormal random fields

A lognormal random field can be defined by a transformation of a Gaussian random field $Y(x,\omega)$ as follows:

$$\widehat{\kappa}(x,\omega) = \exp(Y(x,\omega)), \tag{B.1}$$

Karhunen-Loéve expansion (refer to Section 2.1.2) of a lognormal random field results in a set of random variables whose probabilistic structure cannot be easily determined and hence such expansions are of no practical interest. Ghanem [127] proposed to discretize the underlying Gaussian random field (using Karhunen-Loéve or other such expansions) and then expand the lognormal field in a PC basis using Equation B.1. This approach leads to analytical expressions for this random field model. The Gaussian random field is discretized using one of the many available techniques such as the Karhunen-Loéve expansion scheme so that the random field is characterized by a finite set of random variables as follows:

$$Y(x,\omega) \approx \mu_g(x) + \sum_{i=1}^{d} g_i(x)\xi_i,$$

where $\mu_g(x)$ is the mean of the random field, $\boldsymbol{\xi} = \{\xi_1, \xi_2, \cdots, \xi_d\}$ are uncorrelated random variables and $\mathbf{g}(x) = \{g_1(x), g_2(x), g_3(x), \cdots, g_d(x)\}$ are the product of eigenvectors and square root of eigenvalues of the KL integral eigenvalue problem (refer to Section 2.1.2). The above equation can be re-written using the vectors $\boldsymbol{\xi}$ and $\mathbf{g}(x)$ as follows:

$$Y(x,\omega) \approx Y(x,\boldsymbol{\xi}) = \mu_g(x) + \mathbf{g}(x)^T\boldsymbol{\xi}. \tag{B.2}$$

Substituting Equation B.2 in Equation B.1, the lognormal random field $\widehat{\kappa}(x,\omega)$ can be

expanded in a Hermite PC basis in terms of Gaussian random variables as follows[1]:

$$\widehat{\kappa}(x,\omega) \approx \exp(\mu_g(x) + \mathbf{g}(x)^T\boldsymbol{\xi}) \approx \sum_{i=0}^{P_1}\widehat{\kappa}_i(x)\phi_i(\boldsymbol{\xi}). \tag{B.3}$$

where the coefficients $\widehat{\kappa}_i$ are obtained after orthogonal projection onto the PC basis as follows:

$$\widehat{\kappa}_i(x) = \frac{\langle \exp(\mu_g(x) + \mathbf{g}(x)^T\boldsymbol{\xi})\phi_i\rangle}{\langle\phi_i^2\rangle}, \forall 0 \leq i \leq P_1.$$

Closed form expressions exist for the various expansion coefficients in the above equation. The first coefficient $\widehat{\kappa}_0$ corresponding to $\phi_0 = 1$ is the mean value of the random field $\widehat{\kappa}(x,\omega)$ given by:

$$\widehat{\kappa}_0(x) = \exp(\mu_g(x) + \frac{1}{2}\sum_{i=1}^{d} g_i^2(x)) = \exp(\mu_g(x) + \frac{1}{2}\sigma_g^2(x)), \tag{B.4}$$

where $\sigma_g(x)$ is the standard deviation of the underlying Gaussian field $Y(x,\omega)$. The other terms after some algebraic manipulations simplify to:

$$\widehat{\kappa}_i(x) = \widehat{\kappa}_0(x)\frac{\langle\phi_i(\boldsymbol{\xi} + \mathbf{g}(x))\rangle}{\langle\phi_i^2\rangle}. \tag{B.5}$$

Referring to the representation Equation 2.6 of the polynomials $\phi_i(\boldsymbol{\xi})$, above equation can be simplified as:

$$\widehat{\kappa}_0(x)\frac{\langle\phi_i(\boldsymbol{\xi} + \mathbf{g}(x))\rangle}{\langle\phi_i^2\rangle} = \widehat{\kappa}_0(x)\frac{\prod_{j=1}^{d} g_j(x)^{\beta_j}}{\prod_{j=1}^{d}\beta_j!}. \tag{B.6}$$

As a result of Equation B.4, Equation B.5, Equation B.6, the PC representation of the discretized lognormal random field is as follows:

$$\widehat{\kappa}(x,\boldsymbol{\xi}) = \widehat{\kappa}_0(x)\sum_{\boldsymbol{\beta}}\frac{\prod_{j=1}^{d} g_j(x)^{\beta_j}}{\prod_{j=1}^{d}\beta_j!}\phi_{\boldsymbol{\beta}}(\boldsymbol{\xi}), \tag{B.7}$$

where the summation ranges over the finite number (P_1) of the PC basis functions with $\boldsymbol{\beta}$ defined as in Equation 2.6.

[1]Note that this equation is the most general form to represent any kind of uncertainty including the Gaussian uncertainty in which case the polynomials $\{\phi_i\}$ are of the first order.

Bibliography

[1] Sachin K. Sachdeva. *Subspace projection schemes for stochastic finite element analysis*. PhD thesis, University of Southampton, Southampton, UK, 2006.

[2] B. Sudret and A. Der Kiureghian. Stochastic finite elements and reliability: A state-of-the-art report. Technical report, University of California, Berkley, Technical report no. UCB/SEMM-2000/08, 173p, 2000.

[3] D. Xiu and G. E. Karniadakis. Modeling uncertainty in flow simulations via generalized polynomial chaos. *Journal of Computational Physics*, 187:137–167, 2003.

[4] W. L. Oberkampf, S. M. DeLand, B. M. Rutherford, K. V. Diegert, and K. F. Alvin. Error and uncertainty in modeling and simulation. *Reliability Engineering and System Safety*, 75:333–357, 2002.

[5] C. Soize. A nonparametric model of random uncertainties for reduced matrix models in structural dynamics. *Probabilistic Engineering Mechanics*, 15(3):277–294, 2000.

[6] C. Soize. Maximum entropy approach for modeling random uncertainties in transient elastodynamics. *Journal of the Acoustical Society of America*, 109(5):1979–1996, 2001.

[7] S. Adhikari. Matrix variate distributions for probabilistic structural mechanics. *AIAA Journal*, 45(7):1748–1762, 2007.

[8] S. Adhikari. On the quantification of damping model uncertainty. *Journal of Sound and Vibration*, 305(1–2):153–171, 2007.

[9] E. Vanmarcke. *Random fields: Analysis and synthesis*. MIT Press, Cambridge, MA, 1983.

[10] C. C. Li and A. Der Kiureghian. Optimal discretization of random fields. *Journal of Engineering Mechanics, ASCE*, 119:1136–1154, 1993.

[11] S. P. Huang, S. T. Quek, and K. K. Phoon. Convergence study of the truncated Karhunen-Loève expansion for simulation of stochastic processes. *International Journal for Numerical Methods in Engineering*, 52:1029–1043, 2001.

[12] R. Y. Rubinstein. *Simulation and the Monte-Carlo method*. Wiley, NY, 1981.

[13] M. Shinzouka and C. M. Jan. Digital simulation of random processes and its applications. *Journal of Sound and Vibration*, 25:111–128, 1972.

[14] J. E. Hurtado and A. H. Barbat. Monte-Carlo techniques in computational stochastic mechanics. *Archives of Computational Methods in Engineering*, 5:3–29, 1998.

[15] H. G. Matthies and A. Keese. Galerkin methods for linear and nonlinear elliptic stochastic partial differential equations. *Computer Methods in Applied Mechanics and Engineering*, 194:1295–1331, 2005.

[16] A. Keese. *Numerical solution of systems with stochastic uncertainties-A general purpose framework for stochastic finite elements*. PhD thesis, Technische Universitat Braunschweig, Brunswick, 2004.

[17] D. Xiu and J. S. Hesthaven. High-order collocation methods for differential equations with random inputs. *SIAM Journal on Scientific Computing*, 27(3):1118–1139, 2005.

[18] A. Keese. A review of recent developments in the numerical solution of stochastic PDEs (stochastic finite elements). Technical report, Technische Universitat Braunschweig, Braunschweig, http://opus.tu-bs.de/opus/volltexte/2003/504/, 2007.

[19] I. Babuška, F. Nobile, and R. Tempone. A stochastic collocation method for elliptic partial differential equations with random input data. *SIAM Journal on Numerical Analysis*, 27(3):1118–139, 2007.

[20] F. Nobile, R. Tempone, and C. G. Webster. An anisotropic sparse grid stochastic collocation method for partial differential equations with random input data. Technical report, Technical Report 04/2007, MOX, Dipartimento di Matematica, Milano, Italy, 2007.

[21] J. Foo, X. Wan, and G. E. Karniadakis. The multi-element probabilistic collocation method: Error analysis and applications. *Journal of Computational Physics*, 227(20): 9572–9595, 2008.

[22] B. Ganapathysubramanian and N. Zabaras. Sparse grid collocation schemes for stochastic natural convection problems. *Journal of Computational Physics*, 225(1):652–685, 2007.

[23] D. Xiu and J. S. Hesthaven. High-order collocation methods for differential equations with random inputs. *SIAM Journal on Scientific Computing*, 27(3):1118–1139, 2005.

[24] M. S. Eldred, C. G. Webster, and P. Constantine. Evaluation of non-intrusive approaches for generalized Wiener-Askey polynomial chaos. In *Proceedings of the 10th AIAA Non-Deterministic Approaches Conference*, Schaumberg, USA, 2008.

[25] M. Kleiber and T. D. Hien. *The stochastic finite element method: Basis perturbation technique and computer implementation*. John Wiley & Sons, Chichester, 1992.

[26] G. I Schueller. Special issue- A state-of-the-art report on computational stochastic mechanics. *Probabilistic Engineering Mechanics*, 12:197–321, 1997.

[27] F. Yamazaki, M. Shinzouka, and G. Dasgupta. Neumann expansion for stochastic finite element analysis. *Journal of Engineering Mechanics*, 114:1335–1355, 1988.

[28] T. D. Hien and M. Kleiber. Stochastic finite element modeling in linear transient heat transfer. *Computer Methods in Applied Mechanics and Engineering*, 144:111–124, 1997.

[29] M. Kaminski. Stochastic second-order perturbation approach to stress-based finite element method. *International Journal of Solids and Structures*, 38:3831–3852, 2001.

[30] A. Haldar and S. Mahadevan. *Reliability assessment using stochastic finite element analysis*. John Wiley & Sons, NY, 2000.

[31] M. R. Rajashekhar and B. R. Ellingwood. A new look at the response surface method for reliability analysis. *Structural safety*, 12:205–220, 1993.

[32] P. B. Nair, A. Choudhary, and A. J. Keane. Bayesian surrogate modeling of deterministic simulation codes for probabilistic analysis. In *Proceedings of 42nd AIAA/ASME/ASCE/AHS/ASC Structures, Structural Dynamics and Materials conference*, Seattle, USA, 2001. AIAA Paper 2001-1676.

[33] P. B. Nair, A. Choudhary, and A. J. Keane. Some greedy algorithms for sparse regression and classification with Mercer kernels. *Journal of Machine Learning Research*, 3: 781–801, 2002.

[34] D. M. Tartakovsky and A. Guadagnini. Prior mapping for nonlinear flows in random environments. *Physical Review E*, 64:035302–1 – 035302–4, 2001.

[35] D. M. Tartakovsky, A. Guadagnini, and M. Riva. Stochastic averaging of nonlinear flows in heterogeneous porous media. *Journal of Fluid Mechanics*, 492:47–62, 2003.

[36] L. Li, H. A. Tchelepi, and D. Zhang. Perturbation-based moment equation approach for flow in heterogeneous porous media: Applicability range and analysis of high-order terms. *Journal of Computational Physics*, 188(1):296–317, 2003.

[37] N. Wiener. The homogeneous chaos. *American Journal of Mathematics*, 60:897–936, 1938.

[38] R. H. Cameron and W. T. Martin. The orthogonal development of nonlinear functionals in series of Fourier-Hermite functionals. *Annals of Mathematics*, 48:385–392, 1947.

[39] R. Ghanem and P. Spanos. *Stochastic finite elements: A spectral approach*. Springer Verlag, New York, 1991.

[40] R. Ghanem and P. Spanos. Stochastic Galerkin expansion for nonlinear random vibration analysis. *Probabilistic Engineering Mechanics*, 8:255–264, 1993.

[41] R. Ghanem and V. Brzkala. Stochastic finite element analysis of randomly layered media. *Journal of Engineering Mechanics*, 122:361–369, 1996.

[42] R. Ghanem. Probabilistic characterization of transport in heterogeneous media. *Computational Methods in Applied Mechanical Engineering*, 158:199–220, 1998.

[43] O. L. Maître, M. Reagan, H. Najm, R. Ghanem, and O. Knio. A stochastic projection method for fluid flow; basic formulation. *Journal of Computational Physics*, 173:481–511, 2001.

[44] A. Sarkar and R. Ghanem. Mid-frequency structural dynamics with parameter uncertainty. *Computational Methods in Applied Mechanical Engineering*, 191:5499–5513, 2002.

[45] M. Anders and M. Hori. Stochastic finite element method for elasto-plastic body. *International Journal of Numerical Methods in Engineering*, 46:1897–1916, 1999.

[46] G. D. Manolis and C. Z. Karakostas. A Green's function method to SH-wave motion in random continuum. *Engineering Analysis with Boundary Elements*, 27:93–100, 2003.

[47] D. Xiu and G. E. Karniadakis. The Wiener-Askey polynomial chaos for stochastic differential equations. *SIAM Journal of Scientific Computing*, 24(2):619–644, 2002.

[48] M. Anders and M. Hori. Three-dimensional stochastic finite element method for elasto-plastic bodies. *International Journal for Numerical Methods in Engineering*, 51:449–478, 2001.

[49] O. P. L. Maître, O. M. Knio, H. N. Njam, and R. G. Ghanem. A stochastic projection method for fluid flow I: Basic formulation. *Journal of Computational Physics*, 173: 481–511, 2001.

[50] O. P. Le Maître, M. T. Reagan, H. N. Najm, R. G. Ghanem, and O. M. Knio. A stochastic projection method for fluid flow II: Random process. *Journal of Computational Physics*, 181(1):9–44, 2002.

[51] R. Ghanem and B. Hayek. Probabilistic modeling of flow over rough terrain. *Journal of Fluids Engineering-Transactions of the ASME*, 124(1):42–50, 2002.

[52] V. A. B. Narayanan and N. Zabaras. Variational multiscale stabilized FEM formulations for transport equations: stochastic advection-diffusion and incompressible stochastic Navier-Stokes equations. *Journal of Computational Physics*, 202:94–133, 2005.

[53] R. Li and R. Ghanem. Adaptive polynomial chaos expansions applied to statistics of extremes in nonlinear random vibration. *Probabilistic Engineering Mechanics*, 13(2): 125–136, 1998.

[54] A. Nouy. A generalized spectral decomposition technique to solve a class of linear stochastic partial differential equations. *Computer Methods in Applied Mechanics and Engineering*, 196:4521–4537, 2007.

[55] A. Nouy. Generalized spectral decomposition method for solving stochastic finite element equations: Invariant subspace problem and dedicated algorithms. *Computer Methods in Applied Mechanics and Engineering*, 197:4718–4736, 2008.

[56] A. Nouy and O.P. Le Maître. Generalized spectral decomposition for stochastic nonlinear problems. *Journal of Computational Physics*, 228:202–235, 2009.

[57] O. P. L. Maître, H. N. Njam, R. G. Ghanem, and O. M. Knio. Uncertainty propagation using Wiener-Haar expansions. *Journal of Computational Physics*, 197:28–57, 2004.

[58] O. P. L. Maître, H. N. Njam, R. G. Ghanem, and O. M. Knio. Multi-resolution analysis of Wiener-type uncertainty propagation schemes. *Journal of Computational Physics*, 197:502–531, 2004.

[59] I. Babuška, R. Tempone, and E. Zouraris. Galerkin finite element approximations of stochastic elliptic partial differential equations. *SIAM Journal of Numerical Analysis*, 42:800–825, 2004.

[60] P. B. Nair. On the theoretical foundations of stochastic reduced basis methods. In *Proceedings of 42nd AIAA/ASME/ASCE/AHS/ASC Structures, Structural Dynamics and Materials Conference*, Seattle WA, 2001. AIAA Paper No. 2001-1677.

[61] P. B. Nair and A. J. Keane. Stochastic reduced basis methods. *AIAA Journal*, 40: 1653–1664, 2002.

[62] Sachin K. Sachdeva, Prasanth B. Nair, and Andy J. Keane. Comparative study of projection schemes for stochastic finite element analysis. *Computer Methods in Applied Mechanics and Engineering*, 195:2371–2392, 2006.

[63] Sachin K. Sachdeva, Prasanth B. Nair, and Andy J. Keane. Hybridization of stochastic reduced basis methods with polynomial chaos expansions. *Probabilistic Engineering Mechanics*, 21:182–192, 2006.

[64] D. Xiu and G. E. Karniadakis. Modeling uncertainty in steady state diffusion problems via generalized polynomial chaos. *Computer Methods in Applied Mechanics and Engineering*, 191:4927–4948, 2002.

[65] D. Xiu and G. E. Karniadakis. A new stochastic approach to transient heat conduction modeling with uncertainty. *International Journal of Heat and Mass Transfer*, 46(24): 4681–4693, 2003.

[66] M. Eiermann, O. G. Ernst, and E. Ullmann. Computational aspects of the stochastic finite element method. *Computer Vision and Science*, 10:3, 2007.

[67] H. Elman and D. Furnival. Solving the stochastic steady-state diffusion problem using multigrid. *IMA Journal of Numerical Analysis*, 27:675–688, 2007.

[68] B. Seynaeve, E. Rosseel, B. Nicolaï, and S. Vandewalle. Fourier mode analysis of multigrid methods for partial differential equations with random coefficients. *Journal of Computational Physics*, 224:132–149, 2007.

[69] H. Holden, B. Oksendal, J. Uboe, and T. S. Zhang. *Stochastic partial differential equations- A modeling, white noise functional approach*. Birkauser, Boston, USA, 1995.

[70] A. F. Emery and D. Bardot. Stochastic heat transfer in fins and transient cooling using polynomial chaos and Wick products. *Journal of Heat Transfer*, 129(9):1127–1133, 2007.

[71] K. E. Atkinson. *The numerical solution of integral equations of the second kind*. Cambridge University Press, Cambridge, 1997.

[72] S. P. Huang, S. T. Quek, and K. K. Phoon. Convergence study of the truncated Karhunen-Loève expansion for simulation of stochastic processes. *International Journal for Numerical Methods in Engineering.*, 52:1029–1043, 2001.

[73] P. G. Ciarlet. *The finite element method for elliptic problems*. North Holland, Amsterdam, 1978.

[74] J. N. Reddy. *An introduction to finite element method*. McGraw-Hill, NY, 1993.

[75] J. A. S. Witteveen and H. Bijl. Modeling arbitrary uncertainties using Gram-Schmidt polynomial chaos. In *Proceedings of the 44th AIAA Aerospace Sciences Meeting and Exhibit*, pages AIAA–2006–0896, Boca Raton, Florida, USA, 2006. AIAA.

[76] P. B. Nair. *Projection schemes in stochastic finite element analysis, Engineering Design and Reliability*, chapter 21. CRC Press, 2005.

[77] D. Xiu and D. M. Tartakovsky. A two-scale non-perturbative approach to uncertainty analysis of diffusion in random composites. *SIAM Journal of multiscale modeling and simulation*, 2(4):662–674, 2004.

[78] X. Wan and G. E. Karniadakis. An adaptive multi-element generalized polynomial chaos method for stochastic differential equations. *Journal of Computational Physics*, 209:617–642, 2005.

[79] X. Wan and G. E. Karniadakis. Multi-element generalized polynomial chaos for arbitrary probability measures. *SIAM Journal on Scientific Computing*, 28(3):901–928, 2006.

[80] O. Le. Maître, H. Najm, P. Pébay, R. Ghanem, and O. Knio. Multi-resolution analysis for uncertainty quantification in chemical systems. *SIAM Journal on Scientific Computing*, 29(2):864–889, 2007.

[81] David Darmofal. Steady and transient heat transfer simulation of a turbine blade. Technical report, MIT, http://ocw.mit.edu/NR/rdonlyres/Aeronautics-and-Astronautics/16-901Spring-2005/BB2A3F40-0401-47B1-9790-417C5980B519/0/proj2.pdf, 2005.

[82] G. Taylor. A model for the boundary condition of a porous material, part 1. *Journal of Fluid Mechanics*, 49:319–326, 1971.

[83] S. Richardson. A model for the boundary condition of a porous material, part 2. *Journal of Fluid Mechanics*, 49:327–336, 1971.

[84] H. Homeier and D. Kingham. Effects of local field variations on the contrast of a field-ion microscope. *Journal of Physics D*, 16:L115–L120, 1983.

[85] M. Fyrillas and C. Pozrikidis. Conductive heat transport across rough surfaces and interfaces between two conforming media. *International Journal of Heat and Mass Transfer*, 44:1789–1801, 2001.

[86] M. Blyth and C. Pozrikidis. Heat conduction across irregular and fractal-like surfaces. *International Journal of Heat and Mass Transfer*, 46:1329–1339, 2003.

[87] D. Cajueiro, V. Sampaio, C. De Castilho, and R. Andrade. Fractal properties of equipotentials close to a rough conducting surface. *Journal of Physics: Condensed Matter*, 11:4985–4992, 1999.

[88] C. Everetsz and B. Mandelbrot. Harmonic measure around a linearly self-similar tree. *Journal of Physics A*, 25:1781–1797, 1992.

[89] B. Van den Nieuwenhof and J. P. Coyette. Modal approaches for the stochastic finite element analysis of structures with material and geometric uncertainties. *Computer Methods in Applied Mechanics and Engineering*, 192:3705–3729, 2003.

[90] G. Stefanou and M. Papadrakakis. Stochastic finite element analysis of shells with combined random material and geometric properties. *Computer Methods in Applied Mechanics and Engineering*, 193:139–160, 2004.

[91] T. Haukaas and M. H. Scott. Shape sensitivities in the reliability analysis of nonlinear frame structures. *Computers and Structures*, 84:964–977, 2006.

[92] S. Reh, J.-D. Beley, S. Mukherjee, and E. H. Khor. Probabilistic finite element analysis using (ANSYS). *Structural Safety*, 28:17–43, 2006.

[93] C. Canuto and T. Kozubek. A fictitious domain approach to the numerical solution of PDEs in stochastic domains. *Numerische Mathematik*, 107:257–293, 2007.

[94] R. Honda. Stochastic BEM with spectral approach in elastostatic and elastodynamic problems with geometrical uncertainty. *Engineering Analysis with Boundary Elements*, 29(5):415–427, 2005.

[95] H. Harbrecht, R. Schneider, and C. Schwab. Sparse second moment analysis for elliptic problems in stochastic domains. Technical report, Research report No. 2007-02, Seminar für Angewandte Mathematik, Eigenössische Technische Hochschule, CH-8092, Zürich, 2007.

[96] A. Nouy, A. Clément, F. Schoefs, and N. Moës. An extended stochastic finite element method for solving stochastic partial differential equations on random domains. *Computer Methods in Applied Mechanics and Engineering*, 197(51):4663–4682, 2008.

[97] Dongbin Xiu and Daniel M. Tartakovsky. Numerical methods for differential equations in random domains. *SIAM Journal of Scientific Computing*, 27(3):1118–1139, 2005.

[98] D. M. Tartakovsky and D. Xiu. Stochastic analysis of transport in tubes with rough walls. *Journal of Computational Physics*, 217:248–259, 2006.

[99] R. d'Ippolito, U. Tabak, M. De Munck, S. Donders, D. Moens, and D. Vandepitte. Modeling of a vehicle windshield with realistic uncertainty. *Proceedings of the International Conference on Noise and Vibration Engineering*, 2006.

[100] C. Chauviere, J. S. Hesthaven, and L. C. Wilcox. Efficient computation of RCS from scatters of uncertain shapes. *IEEE transactions on Antennas and Propagation*, 55(5): 1437–1448, 2007.

[101] G. Stefanou, A. Nouy, and A. Clement. Identification of random shapes from images through polynomial chaos expansion of random level set functions. *International Journal for Numerical Methods in Engineering*, DOI: 10.1002/nme.2546, 2009.

[102] V. Garzon. *Probabilistic aerothermal design of compressor airfoils*. PhD thesis, Department of aeronautics and astronautics, MIT, USA, 2002.

[103] A. Rao, P. Aljabar, and D. Rueckert. Hierarchical statistical shape analysis and prediction of sub-cortical brain structures. *Medical Image Analysis*, 12(1):55–68, 2008.

[104] D. Rueckert, A. F. Frangi, and J. A. Schnabel. Automatic construction of 3D statistical deformation models of the brain using non-rigid registration. *IEEE Transactions on Medical Imaging*, 22(8):1014–1025, 2003.

[105] A. F. Frangi, D. Rueckert, and J. A. Schnabel. Automatic construction of multiple-object three dimensional statistical shape models: Application to cardiac modeling. *IEEE Transactions on Medical Imaging*, 21(9):1151–1166, 2002.

[106] I. T. Jolliffe. *Principal Component Analysis*. Springer Verlag, NY, USA, 2002.

[107] R.G. Ghanem and A. Doostan. On the construction and analysis of stochastic models: Characterization and propagation of the errors associated with limited data. *Journal of Computational Physics*, 217:63–81, 2006.

[108] I. S. Sokolnikoff. *Tensor analysis: Theory and applications to geometry and mechanics of continua*. John Wiley & Sons, New York, 1967.

[109] V. Akcelik, B. Jaramaz, and O. Ghattas. Nearly orthogonal two-dimensional grid generation with aspect ratio control. *Journal of Computational Physics*, 171:805–821, 2007.

[110] M. Renardy and R. C. Rogers. *An introduction to partial differential equations*. Springer, New York, USA, 1996.

[111] Brian T. Helenbrook. Mesh deformation using the biharmonic operator. *International Journal for Numerical Methods in Engineering*, 56:1007–1021, 2003.

[112] I. Robertson and S. Sherwin. Free-surface flow simulation using hp/spectral elements. *Journal of Computational Physics*, 155:26–53, 1999.

[113] C. Burg. Analytic study of 2D and 3D grid motion using modified Laplacian. *International Journal for Numerical Methods in Fluids*, 52:163–197, 2006.

[114] S. M. Shontz and S. A. Vavasis. A mesh warping algorithm based on weighted Laplacian smoothing. In *Proceedings of the 12th International Meshing Round-table, Santa Fe, USA*, pages 147–158, 2003.

[115] S. M. Shontz and S. A. Vavasis. An algorithm based on finite element weights for warping tetrahedral meshes. *submitted to SIAM Journal of Scientific Computing*, 2004.

[116] P. I. Crumpton and M. B. Giles. Implicit time-accurate solutions on unstructured dynamic grids. *International Journal for Numerical Methods in Fluids*, 25(11):1285–1300, 1997.

[117] K. Stein, T. Tezduyar, and R. Benney. Mesh moving techniques for fluid-structure interactions with large displacements. *ASME Journal of Applied Mechanics*, 70:58–63, 2003.

[118] R. Cools. An encyclopedia of cubature formulas. *Journal of Complexity*, 19:445–453, 2003.

[119] D. Xiu. Efficient collocational approach for parametric uncertainty analysis. *Communications in Computational Physics*, 2:293–309, 2007.

[120] R. V. Grandhi and L. Wang. Reliability-based structural optimization using improved two-point adaptive nonlinear approximations. *Finite Elements in Analysis and Design*, 29:35–48, 1998.

[121] M. Voigt, R. Mücke, K. Vogeler, and M. Oevermann. Probabilistic lifetime analysis for turbine blades based on a combined direct Monte Carlo and response surface approach. *ASME Turbo Expo*, pages GT2004–53439, 2004.

[122] C. W. Moeckel. Probabilistic turbine blade thermal analysis of manufacturing variability and tolerated designs. Master's thesis, MIT, 2006.

[123] T. Harter and T. C. J. Yeh. Flow in unsaturated porous media, nonlinear numerical analysis and comparison to analytical stochastic models. *Advances in Water Resources*, 22(3):252–272, 1998.

[124] C. Brenner and C. Bucher. A contribution to the SFE-based reliability assessment of nonlinear structures under dynamic loading. *Probabilistic Engineering Mechanics*, 10(4):265–273, 1995.

[125] G. A. Bécus and F. A. Cozzarelli. The random steady state diffusion problem. II: Random solutions to nonlinear, inhomogeneous steady-state diffusion problems. *SIAM Journal of Applied Mathematics*, 31:148–158, 1976.

[126] D. Gilbarg and N.S. Trudinger. *Elliptic partial differential equations of second order*. Springer-Verlag, Berlin, 1977.

[127] R. Ghanem. The nonlinear Gaussian spectrum of log-normal stochastic processes and variables. *ASME Journal of Applied Mechanics*, 66(4):964–974, 1999.

[128] P. Surya Mohan, P. B. Nair, and A. J. Keane. Multi-element stochastic reduced basis methods. *Computer Methods in Applied Mechanics and Engineering*, 197:1495–1506, 2008.

[129] R. W. Walters and L. Huyse. Uncertainty analysis for fluid mechanics with applications. Technical report, NASA, http://historical.ncstrl.org/tr/ps/icase/TR-2002-1.ps, 2002.